Technical University of Denmark

Validation of a Sensor System Solution for Process Monitoring in Robot Assisted Polishing

M.Sc Thesis by:

MATTIA DAZZI

Under the supervision of:

Prof. Paolo F. Bariani, Università degli Studi di Padova

Prof. Giuliano Bissacco, DTU Mekanik

February 2013

Abstract

This work is a Master Thesis carried out from September 2012 to February 2013 as International Exchange student at the Mechanical Engineering Department (MEK) of Technical University of Denmark (DTU) inside the European project IFaCOM.

The project deals with the validation of a sensor system composed by a three-component force transducer on which the workpiece was clamped, 2 AE sensors positioned on the workpiece and a Hall sensor for the measurement of the power consumed by oscillation module, applied in robot assisted flat diamond polishing of Uddeholm Stavax; on the machine is mounted a scattered light instrument OptoSurf OS 500 for the feasibility of on machine surface roughness evaluation. The goal is to validate possible correlation of the progress of the surface roughness during polishing with the sensors output signals acquired in-process or on machine for the subsequent implementation on the RAP (Robot Assisted Polishing) machine.

In order to achieve these results, tests were performed where the development of the surface roughness is divided in different time intervals to define the roughness behavior curve along the polishing process duration and to evaluate possible correlation with the different sensor signals acquired during the process. Roughness was measured both with a scattered light instrument (Optosurf OS 500) directly on the polishing machine and with a white light interferometer in a specialized laboratory as a reference instrument.

The polishing process itself, using loosen abrasives by means of a diamond gel, is studied to achieve the best possible results in terms of surface uniformity and duration of the process. Several preliminary tests have brought to the definition of all the parameters and the settings for the final tests. For the tests the polishing module that allows the oscillation is mounted on a CNC.

The correlation between the roughness curve obtained with the white light interferometer and the different signals acquired with all the sensors and the roughness measurements performed with Optosurf is finally analyzed to state if these hidden process variables can be used to characterize the development of surface finish.

Contents

Chapter 1

Introduction

1.1 IFaCOM Project

The vision of IFaCOM (Intelligent Fault Correction and self Optimizing Manufacturing systems) is to achieve near zero defect level of manufacturing for all kinds of manufacturing, with emphasis on production of high value parts, on large variety custom design manufacturing and on high performance products.

This shall be achieved through:

- Improved performance process control to reduce defects output and reduce the costs of defect avoidance
- Enhanced quality control to obtain more predictable product quality
- Enhanced manufacturing process capability independent of manufactured parts

The objectives are to reach a level of excellence for a systematic body of knowledge on near zero defect manufacturing output through improved process control.

In IFaCOM this will be obtained through development of new manufacturing strategies and methods which will be demonstrated in industrial cases. The fulfillment of these topics of the objective will lead to better performance in industries that apply the new technologies developed and an opportunity for equipment manufacturers to offer new high performance products, machine tool and auxiliary equipment on the market. [44]

1.2 Robot Assisted Polishing (RAP) Machine

The polishing machine is a new, alternative and flexible polishing machine tool solution that provides a qualitative and cost-effective polishing process developed by Strecon.

RAP is a robot arm polishing machine and its flexibility is given by its particular movement system with 6 axes and by its open structure. This particular geometry permits to polish different kind of parts with different shapes as:

- Part with 2D round and rotation-symmetric geometries.
- Parts with 3D simplified geometries
- Flat part surface

On the machine is mounted a proper polishing module developed by Strecon which controls normal force, oscillation rate and stroke. [46]

The force is controlled by two pressed air valves, the oscillation frequency is fully controlled by the operator, and the stroke of the pulse oscillation can be adjusted by the operator. Different polishing arms can be mounted on the module. The polishing arm can be easily mounted to the polishing module with the help of a conical connector. The need of different polishing media (e.g. stone, wood, diamond paste, etc.) can be easily mounted on the polishing end of the arm. This ensures a flexible and time efficient adjustment of the media and the individual polishing job.

The polishing module is a complete unit integrating both the force control and the oscillation system. The design ensures a fast and flexible, but also robust mounting and demounting on the robot arm.

1.3 Project Goals

A robust method for the determination of the right moment for tool change in RAP process has to be established by the process monitoring and control. Recognition of a steady state in the polishing process when additional material removal would no longer improve the surface roughness, resulting in an automatic stop and/or change of tool to proceed to the next step of the polishing sequence would provide:

- Significant reduction in the cycle time of the polishing job
- Maintaining the specified geometrical tolerances

This could be made by the assessment of few vital quality characteristics (VQC) as the surface roughness or the gloss of the surface. The easiest way is to monitor the variation of the surface roughness over polishing time, but this implies stopping of the process, proper cleaning of the surface to be measured and actual surface finish measurement. Since the produced surfaces can reach mirror like finish down to a few nm in Ra, unclamping the piece

and laboratory surface finish measurement is often required to reach necessary robustness due to hostile environment on the machine (e.g. presence of dust, debris, vibrations).

The steady state in the polishing process, where the variation in surface roughness over a certain number of polishing passes is negligible and there is no longer improvement adding value to the surface, represent the right moment for process stop and tool change. Such moment is designated by N_1 number of polishing passes in Figure 1, showing the improvement in polished surface roughness by subsequent polishing steps using different tools.

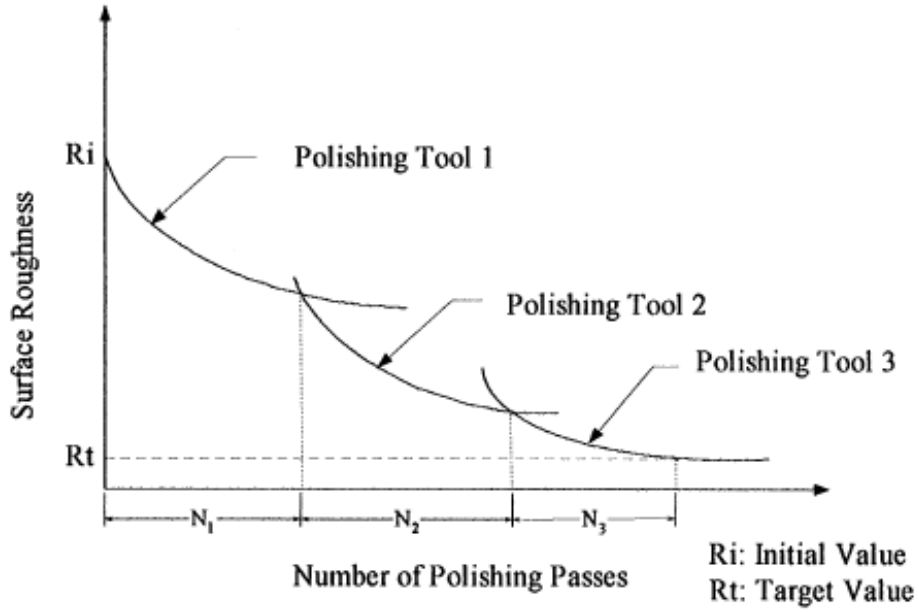

FIGURE 1 Surface roughness in polishing operation [2]

Based on literature survey and available process knowledge [2], [7], [14], [13],[3], [16] different kinds of indirect measurement of hidden process variables (HPVs) are expected to provide necessary information to determine the optimal point for the tool change such as:

- Acoustic emission (AE)
- Power consumption
- Force

This project will evaluate if there is a correlation between these HPV and the progress of the surface roughness in order to robustly monitor, control and optimize the process, as

described before; without the necessity of measuring every time the surface roughness unclamping and cleaning the piece, but relying on the data acquired with the different sensors applied on the machine.

Forces are measured in the oscillation direction while clamping the workpiece on a dynamometer, AE is measured positioning 2 different sensors directly on the workpiece and the power consumption of the oscillation module is acquired using Hall sensors.
Another issue is the validation of on-line roughness measurement with scattered light instrument (Optosurf 500) for future implementation on the polishing machine.

1.4 Thesis outline

First of all a literature survey on finishing processes, sensors typologies and surface roughness technologies are introduced.

Then the preliminary test campaign is exposed during which the polishing process was studied and all the parameters for the final tests were set.

Afterwards the final test campaign, where the knowledge from the preliminary tests is implemented, is explained focusing on every specific procedure and setting studied before.

Finally the results from the experimental campaign are shown and commented.

Chapter 2

Introduction to Finishing Techniques, Monitoring and Roughness

2.1 Introduction to Surface Finishing Techniques

Grinding, lapping and polishing are three important mechanical processes used to achieve desired dimension, surface finishing and very fine shapes of the machining workpiece, causing a little amount of material removal.

For these three techniques, the mechanism employed could seem very similar (for example a rotating wheel which rubs against a wafer is common both in lapping and in polishing), but the aims are different for each process. In fact, they are three different mechanical processes with different characteristics from each other and each of them has to be employed to obtain a precise result. An example of this is that these three techniques may belong to a mechanical machining sequence to achieve the desired final roughness value, or a free-damage surface of the machining part (in this particular case, the grinding process is applied firstly on the workpiece and then lapping and polishing follow). Nevertheless, the design specifications may require tolerances or sizes that a grinding wheel is not capable to obtain, without the employment of the other two. Or, it could happen a mechanical machining which requires a great material removal in the beginning, but a close roughness tolerance in the end because these are the required specifications of the design. In this last case, the workpiece has to be firstly machined with a grinding process to remove a large amount of material, and then with a polishing process in the end to satisfy the requests.[17],[1],[10]

But to better understand which are the characteristics and the capabilities of each process and to see where and how these particular processes are employed in the mechanical field, they will be introduced below.

2.1.1 Grinding

Grinding is used to produce a smooth finish on flat surfaces. It is a widely used abrasive machining process in which a spinning wheel covered in rough particles (grinding wheel) cuts chips of metallic substance from a workpiece, making a face of it flat or smooth.

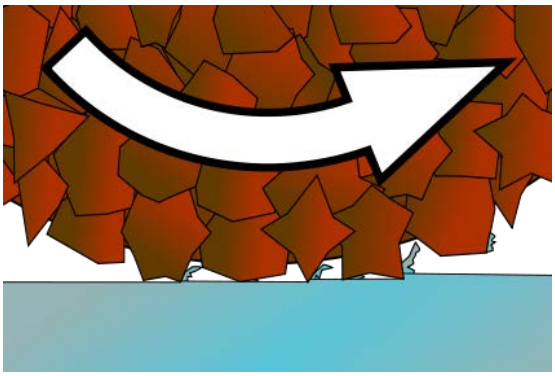

FIGURE 2.1 Sketch of how the abrasive particles in a grinding wheel remove material from a worpiece (source it.wikipedia.com)

The surface grinder is composed of an abrasive wheel, a workholding device known as a chuck, and a reciprocating or rotary table. The chuck holds the material in place while it is being worked on. It can do this one of two ways: ferromagnetic pieces are held in place by a magnetic chuck, while non-ferromagnetic and nonmetallic pieces are held in place by vacuum or mechanical means. A machine vise (made from ferromagnetic steel or cast iron) placed on the magnetic chuck can be used to hold non-ferromagnetic workpieces if only a magnetic chuck is available.

Factors to consider in surface grinding are the material of the grinding wheel and the material of the piece being worked on.

Typical workpiece materials include cast iron and mild steel. These two materials don't tend to clog the grinding wheel while being processed. Other materials are aluminum, stainless steel, brass and some plastics. When grinding at high temperatures, the material tends to become weakened and is more inclined to corrode. This can also result in a loss of magnetism in materials where this is applicable.

The grinding wheel is not limited to a cylindrical shape and can have a myriad of options that are useful in transferring different geometries to the object being worked on. Straight wheels can be dressed by the operator to produce custom geometries. When surface

grinding an object, one must keep in mind that the shape of the wheel will be transferred to the material of the object like a mirror image.

Spark out is a term used when precision values are sought and literally means "until the sparks are out (no more)". It involves passing the workpiece under the wheel, without resetting the depth of cut, more than once and generally multiple times. This ensures that any inconsistencies in the machine or workpiece are eliminated.

A surface grinder is a machine tool used to provide precision ground surfaces, either to a critical size or for the surface finish.

FIGURE 2.2 Surface grinder (source maxgrind.com)

The typical precision of a surface grinder depends on the type and usage, however +/- 0.002 mm should be achievable on most surface grinders.

The machine consists of a table that traverses both longitudinally and across the face of the wheel. The longitudinal feed is usually powered by hydraulics, as may the cross feed, however any mixture of hand, electrical or hydraulic may be used depending on the ultimate usage of the machine (i.e.: production, workshop, cost). The grinding wheel rotates in the spindle head and is also adjustable for height. Modern surface grinders are semi-automated, depth of cut and spark-out may be preset as to the number of passes and once setup the machining process requires very little operator intervention.

The machine has provision for the application of coolant as well as the extraction of metal dust (metal and grinding particles).

Aluminum oxide, silicon carbide, diamond, and cubic boron nitride (CBN) are four commonly used abrasive materials for the surface of the grinding wheels. Of these materials, aluminum oxide is the most common. Because of cost, diamond and CBN grinding wheels are generally made with a core of less expensive material surrounded by a layer of diamond or CBN. Diamond and CBN wheels are very hard and are capable of economically grinding materials, such as ceramics and carbides that cannot be ground by aluminum oxide or silicon carbide wheels.

As with any grinding operation, the condition of the wheel is extremely important. Grinding dressers are used to maintain the condition of the wheel, these may be table mounted or mounted in the wheel head where they can be readily applied.

The high temperatures encountered at the ground surface create residual stresses and a thin martensitic layer may form on the part surface; this decreases the fatigue strength. In ferromagnetic materials, if the temperature of the surface is raised beyond the Curie temperature then it may lose some magnetic properties. Finally, the surface may be more susceptible to corrosion. [17], [18]

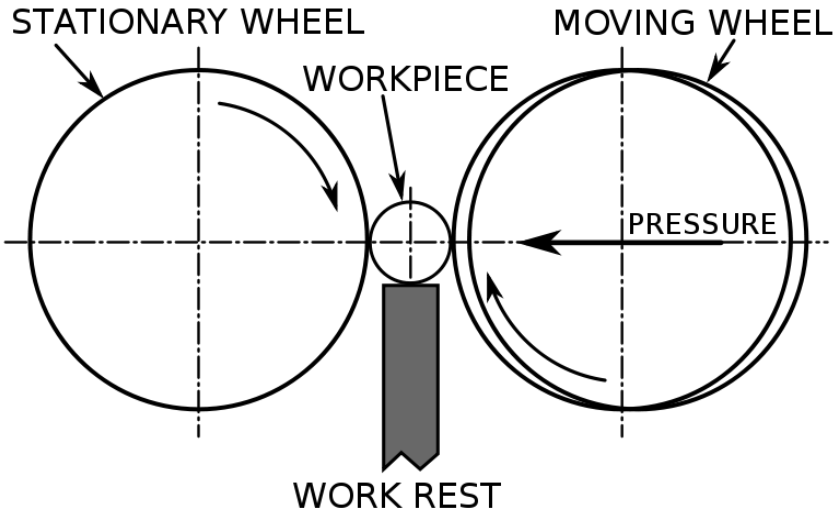

FIGURE 2.3 Centerless grinding (source cnx.org)

2.1.2 Polishing

Polishing is a finishing process for smoothing a workpiece's surface using an abrasive and a work pad or wheel. Technically polishing could refer to processes that use an abrasive that is glued to the work pad or wheel, or uses a loose abrasive applied to the work wheel. The first is a more aggressive process while the second is less harsh, which leads to a smoother, brighter finish.

Silicon-based polishing pads or a diamond solution can be used in the polishing process.

To prevent further unwanted oxidization, polished metal surfaces may be coated with wax, oil, or lacquer. This is of particular concern for copper alloy products such as brass and bronze.

FIGURE 2.4 Polishing cloths [42]

The improvement of products has created a higher demand for mirror finish of moulding tools. The highest demands for surface finish are in the optical lens mould where an extreme requirement on polishability is desired. However, in general there are other advantages with high surface finish, including:

- Easier ejection of the plastic parts from the moulding tool (applies to most plastics)
- Reduced risk of local corrosion
- Reduced risk of fracture or cracking due to temporary over loading or pure fatigue.

Two things are important when judging the surface. The surface must first have a geometrically correct shape without any long macro waves. This macro shape is mostly an inheritance from earlier grinding and stoning steps.

Secondly, the mirror finish of the mould surface must be free from scratches, pores, orange peel, pitting (pin-holes) etc. The surface finish is normally judged by the naked eye. There are certain difficulties involved in such a visual evaluation. A “flat” surface can look perfect despite the fact that it is not geometrically completely flat. Thus, the eye can be “fooled”. In more sophisticated cases, the finish can be judged by instrumental methods, such as optical interference techniques.

FIGURE 2.5 Examples of polished surfaces (source harrisonhep.com)

The first stage of polishing starts with a rough abrasive and each subsequent stage uses a finer abrasive until the desired finish is achieved. The rough pass removes surface defects like pits, nicks, lines and scratches. The finer abrasives leave very thin lines that are not visible to the naked eye. Lubricants like wax and kerosene may be used as lubricating and cooling media during these operations, although some polishing materials are specifically designed to be used "dry."

FIGURE 2.6 Polishing pads and arm [41]

There is a wide selection of abrasives to choose from when selecting a lapping and polishing process. Selecting an abrasive is dependent upon the specimen hardness, desired surface finish, desired removal rate, lifetime, and price. There are four basic types of abrasives that are used in lapping and polishing processes: silicon carbide (SiC), aluminum oxide or alumina (Al2O3), boron carbide (B4C), and diamond (C).

All of these abrasives have distinct properties and are used for different materials and applications.

- SiC: SiC is hard and generally has a needle or blocky structure. SiC is used in many applications where rough lapping is required. It seldom is used for polishing or applications that require smooth surface finishes.
- Al2O3: Al2O3 is relatively hard and has a sharp, angular structure. Alumina is commonly used where fine surface finishes are required as it breaks down over time and gives excellent surfaces during lapping and polishing. Alumina is also relatively inexpensive.
- B4C: B4C is harder than most other abrasives (excluding diamond) and has a blocky crystal structure. B4C provides excellent removal rates and is typically used when fast removal with moderate surface quality is needed.

- Diamond: Diamond is the hardest material known and has a sharp, angular structure. Diamond is extremely useful in lapping and polishing due to its removal rates and surface finishing qualities. Diamond can produce excellent surface finishes combined with high removal rates.

Polishing pads and wheels come in a wide variety of types to fulfill a wide range of needs. The most common materials used for polishing pads and wheels are wood, leather, canvas, cotton cloth, plastic, felt, paper, sheepskin, impregnated rubber, canvas composition, and wool; leather and canvas are the most common. Wooden pads and wheels have emery or other abrasives glued onto them and are used to polish flat surfaces and maintained good edges.

Other polishing cloths also known as mops, are either made from cotton or wool cloth and come bleached or unbleached.

FIGURE 2.7 Diamond gel [41]

Polishing is one of the last processes in the manufacturing chain and because of his nature is very time-consuming and then expensive. Optimize this process could be very useful and leads to significant improvement in several factors like tool wear, final roughness, time elapsed, production rate and finally cost of the part. [1],[6],[10],[19]

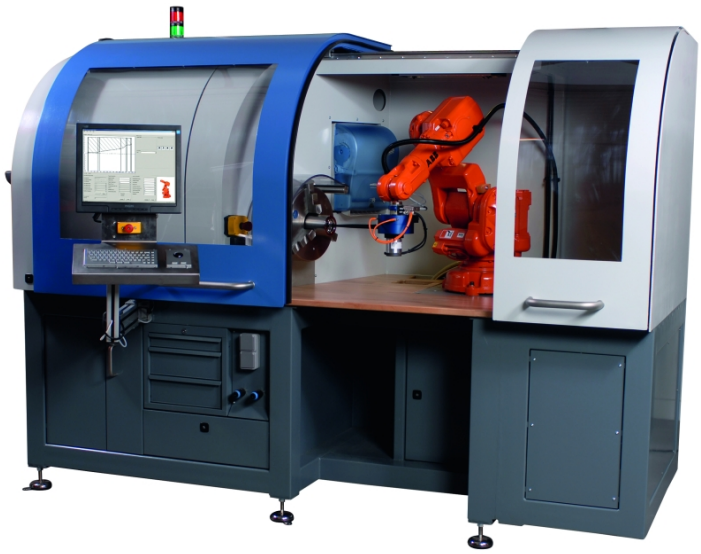

FIGURA 2.8 RAP machine [46]

In this project the process studied is a robot assisted diamond polishing, in which the oscillation motion is driven by an electric motor and the pressure is applied by a compressed air circuit. The polishing module that allows both actions is mounted on a CNC milling machine.

2.1.3 Lapping

Lapping is a material removal process that produces smooth and flat surfaces. The magnitude of the generated material removal is lower than the one generated by grinding. This technique is usually used to obtain dimensionally accurate specimens to high tolerances. The reached speeds of the lapping plates are usually lower than the ones of the grinding wheels (less than 80 RPM) and the employed abrasive size is between 5 and 20 µm. Lapping process is mainly used to produce the desired flatness of the machining part

Lapping can be run in two different regimes: free abrasive lapping and fixed abrasive lapping (in both cases, the caused surface damage is lower than in grinding).

FIGURA 2.9 Lapping machine (testbourne.com)

In fixed abrasive lapping two plates rub together (one of them is the workpiece) and the abrasive is bounded on the polishing plate surface. This process could be seen like a grinding process, but the employed grain size and speed in this last technique are higher and the final effect on the part surface results very different.

The most used regime is the free abrasive lapping. In this case, two plates are not directly touching each other. The abrasive is free to move, roll and scratch the surface without a preferential way. The abrasive is applied towards slurry that acts as lubricant and at the same time moves the abrasive on the lapping surface, washing out the chip. This is the most accurate method for producing specimens and causing the least amount of damage. It is noteworthy that in the end of this process, as for polishing, the surface doesn't show any directional marks. [1], [10]

FIGURE 2.10 Examples of lapped surfaces (source legitreviws.com)

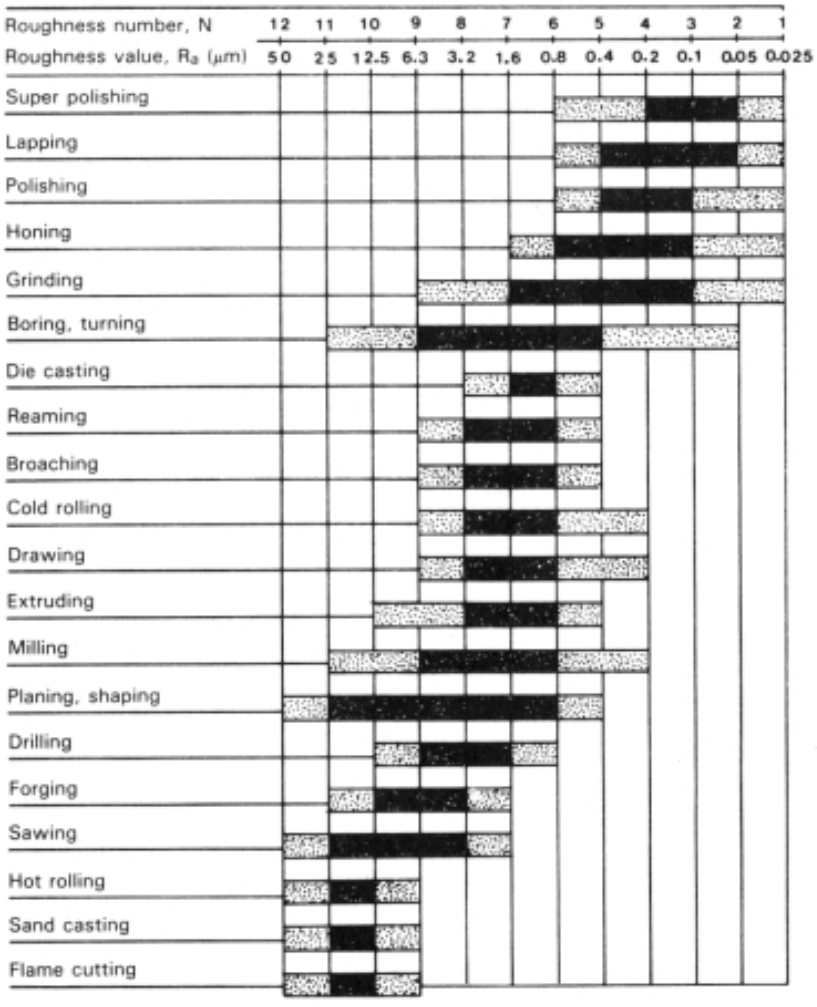

FIGURE 2.11 Final roughness in machining processes [1]

2.2 Introduction to process monitoring

The application of sensors can be twofold, either for measurement or for process monitoring of a property. Note that process monitoring can be based on the quantitative measurement of a property, but does not necessarily need to do so. While measurement has the aim of quantitatively identifying a certain property, process monitoring is often based on defining a threshold or an operating range determining whether some condition is acceptable or not.

For process monitoring it is often sufficient to apply simple, cheap but fast sensors (like accelerometers) for acquiring some kind of signal being in context with the characteristic process behavior. Although desirable, the physical context between the signal and the process does not necessarily need to be known or understood. The signal can even be composed of several mechanisms leading to a complex value difficult to explain physically – and impossible to reduce to the original physical values behind.

However, for successful process monitoring a reliable correlation between a signal characteristics and some process or product property is sufficient, even if achieved in an empirical manner. As a subsequent step process monitoring is an essential base for realizing a closed loop control. Monitoring provides on-line (i.e. with a certain sampling rate) the information on the status of the process or product property that can be followed by a certain control strategy for readjusting some process parameter in order to keep the property within the tolerance window.

2.2.1 Monitoring of machining

Machining is a mechanical process, thus accelerometers and force sensors are the most suitable.

Although the identification of empirical correlations can already be sufficient for successful process monitoring and even control, improved understanding of the physics and dynamics of the combination system-process-product is desirable in order to develop methods in a more controlled, systematic manner. Note that not only the machining process itself but the combined interaction system-process-product is essential for the process behavior and for its monitoring, being a complex task.

The ability to monitor processes has rapidly increased during the past years, mainly depending on the fact that powerful low cost computers are available nowadays and that faster sensors and data acquisition cards have been developed. Also the global competition

has forced the manufacturing companies to automate their machines to become less dependent on personnel. To achieve a higher degree of automation some kind of monitoring devices are needed. The monitoring devices are also necessary to uphold product quality and productivity. The effectiveness of these systems depends on their ability to detect any errors and correct them with the right response.

The trend is towards systems that use multiple sensors simultaneously (sensor fusion).

The sensors can be placed almost anywhere depending of the type. They can roughly be divided in two groups, external and internal sensors. External sensors are retrofitted to the machine while internal sensors generate signals that can be read from the machine controller. The external sensor types used are mainly accelerometers, force transducers and acoustic emission sensors. Occasionally also ultrasonic sensors and microphones are used.

It is obvious that depending on the information to be measured from the process, it is important to choose the most suitable sensor and to employ it correctly. For example if an accelerometer is placed too far away from the cutting zone it will be impossible to monitor the cutting process, but it will probably be possible to evaluate the structural vibrations of the machine during machining, this depending on the sensitivity of the sensor. For the force sensor it is important to place it in a manner that the forces from the machining process interact with it.

Although much research has been carried out only few solutions have reached the industry, (e.g. force sensors based on measuring the electrically induced currents from the electric drive of the spindle). This is dependent on the complexity of most systems but also of the process. This shows the need for either highly automated systems or for systems easy to use. Even if the education level of the operators has increased it is paramount that the system has to be simple enough for them to use in order to ensure reliable production. For industry the avoidance of long down-time is important, in particular it must not be caused by failing monitoring systems, otherwise they will not be used any more, as often is the case. [26]

2.2.2 Measurement technologies

Many different sensors can be used for monitoring the status of the machine and environment and make it understandable for a computer.

The characteristics of a sensor are usually related to the application it is being used for. The amount of data that a sensor outputs is an important factor to consider, both from the point

of data logging, but also since this data must be subsequently processed and analyzed. For the sensors that considered this can range from one reading per second up to 1,5 million readings per second, so the amount of data that one sensor can generate is enormous, and place significant demands on the real time processing capabilities of the data logging equipment.

For this project according to the literature survey and previous works the sensors typology used for monitoring the polishing process are three: acoustic emission, force and power consumption.

2.2.3 Acoustic Emission (AE)

Acoustic Emission (AE) testing is a powerful method for examining the behavior of materials deforming under stress. Acoustic Emission may be defined as a transient elastic wave generated by the rapid release of energy within a material. Materials "talk" when they are in trouble: with Acoustic Emission equipment you can "listen" to the sounds of cracks growing, fibers breaking and many other modes of active damage in the stressed material.

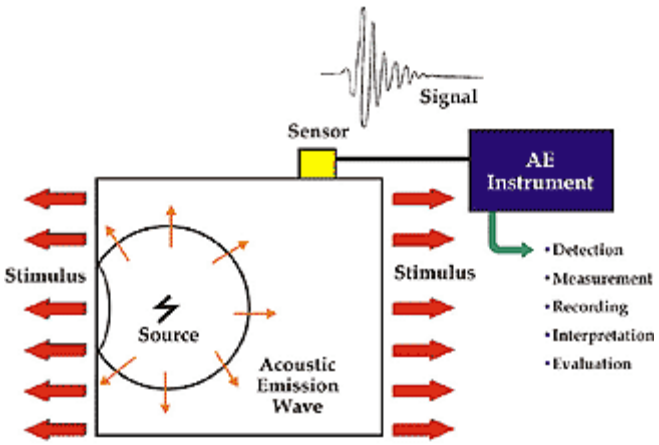

FIGURE 2.12 AE sensor setup (source http://www.pacndt.com)

Small-scale damage is detectable long before failure, so AE can be used as a non-destructive technique to find defects during structural proof tests and plant operation. AE also offers unique capabilities for materials research and development in the laboratory. Finally, AE

equipment is adaptable to many forms of production quality control testing, including weld monitoring and leak detection.

Some typical applications of the Acoustic Emission principle in testing materials are as follows:

Behavior of materials: metals, ceramics, composites, rocks, concrete:

- Crack propagation
- Yielding
- Fatigue
- Corrosion, Stress corrosion
- Creep
- Fiber fracture, delamination

Nondestructive testing during manufacturing processes:

- Material processing
- Phase transformation in metals and alloys (martensitic transformation)
- Detection of defects such as pores, quenching cracks, inclusions, etc.
- Fabrication
- Deforming processes
- Welding and brazing
- TIG, MIG, spot, electron beam, etc.
- Weld monitoring for process control

Monitoring structures:

- Continuous monitoring (metallic structures, mines, etc.)
- Periodic testing (pressure vessels, pipelines, bridges, cables)
- Loose Part Detection
- Leak Detection

Several studies were carried on dealing with AE and finishing techniques during the past years. The results were that there is correlation between the progress of the process and the Acoustic emission acquired [3], [4], [5], [7], [8], [12], [2].

2.2.4 Force

Force is one of the most important signals. This is because of the direct effect the cutting force have on the machining accuracy and so if the forces can be controlled within certain predetermined limits it can, amongst other things, result in better surface of the workpiece.

This type of sensor can be of two major types: piezoelectric and resistance. Piezoelectric sensors are fast but cannot measure low frequency force fluctuations i.e. static force, they are also more expensive.

A force transducer generally measures the applied force from the proportional deformation of a spring element: the larger the force, the more this element deforms. However, the frequency range of this type of transducer is limited by this element having to be sufficiently elastic to undergo large-amplitude deflections reflecting the load.

To overcome this limitation, force transducer relies on the piezoelectric principle exhibited by quartz. Under load, quartz crystals produce an electric charge proportional to the mechanical load applied: the higher the load, the higher the charge. Thus, in piezoelectric force transducers, quartz serves as both the spring element and the measurement transducer.

Thanks to the high rigidity of the crystal, the measuring deflections are very small, usually just a few microns. Where slow, quasi-static processes are being measured, this virtual absence of displacement keeps measurement error to an absolute minimum. Yet quartz also offers unrivalled accuracy in the case of much faster processes.

The quartz crystal converts each physical quantity to be measured (force, pressure or acceleration) into an output signal that is precisely linear and hysteresis-free. A quartz force transducer consequently has an extremely wide measuring range while remaining compact, robust and highly sensitive. [28]

2.2.4.1 Three-Component Force Transducer

This force transducer with two shear-sensitive quartz washers (Fx and Fy) and one pressure-sensitive quartz washer (Fz) is particularly compact.

Typical Force Transducer Applications:

- Quality assurance in manufacturing and assembly
- Monitoring of presses
- Measurement of cutting forces involved in machining
- Biomechanics

- Product testing
- Materials testing
- Dynamic weighing of moving vehicles
- Wheel force measurement

2.2.5 Power consumption

Power consumption is an important area which has various applications. However, in most cases, the amount of electricity consumed by an appliance is not readily apparent.

The total power is obtained by multiplying the instantaneous voltage of the load from voltage sensor by instantaneous current of load from hall sensor and summing the results of multiple phases. The total power is calibrated to the full scale of power meter for display to the operator.

2.2.5.1 Hall Effect

When a current carrying conductor is placed into a magnetic field, a voltage will be generated perpendicular to both the current and the magnetic field. The principal is known as the Hall Effect.

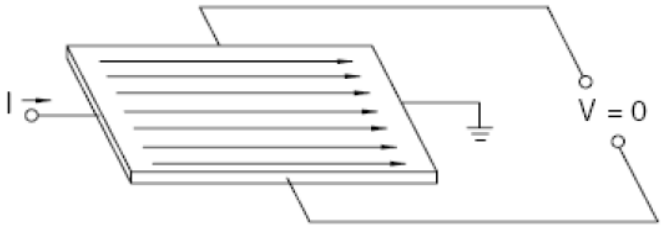

FIGURE 2.13 Hall Effect principle when no magnetic field is present [29]

Figure 2.6 shows a thin sheet of semi conducting material (Hall element) through which a current is passed. The output connection are perpendicular to the direction of current when

no magnetic field is present current distribution is uniform and no potential difference is seen across the output.

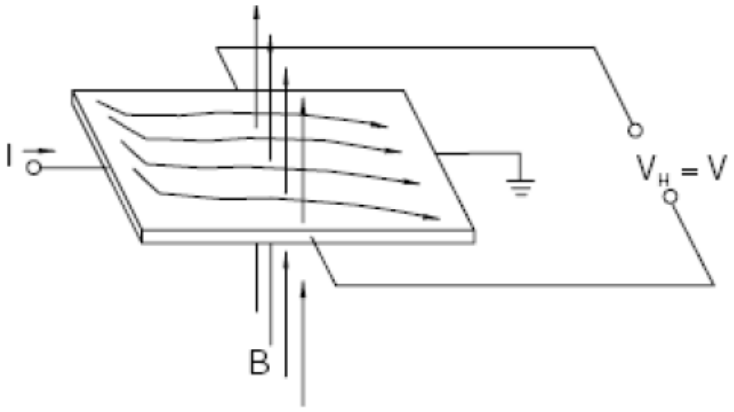

FIGURE 2.14 Hall Effect principle when magnetic field is present [29]

When a perpendicular magnetic field is present, as shown a Lorentz force is exerted on the current. The force disturbs the current distribution, resulting in a potential difference (voltage) across the output. This voltage is called Hall voltage (VH). The interaction of the magnetic field and current is shown in the equation below

$$\mathbf{V_H \rightarrow I \times B}$$

2.2.5.2 Hall Effect current sensors

An open-loop Hall Effect current (Figure 2.8) measurement system is the easiest to understand. The Hall generator is mounted in the air gap of a magnetic core placed around the current carrying conductor or bus. This Hall Generator “chip”. The conductor produces a magnetic field proportional to the current it is carrying. The magnetic core concentrates the magnetic field which is then sensed by the Hall Generator “chip” together with its electronic driving. Because the output of the Hall Generator “chip” is quite low, it is amplified to a useful level. In open loop designs, this amplified signal is the measurement output.

The performance of an open loop technology sensor is dependent upon the linearity of the Hall Generator “chip” and the linearity of the magnetic core. At higher currents, the linearity of the magnetic core declines quite rapidly dramatically degrading performance.

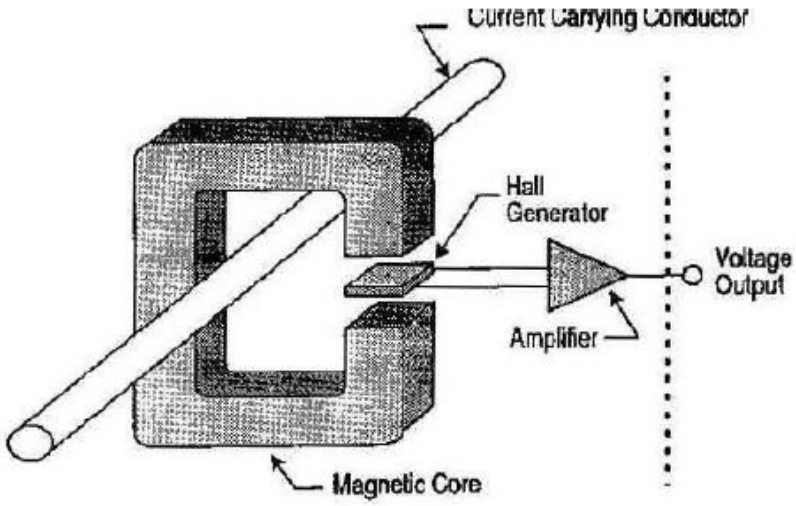

FIGURE 2.15 Open loop Hall Effect current sensor [29]

A Closed loop Hall Effect (Figure 2.9) current measurement system starts with the same five basic building blocks: The magnetic core, Hall Generator “chip”, its constant current source and its amplification. However, in a closed loop design, this amplified Hall Generator “chip” signal is used quite differently.

In a closed loop design, this signal is passed through coils wound around the core at a precise number of turns to offset or “null” the concentrated magnetic field in the core from the current carrying conductor or bus.

The measurement output is simply the current it takes to null the flux in the core accounting for the turns ratio of the coil around the core to accomplish this. The Closed loop technique allows great improvements in sensor performance. By driving the core to nearly zero magnetic flux, the effects of magnetic core linearity as well as the effects of Hall Generator “chip” linearity are practically eliminated. This also eliminates the performance effects of temperature on the performance of the Hall Generator “chip”. The result is superior linearity, low temperatures drifts and fast measurement response.

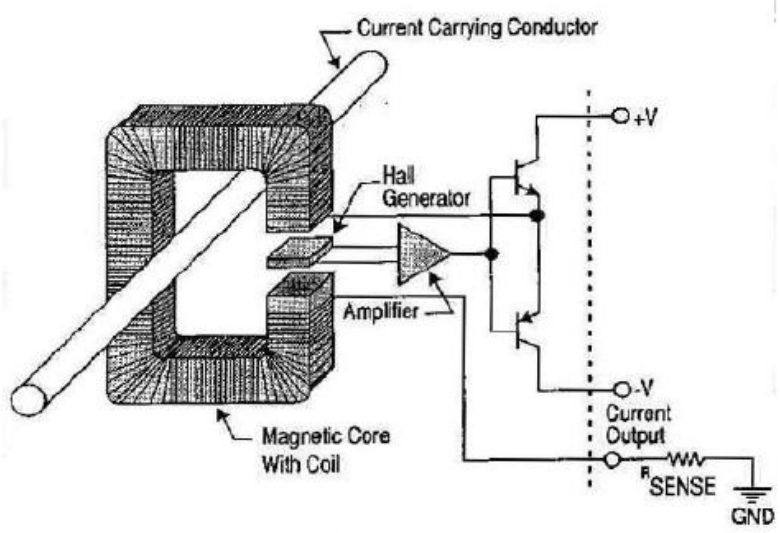

FIGURE 2.16 Close loop hall effect current Sensor [29]

Instantaneous voltage is obtained from the voltage sensor (potential transformer) and instantaneous current is obtained from hall current sensor. Instantaneous current and instantaneous voltage is multiplied to calculate power. [29], [30]

2.3 Roughness measurements

Roughness is an important parameter and issue in many mechanical applications. It is directly related to the surface conditions of the products, and this means that it is a good factor that clarifies on the presence of scratches or scrapes on the part.

There are many parameter used to define the roughness, the one used in this project is the Arithmetical Mean Roughness commonly abbreviated Ra. The Ra represents the average roughness amplitude of the analysed surface. This parameter is highly robust under statistical point of view. The measurements of Ra values are performed with a white light interferometer and then compared with the Aq values measured with a scattered light instrument.

In this way a validation of the Optosurf is carried on comparing the values measured with the WLI with the ones measured with Optosurf. The technology behind these two

instruments are now presented, it is to be noticed that Optosurf is the only instrumwent using scattered light technique in commerce.

A stylus profilometer FTS and an Infinite Focus Alicona instruments were also used for some quick roughness measurements, these will be briefly introduced in chapter 4.

2.3.1 Optosurf OS 500

FIGURA 2.17 Optosurf OS 500 [25]

The surface measuring instrument Osposurf OS 500 uses angular resolution of scattered light and can capture surface roughness as well as the reflection angle of machined surfaces by evaluating the distribution curve.

The parameter Aq is a statistical characteristic value (variance of the scattered light distribution) and reacts with high sensitivity to changes in surface roughness.

The intensity value (surface under the distribution curve) means the intensity of the reflection from the surface and thus shows if the surface is dark or light.

Calibration prevents the value Aq from being influenced by the intensity. The intensity value can be used to measure different reflections or control the position of the sensor.

The diameter of the measuring spot is normally 0.9 mm (optionally 0.3 mm) the extra parameter M (centre of gravity of the distribution) can be used to measure form errors in round and flat parts. Evaluating with the help of the sensor geometry enables the derivation of the angle of reflection from M. By integrating the angle of reflection, the absolute form error is obtained in µm. For this type of measurement, perfect movement (rotation for round parts) of the object under test and knowledge of the measurement length (diameter for round parts) are both necessary.

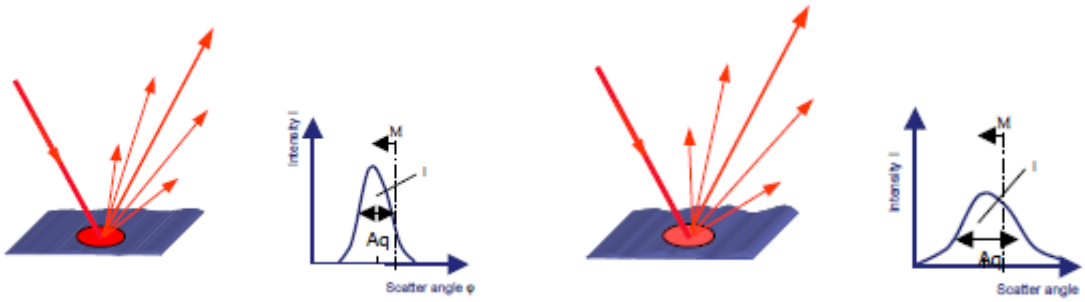

a *b*

FIGURE 2.18 Smooth surface with low value of Aq(a), rougher surface with increased value of Aq (b) [25]

2.3.1.1 Sensor Principle

A light beam source projects a spot, which size depends on the type of sensor in use, on to the surface. The light reflected back from the surface, scattered by the surface imperfections, is collected by the sensor optics and directed onto a linear detector array, which converts the incident distribution of light intensity into electrical current. After digitalisation, a microprocessor processes the data thus gained.

For a standard sensor, the capture angle is 32º. Depending on how the sensor is oriented, either the characteristic across the machining direction or the characteristic parallel to it is captured. In other words, either the cross-wise or the long-wise roughness is measured.

The sensor optics are corrected for angle, which means that it is relatively insensitive to working distance. The working distance set to 5 mm can vary, for notionally flat surfaces, by

±1 mm with no change to the distribution curve and thus the roughness characteristic measured. [24]

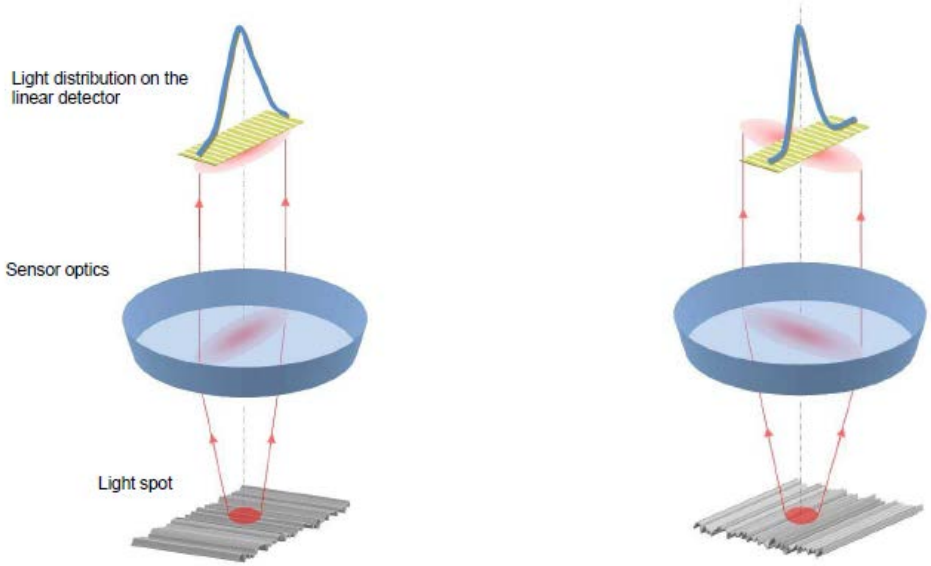

FIGURE 2.19 Cross-wise roughness measurement: diode array oriented across the machining direction (a); Long-wise roughness measurement: diode array oriented parallel to the machining direction (b) [24]

2.3.1.2 Correlation of Aq to Ra or Rz

The scattered light technique cannot directly make Ra and Rz measurements, since the optical value Aq is measured, which is not absolutely related to the standard coefficients Ra or Rz. It is, however, always possible to carry out these measurements by means of a prior onetime comparison measurement with a profilometer. The best method of doing this is to take a number of parts from serial production, whose origin is traceable, e.g. the first part after dressing of a grinding wheel, and then every 10th or 20th part during the following cycle before re-dressing of the wheel. This guarantees a known increment in roughness values, since the Rz value is always higher after dressing than at the end of the cycle, just before re-dressing.

At least five measurements should be carried out with each instrument on various places on each part, to achieve measurement certainty. The characteristic values (Ra or Rz) should be

captured in a table, and the coefficients a and b calculated for converting Aq to Rz, Ra or Rdq.

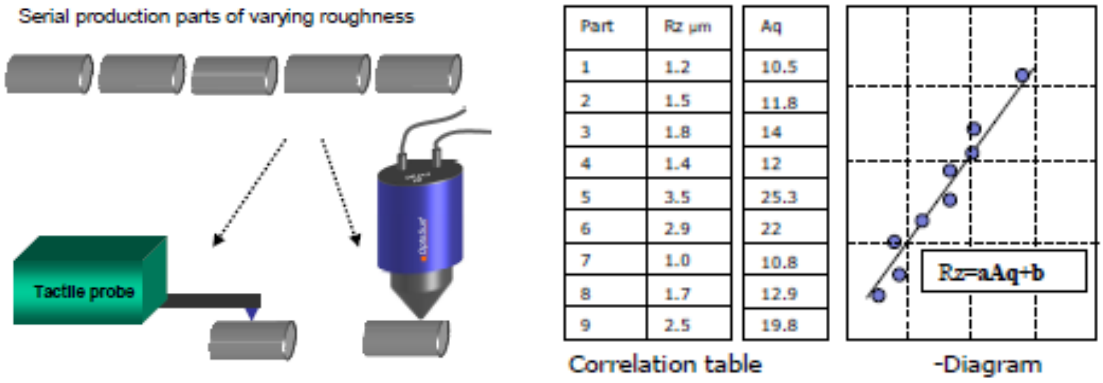

a *b*

FIGURE 2.20 Serial production parts of varying roughness (a), Correlation table and diagram (b) [25]

2.3.1.3 Adjusting the Sensor

For correct measurement, the sensor must always be positioned to be normal to the surface of the object to be measured. This is done with the help of two measurement parameters:

- I
- M

Adjust the sensor to maximize I and bring M as close to zero as possible. This can best be achieved using the cable entry points as a guide to orientation of the sensor.

If they are at right angles to the observer, then tilting the sensor to left or right will change the value of M. When M is negative, the scattered light distribution will move left, if M is positive, it will move to the right. Try to bring M to zero, i.e. bring the peak of the distribution into the middle of the display. A value of up to ±2º can be accepted, provided

the edges of the distribution curve are not cut off. If the cable entry points are in line with the observer, then tilting the sensor to left or right will change the intensity value I. When the sensor is perfectly normal to the surface of the object to be measured, the intensity will be maximal. Tilting the sensor to left or right will reduce this value. It is important to try to get the sensor normal, achieving the highest value of I. [25]

2.3.2 White Light Interferometer

As reference instrument for the roughness measurements a White Light Interferometer was used, thanks to Kaledio-Technology Company based in Farum that allowed the use of their instrument. This choice was made because the final roughness, around 2 nm, could be measured with this instrument that has an accuracy lower then 1 nm.

2.3.2.1 White light interferometry

Scanning white light interferometry is a versatile technology that provides a noncontact, 3-D method of measuring surface roughness. The interference microscopy technology combines an interferometer and microscope into one instrument.

Illumination from a white light beam passes through a filter and then a microscope objective lens to the sample surface. The objective lens is coupled with a beam splitter so some of the light is reflected from a reference mirror. The light reflecting back from the surface recombines with the reference beam. The recombined beams create bright and dark bands called “fringes,” which make up the interferogram. Fringes represent the object’s topography.

The pattern of these fringes is captured on a CCD camera array for software analysis. By obtaining several frames of intensity information for each point, the system can recreate the sample surface. The frames are passed through an algorithm to convert those intensity signals into height information.

Microscope-based white light optical profilers are capable of measuring a variety of surface types, including ground and polished surfaces, steps and films. They do this by mapping surface heights that range from sub nanometers to microns across areas that range from microns to millimeters in a single measurement. This rapidly provides surface roughness, shape and waviness data.

When the required measurement areas are larger than the field of view, a stitching procedure can be employed that involves a number of partially overlapping measurements being combined into one surface profile. Stitching, however, requires that regions overlap,

with the overlapping data aligning adjacent measurements. Because overlap regions are measured more than once, overall measurement time increases.

While other metrology solutions provide either high resolution or high speed, white light interferometry offers both. It combines noncontact measurement, repeatable 3-D surface measurement, high speeds and subnanometer resolution. WLI is employed for surfaces with average roughness down to 0.1nm Ra and peak-to-valley heights up to several millimeters, and repeatability can be 0.1nm or better. [33]

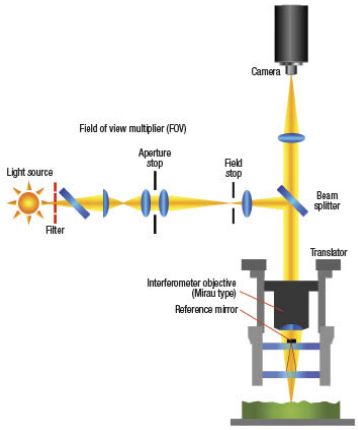

FIGURA 2.21 White light interferometer working principle [45]

2.3.2.2 Pros and cons

WLI offers many advantages over other methods, such as stylus profilometry and atomic force microscopy (AFM). Two principle advantages are WLI's high-speed and noncontact capabilities. The user can rapidly acquire a 3-D rendered surface to make measurements immediately.

On the other hand, AFM is a very high-resolution technique, but it takes a lot of time to perform and stylus profilometry is a contact technique, which may not be desired. When you drag a stylus across the surface and it touches the part, it has the potential to damage or even destroy the surface you are interested in characterizing.

Another benefit of WLI is that it is an area-based technique, wherein the sensor images the interference signal from an area of the part and communicates that signal to the camera. Other topography techniques only sense the surface at a single point or along a single line.

When compared to techniques such as video microscopy, WLI is advantageous because it does not depend on part color to obtain high-quality data. Even if the surface being

measured reflects a small amount of light, that reflected light interferes with the light that reflects off of the reference surface. This interference signal is what defines the surface measurement data. Because WLI uses the interference signal to measure the height of the surface—and not simply a raw camera image like a video system—it is possible to measure structures that visibly have little color contrast, but are easy to see by their topography.

Lastly, SWLI is an easy-to-learn technique and does not require sample preparation. The principle disadvantage of WLI, or any optical technique, is that it depends on the optical properties of the medium through which it is looking, whether it's glass, air or, for semiconductor manufacturing, thin films.

Each of those dielectric thin films has it own optical properties and this can produce anomalous results, such as inaccurate film thickness or step measurements, due to the different optical properties of the films. Most instrument manufacturers have proprietary methods of overcoming these anomalies, but the ambiguity remains.

Also, WLI is typically focused on the part's vertical resolution, or topography, and less on lateral resolution, such as the part's geometric dimensions. WLI tools do focus on high lateral resolution, but if the user is primarily interested in lateral information, other less-expensive measurement methods are available.

2.3.3 Stylus profilometer

Stylus profilometer are instruments which come in contact with the measuring surface. A diamond tip is usually employed to come in touch with surface. The stylus makes a certain load on the tip which has to stay in contact with the surface. The tip runs across the surface for a determined length called evaluation length and records the vertical displacements of the surface profile. The vertical displacement of the tip is usually translated by the transducer which send signal to the software that elaborate it in roughness parameters. The problems related with this kind of measurement instruments are mainly two: the first one is that the type of employed transducer affects the measurements, and the second one is that in the contact zone between the tip and the surface a plastic deformation occurs and thus the beginning surface condition are modified

2.3.4 Optical instruments

These kinds of instruments do not come in contact with the measuring surface. In fact, they do not use a tip to find out the vertical displacement of the surface but "take a picture" of the analyzing region. The principle with these instruments work is simple. A beam of radiation is reflected by the interested surface. Depending on the surface roughness the reflected light can specular, diffuse, specular and diffuse. Depending on the amount of specular or diffuse radiation the roughness surface is estimated. The main problem with

these measurement instruments is that the roughness of too smooth surface is difficult to measure, because in this case the radiation is reflected back with a very small angle of deviation.

Chapter 3

Planning of Experimental Work

3.1 Goal and approach

This section of experimental tests describes investigations performed on the polishing process, the sensor system and Optosurf. A number of different process parameters, tools, and influence of other factors were evaluated in order to find suitable solutions for optimizing the polishing process and assuring the maximum reliability and uniformity during the final tests.

The experimental parameters were selected based on earlier experimental studies discussed in literature survey (see Chapter 2), recommendation of manufacturers' equipment used during tests and experience gained.

3.2 Organization of experimental work

The experimental work was done in two subsequent tests as follows:

- *Experimental equipment and preliminary tests* (see Chapter 4)
- *Experimental validation of monitoring solutions for RAP process* (see Chapter 5)

The first experimental tests, hereinafter referred by the notation Preliminary test (Chapter 4), were performed to find out all the parameters influencing the polishing process, define the procedures for the final tests, set the sensors and the accessory equipment and choose the best combination of products on the market to perform the final tests.

The final tests were carried on to acquire all the data needed to evaluate the possible correlation between the critical hidden process variables (acoustic emission, force and power consumption) and the vital quality characteristic (surface roughness).

During these final tests also the validation of on-line roughness measurement with scattered light technique is investigated, for possible future implementation on the robot assisted polishing machine.

Description of tests setup, conditions, data analysis and conclusions are presented forth in particular chapters

CHAPTER 4

Experimental Equipment and Preliminary Tests

Diamond polishing process has to deal with several variables that could definitely affect the process itself and the final surface to be reached.

In the preliminary test campaign the most critical factors that were tuned for the final test setting were: the alignment between arm and workpiece to be properly parallel, the holding down pressure to have a constant contact force on the workpiece induced by the polishing arm, the type of pad and arm to get a full contact area and uniform polished surface, the feed rate, the oscillation, the stroke, the polishing path, the polishing time, the abrasive and at last the stone pre-polishing process.

This was long preparatory phase during which were tested a lot of different set-ups led to important conclusions necessary to have a reliable and repeatable process able to fully represent the real conditions available in the process. The different factors here are subsequently studied in deep.

4.1 Experimental setup

4.1.1Machine tool

The oscillation module is mounted on a CNC milling machine Cincinnati Milacron sabre 750 with 3 CNC controlled axes and both the preliminary tests and the final campaign were performed on that machine. The main characteristics of the machine are summarized in Table 4.1.

Characteristic	Unit	Magnitude
X/Y/Z axis travel	[mm]	762/381/508
Feed speed range	[m x min^{-1}]	3-15
Rapid traverse speed	[m x min^{-1}]	15
Tool stations		12
Motor power	[kW]	11
Machine type		Vertical
Control		Acramatic

TABLE 4.1 Cincinnati Milacron Sabre 750 CNC characteristics

FIGURE 4.1 Cincinnati with the polishing module and Optosurf mounted on

4.1.1.1 Oscillation module

The oscillation module is what permits the application of the normal force and the vibratory motion. The module developed by Strecon and briefly described in paragraph 1.2 is essentially made of an electric motor, an air piston and a conical connector.

The electric module allows the proper vibrating motion with some mechanisms. The setting of the stroke at different amplitudes is made modifying the relative position of the motor in the module using screws. The vibrating frequency can be fully controlled with software. The normal force is applied by a piston fed with pressed air. This piston permits the module to get in contact with the surface to be polished rotating it around an axis .The conical connector allows mounting different kind of arms on the oscillation module for different purposes. All the parameters and tools playing an important role will be discussed in deep later in this chapter.

The polishing module is a complete unit integrating both the force control and the oscillation system. The design ensures a fast and flexible, but also robust mounting and demounting on the robot arm.

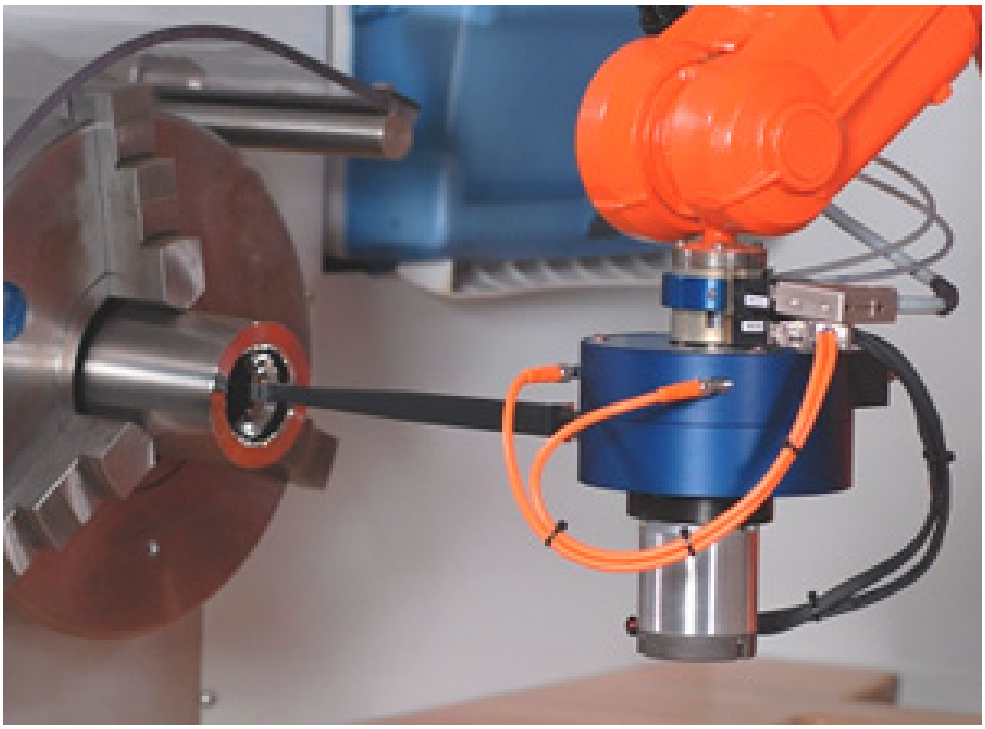

FIGURE 4.2 The polishing module on the RAP machine [46]

4.1.2 Sensors

4.1.2.1 R15α by MISTRAS

The R15α is a narrow band resonant sensor with a high sensitivity. The sensor cavity is machined from a solid stainless steel rod, making the sensor extremely rugged and reliable. The ceramic face along with a 30 degree chamfer to cavity electrically isolates the sensor cavity from the structure under test assuring a low noise operation. The compact size of the sensor makes it readily suitable for deploying in tight spaces for monitoring.

FIGURE 4.3 R15α by MISTRAS [37]

This general purpose sensor provides a good combination of high sensitivity and low-frequency rejection. These properties make the sensor very useful for monitoring common structures such as pipelines, vessels, bridges, and storage tanks in petroleum, refineries, chemical plants, offshore platforms, as well as factory and process monitoring applications. [36],[37]

Operating Specifications

Dynamic
Peak Sensitivity, Ref V/(m/s)..... 80 dB
Peak Sensitivity, Ref V/µbar..... -63 dB
Operating Frequency Range..... 50-400 kHz
Resonant Frequency, Ref V/(m/s).....75 kHz
Resonant Frequency, Ref V/µbar.....150 kHz

Directionality..... +/-1.5 dB

Environmental

Temperature Range..... -65 to 175ºC

Shock Limit.....500 g

Completely enclosed crystal for RFI/EMI immunity

Physical

Dimensions.....19 mm OD X 22.4 mm H

Weight.....34 grams

Case Material.....Stainless steel

Face Material..... Ceramic

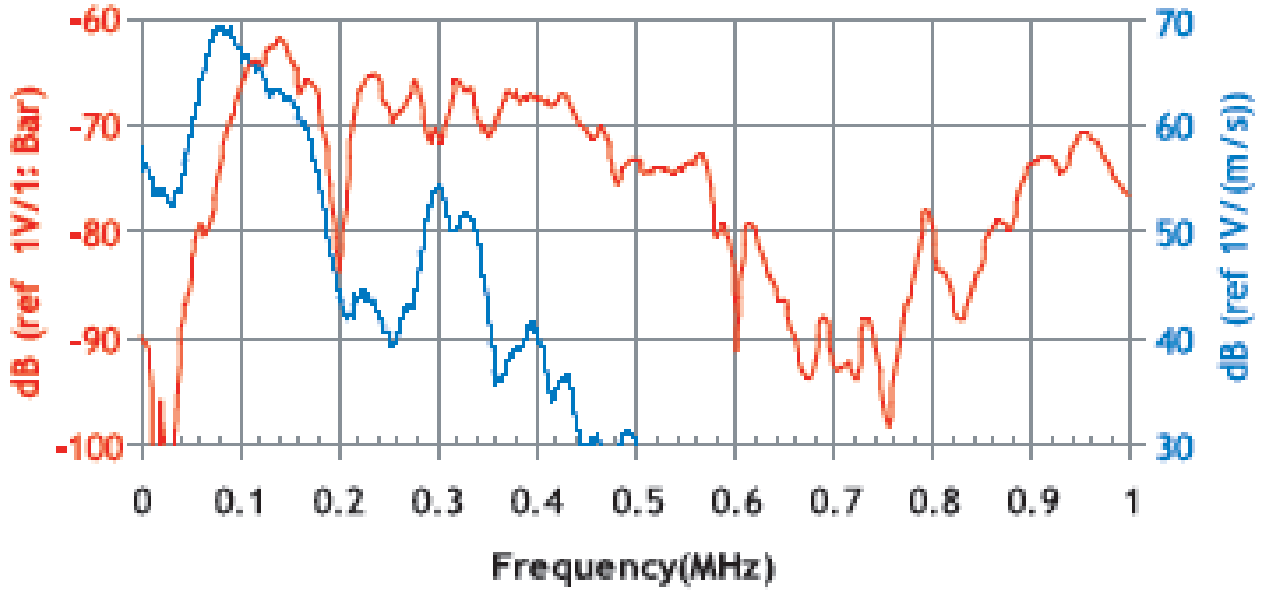

FIGURE 4.4 R15α sensitivity [37}

4.1.2.2 BV100 by MONTRONIX

The Montronix BV100 Broadband Vibration Sensor measures both low frequency mechanical vibration of a machine structure or part fixture and high frequency acoustic emission (AE) in machine structures to detect tool and process failures. The BV100 measures vibration from continuous cutting operations or from impact events common with pressing, stamping or forming. Plastic deformation, fracture or friction events commonly found in metalworking processes generate AE signals. For example, as a tool begins to fail, microscopic cracks form on the tool body. These propagate quickly and generate distinctive acoustical energy signals, which the BV100 is able to measure.

The BV100 design features small size, single-bolt installation and rugged construction, making it ideal for industrial monitoring applications.

FIGURE 4.5 BV100 by MONTRONIX [40]

This sensor has been designed for application on machining centers that use a wide variety of tooling. It is able to detect vibrations characteristic of individual cutting tooth disturbances that develop as inserts fail on larger diameter (multi-tooth milling cutters ~ 50 Hz to 600 Hz). It can also detect the AE bursts that are common when very small diameter drills and taps break (50 kHz to 500 KHz).

ITEM	General Data
Frequency Range	0.1 Hz – 500 kHz
Sensitivity, ± 10 %	60 dB (Ref. 1V/ms^{-1}) / 100 mV/g
Power Supply Voltage	15 VDC
Power Supply Current (Constant Current Diode)	2 – 6 mA (The Montronix systems provides 4 mA constant current.)
Output Impedance, max.	< 100 Ω
Bias Output Voltage, nominal	2.0 VDC / 8 - 10 VDC
Ground Isolation	> 1MΩ
Case Material	Stainless Steel
Weight	300 grams incl. cable (approx.)
Cable	Integral, 100% shielded, PUR-jacket, stainless steel overbraid
Cable Length	5 m (16.4 ft)
Mounting	M6 x 1 x 16 or (¼ x 28 x 5/8) Screw
Protection	IP67
Shock Limit	7,000 g
Temperature Range	-45 to 80ºC (-49 to 176ºF)
BV100 Certifications (When connected to a Montronix system)	ETL, CSA, CE

TABLE 4.2 BV100 specifications [40]

The most suitable machining center mounting location for this sensor is on the part fixture. It can also be mounted on the head of the spindle, but almost no AE information can be detected in this location. [27], [40]

4.1.2.3 Minidyn 9256 by KISTLER

Minidyn 9256 is a multicomponent dynamometer for measuring the three orthogonal components of a force; its very low threshold allows measuring extremely small forces.

- For cutting force measurements in ultra-precise machining
- Small design
- High sensitivity and natural frequency
- Small temperature error
- Top plate made of titanium

The dynamometer consists of four 3-component force sensors mounted under high preload between the cover plate and the two lateral base plates. A low temperature error is obtained by this special mounting of the sensors. Each force sensor contains three crystal

rings, of which one is sensitive to pressure in the y-direction and the two others to shear in the x- and z-directions.

The forces are measured practically without displacement.

The outputs of the four mounted force sensors are fed to the 7-pole flanged socket. There are also multicomponent force moment measurements possible. The four sensors are fitted so that they are ground-isolated. This largely eliminates ground loop problems. The dynamometer is corrosion-resistant and protected against penetration by splashing water or cutting fluid.

FIGURE 4.6 Minidyn 9256 by KISTLER [38]

Examples of Application

- Cutting force measurement in precision machining such as:
- Cutting wafers
- Grinding hard-disk read heads
- Diamond turning
- High speed machining

- Micromachining
- Ultra-high precision machining of brittle hard materials
- Multicomponent force measurement of small forces
- Force measurement in confined spaces

Measuring range	F_x, F_y, F_z	N	–250 … 250
Type 9256C1	M_x, M_z	N·m	–8 … 8
Type 9256C2	M_x, M_z	N·m	–11 … 11
Calibrated measuring range			
100 %	F_x, F_y, F_z	N	0 … 250
10 %	F_x, F_y, F_z	N	0 … 25
Overload	F_x, F_y, F_z	N	–300/300
Threshold		N	<0,002
Sensitivity	F_x, F_z	pC/N	≈–26
	F_y	pC/N	≈–13
Linearity, all ranges		%FSO	≤±0,4
Hysteresis, all ranges		%FSO	≤0,5
Crosstalk		%	≤±2
Rigidity	c_x, c_z	N/µm	>250
	c_y	N/µm	>300
Natural frequency (mounted on rigid base)			
Type 9256C1	f_n (x)	kHz	≈5,1
	f_n (y)	kHz	≈5,5
	f_n (z)	kHz	≈5,6
Type 9256C2	f_n (x)	kHz	≈4,0
	f_n (y)	kHz	≈4,8
	f_n (z)	kHz	≈4,6
Operating temperature range		°C	0 … 70
Insulation resistance		Ω	$>10^{13}$
Ground isolation		Ω	$>10^{8}$
Degree of protection EN60529 (with connecting cable Type 1696A5/1697A5)			IP67
Weight			
Dynamometer	Type 9256C1/C2	kg	0,75/0,87
Top plate	Type 9256C1/C2	kg	0,24/0,36
Clamping area			
Type 9256C1		mm	39x80
Type 9256C2		mm	55x80

TABLE 4.3 Minidyn 9256 specifications [38]

The dynamometer can be mounted with screws or clamps to any face-ground, clean mounting surface such as on a machine tool table. The measuring instrument can also be mounted on a magnetic plate. It must be noted that uneven contact surfaces may cause internal distortions, placing additional heavy stresses on the individual measuring elements and increasing the cross talk. There are M3 tapped blind holes in the mounting plate for clamping the force-introducing components such as workpieces or toolholder. The contact surfaces of the force-introducing parts must be surface ground to achieve good mechanical coupling to the mounting plate. [38]

4.1.2.4 PS200-DGM by MONTRONIX

The Montronix power sensor PS-200-DGM measures the input of effective electrical power of the polishing module with the highest possible resolution. The power signal provided is perfectly suited for process monitoring.

The PS200-DGM can be used with direct current motors as well as with one- or three-phase AC motors. Via current and voltage, the PS200-DGM determines the input of effective power and creates a corresponding analog output signal. A multitude of amplification and filter settings are available to optimally adapt the output signal to the respective drive and process. [27], [40]

Properties:

- Maximal measurable active power: 156 kW (with 200 A sensors)
- Maximal measurable voltage: 600 V
- Maximal measurable power: 150 Arms
- Adjustable bandwidth: 2 Hz, 7.5 Hz, 15 Hz, 60 Hz
- 2 outputs for total power and DGM signal

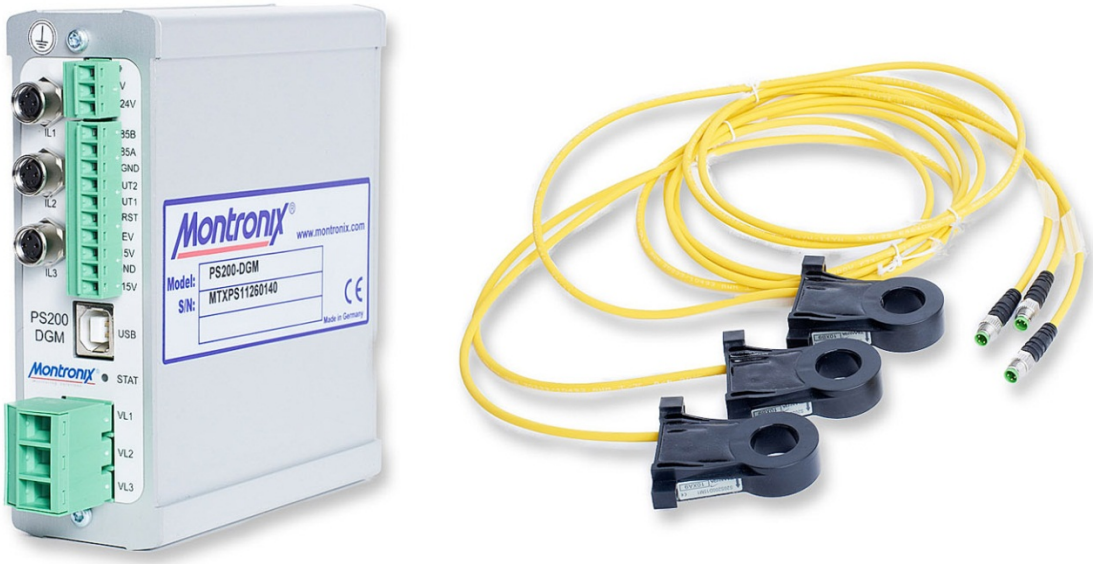

FIGURE 4.7 PS200-DGM by MONTRONIX [40]

4.1.3 Roughness measurement instruments

4.1.3.1 Optosurf Traceability and repeatability

Before all the measurements are carried traceability and repeatability documentation for our purpose has to be provided.

The Optosurf is usually placed in the Metrological Laboratory of DTU in a controlled environment, in this project it is used mounted on a Cincinnati CNC so the first step is to discover if this different location involves any change in the measurements. Afterwards the repeatability of the instrument has to be checked.

Also the influence of day light is to take into account performing the measurements both with the sun up and down.

As a reference for traceability and repeatability a Si wafer plate was used; Si wafer has an ultra-shiny, smooth and uniform surface, this last is the main reason of its use. One cannot ensure exact position of measurements while moving the sample from Metrolab to Cincinnati. Therefore Si wafer, as the most unifirm surface was chosen

Dealing with the repeatability at first 625 measurements were taken on 5 different random spots of the Si wafer in the MetroLab with the day light (13/01/2013 at 11:20am). The results are shown in the Table 4.4.

Num. meas.	Aq	Aq max	I	M
1	1,61	1,63	1454	0,00
2	1,61	1,63	1455	0,00
3	1,61	1,64	1455	0,00
4	1,61	1,63	1456	0,00
5	1,61	1,63	1458	0,00

TABLE 4.4 Measurement performed in the MetroLab with day light

It can be seen the repeatability is definitely good, all the spots present an average Aq value of 1,61. Even the maximum Aq =1,63 is the same 4 out of 5 times.

This shows that the repeatability of the instrument in laboratory conditions is good.

Afterwards other 5 measurements on random spots were performed when the sun went down to check the influence of daylight on the instrument (14/01/2013 at 5:05pm). The results are shown in Table 4.5.

Num. meas.	Aq	Aq max	I	M
1	1,61	1,63	1455	0,00
2	1,61	1,64	1455	0,00
3	1,61	1,62	1455	0,00
4	1,61	1,63	1455	0,00
5	1,61	1,63	1455	0,00

TABLE 4.5 Measurement performed in the MetroLab without day light

One can see that the repeatability is, another time, very good, all the spots present an average Aq value of 1,61. The maximum Aq value is varying a bit more from 1,62 to 1,63. These changes are negligible.

The study of the day light influence in laboratory conditions gave excellent results; one can say then that Optosurf is not influenced by the presence of the sun.

The Optosurf was then moved on the Cincinnati, where it will be positioned during the tests performed in this project, to check if the behaviour showed in laboratory condition about day light is confirmed in a workshop environment. The same Si wafer was used.

Suddenly the main problem was the alignment procedure, as stated before the measurement made with Optosurf deals with the I and M value that have to be respectively the maximum one and as close to zero as possible. In the MetroLab a mobile support was available and the adjustment of the values was easily made by two screws that controlled the two angular degrees of freedom. On the Cincinnati this mobile support is not available. The setting of the I value is performed manually rotating the support rod of the Optosurf and looks quite easy; the M value is more critical because the whole workpiece has to be unclamped and then rotated. This operation made manually is not easy and could be very long. As a solution some wedges were used to align it in an easiest way.

Despite of the problems dealing with alignment the performances of the instrument was also in this case checked both with day light and without. Another measurements campaign made without day light and artificial lighting was carried on.

The results of the measurements made on the Cincinnati with day light (15/01/2013 at 11:30am) are shown in Table 4.6.

Num. meas.	Aq	Aq max	I	M
1	1,56	1,59	1416	-0,01
2	1,56	1,59	1413	-0,01
3	1,56	1,59	1414	0,00
4	1,56	1,59	1418	0,00
5	1,56	1,59	1418	-0,01

TABLE 4.6 Measurement performed on the Cincinnati with day light

In Table 4.6 can be seen that in this case the Aq value is a bit lower than the ones measured in the MetroLab. The difference between the two measurements campaigns are of the same order of magnitude as the difference between the average Aq value and the maximum Aq value. This difference is negligible and it's possible to say that the behaviour of the instrument in workshop environment conditions is almost the same that the one in laboratory conditions. This result was expected because Optosurf was designed to be used in in-line measurements during the manufacturing process, but is also an important confirmation for the implementation by the company on their own robot for automated polishing.

Afterwards other 5 measurements on random spots were performed when the sun went down to check the influence of daylight on the instrument (15/01/2013 at 5:00pm). The results are shown in Table 4.7.

Num. meas.	Aq	Aq max	I	M
1	1,59	1,61	1420	0,01
2	1,58	1,61	1421	0,01
3	1,58	1,61	1421	0,01
4	1,58	1,61	1419	0,01
5	1,58	1,61	1418	0,01

TABLE 4.7 Measurement performed on the Cincinnati without day light

Table 4.7 shows that the measurement performed without day light are closer to the one made in the MetroLab. This is because the workshop has bigger windows than the laboratory and so more light could enter and affect the measurements. Even in this case, however, the difference is negligible and the Optosurf shows again a perfect behaviour dealing with repeatability.

The last series of measurements for the repeatability and the traceability was made with the artificial lighting switched off, to check if it could affect the performances of the instrument (15/01/2013 at 5:05pm). The results are shown in Table 4.8.

Num. meas.	Aq	Aq max	I	M
1	1,57	1,60	1414	-0,01
2	1,57	1,60	1414	-0,03
3	1,57	1,60	1417	-0,03
4	1,57	1,60	1414	-0,01
5	1,57	1,60	1415	-0,02

TABLE 4.8 Measurement performed on the Cincinnati without day light and artificial lighting off

4.1.3.2 Zygo NewView 200

Thw white light interferometer (WLI) owned by Kaleido_technology is a Zygo NewView 200 biult in 1994.

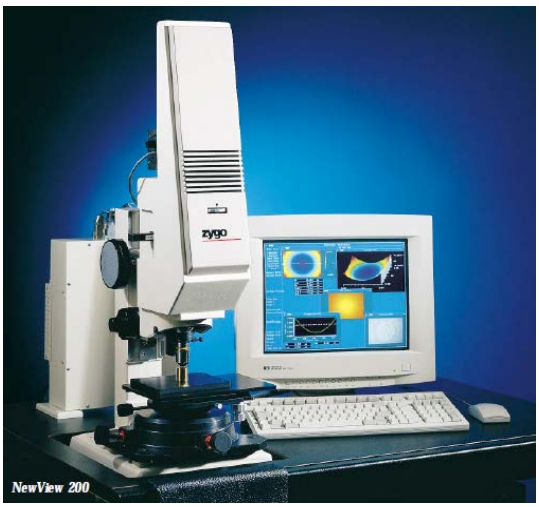

IGURA 4.9 Zygo Matrix GP200 [45]

The Zygo NewView is a general purpose, three dimensional, imaging surface structure analyzer. It provides both imaged surface details of test parts and accurate measurements to characterize these details.

The NewView uses scanning white light interferometry to image and measure the micro structure and topography of surfaces in three dimensions.
There are two major parts to the NewView system: the Microscope and the Computer. The Microscope combines optical microscopy and interferometry to provide the raw data needed for imaging and for surface structure analysis. The computer controls the measurement process, performs calculations, and displays measurement results on a color monitor. [45]

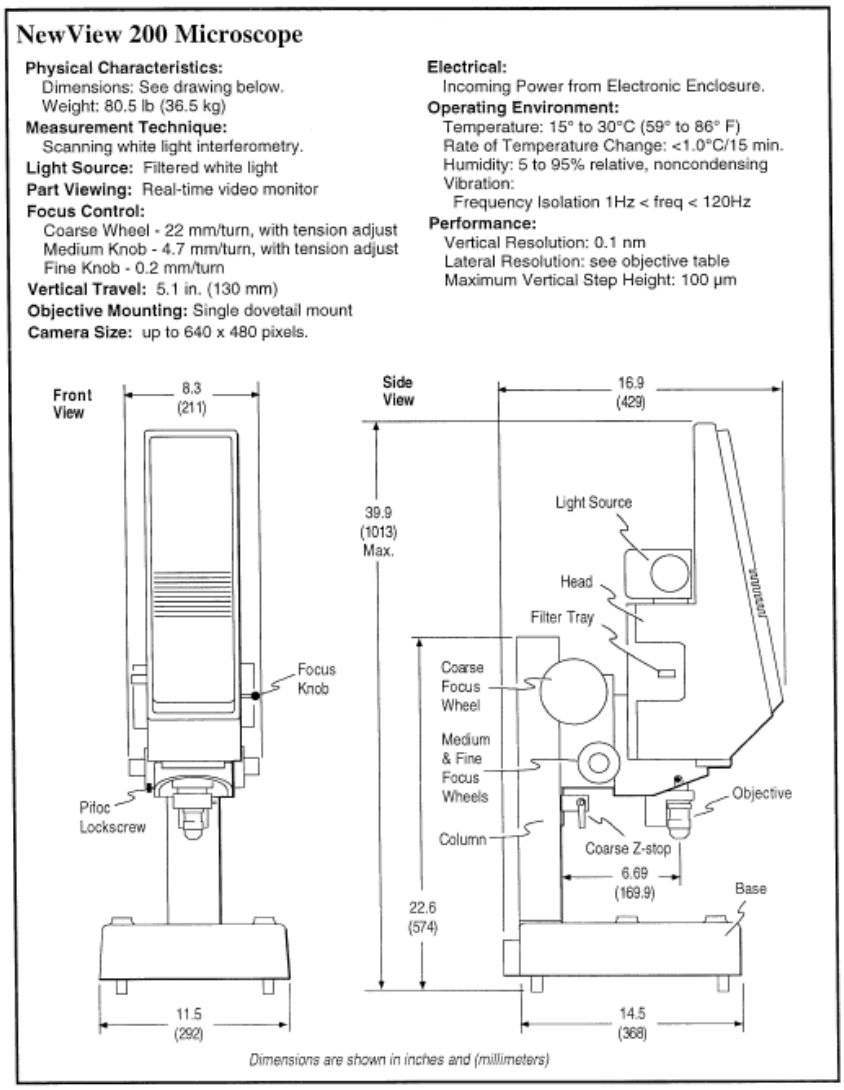

FIGURA 4.10 Zygo Matrix GP200 specifications [45]

4.1.3.3 FTS and Alicona

FTS is a profilometer which uses a tip of diamond to measure the profile and the roughness surface of an analysing part. The action of this measurements machine is simple. In fact, on top of the FTS there is a small automatic arm with a diamond tip in the end (called stylus) which goes in contact with the analysing surface and with a horizontal movement it is able to extrapolate the shape of the surface, and therefore to memorize the profile of the surface and its roughness parameters. The device is simple but not fast and can measure single profiles or scan an area. The operating principle of this instrument is simple, it analyses the roughness of the part for a predefined length. From this length, it takes five reference lengths and from these it computes Ra and the other roughness and waviness parameters.

Alicona Infinite Focus is a non-contact, high resolution optical 3D measuring device. The measurement system is based on Focus-Variation. Its operating principle combines the small depth of focus of an optical system with vertical scanning to provide topographical information from the variation of focus. The ayatem provides the functionalities of an optical profiler and a micro coordinate measurements. Results are able to be reproduced with avertical resolution of up to 10 nm.

4.1.4 Material

For this project a typical mould metal was chosen; known for his good polishability and hardness. Uddeholm Stavax is produced by the Swedish steel company Uddeholm, a factory born in the 1668 and one of the leading suppliers of tooling material.

4.1.4.1 General informations

Uddeholm Stavax is a premium grade stainless tool steel with the following properties:

- Good corrosion resistance
- Excellent polishability
- Good wear resistance
- Good machinability
- Good stability in hardening

The combination of these properties gives steel with outstanding production performance.

The practical benefits of good corrosion resistance in a plastics mould can be summarized as follows:

• *Lower mould maintenance costs*

The surfaces of cavity impressions retain their original finish over extended running periods. Moulds stored or operated in humid conditions require no special protection.

• *Lower production costs*

Since water cooling channels are unaffected by corrosion (unlike conventional mould steel), heat transfer characteristics, and therefore cooling efficiency, are constant throughout the mould life, ensuring consistent cycle times.

These benefits, coupled with the high wear resistance of Uddeholm Stavax , offer the mould low-maintenance, long-life moulds for the greatest overall moulding economy.

Typical analysis %	C 0.38	Si 0.9	Mn 0.5	Cr 13.6	V 0.3
Standard specification	AISI 420 modified				
Delivery condition	Soft annealed to approx. 190 HB.				
Colour code	Black/Orange				

TABLE 4.9 Stavax composition

4.1.4.2 Applications

Uddeholm Stavax is recommended for all types of moulding tools and its special properties make it particularly suitable for moulds with the following demands:

• Corrosion/staining resistance, i.e. for moulding of corrosive materials, e.g. PVC, acetates, and for moulds subjected to humid working/storage conditions.

• Wear resistance, i.e. for moulding abrasive/filled materials, including injection-moulded termosetting grades. Uddeholm Stavax ESR is recommended for moulds with long production runs, e.g. disposable cutlery and containers.

• High surface finish, i.e. for the production of optical parts, such as camera and sunglasses lenses, and for medical containers, e.g. syringes, analysis phials.

4.1.4.3 Mechanical properties

Temperature °C	Temperature °F	Soaking time* minutes	Hardness before tempering
1020	1870	30	56±2 HRC
1050	1920	30	57±2 HRC

TABLE 4.10 Hardening

Temperature	20°C (68°F)	200°C (390°F)	400°C (750°F)
Density, kg/m^3 lbs/in^3	7 800 0.282	7 750 0.280	7 700 0.277
Modulus of elasticity N/mm^2 tsi psi	200 000 12 900 29.0 x 10^6	190 000 12 300 27.6 x 10^6	180 000 11 600 26.1 x 10^6
Coefficient of thermal expansion /°C from 20°C /°F from 68°F	– –	11.0 x 10^{-6} 6.1 x 10^{-6}	11.4 x 10^{-6} 6.3 x 10^{-6}
Thermal conductivity* W/m °C Btu in/(ft^{2}h °F)	16 110	20 138	24 166
Specific heat J/kg °C Btu/lb, °F	460 0.110	– –	– –

TABLE 4.11 Mechanical proprieties

Hardness	50 HRC	45 HRC
Tensile strength R_m N/mm^2 kp/mm^2 psi	 1 780 180 258 000	 1 420 145 206 000
Yield point $R_{p0,2}$ N/mm^2 kp/mm^2 psi	 1 360 150 197 000	 1 280 130 186 000

TABLE 4.12 Tensile strength

Uddeholm Stavax has a very good polishability in the hardened and tempered condition. A slightly different technique, in comparison with other mould steel, should be used. The main principle is to use smaller steps at the fine-grinding/polishing stages and not to start polishing on too rough a surface. It is also important to stop the polishing operation immediately the last scratch from the former grain size has been removed. [20]

4.2 Experimental campaign

4.2.1 Down pressure

Prior to the polishing operation the contact force acting on the workpiece needs to be set. The down pressure is one of the most important parameter in the process because the abrasive particles are pushed against the workpiece and during their motion they remove the material. The application of the force is made varying the pressure trough 2 valves, one that applies the real pressure and another one that applies the backpressure to lift the tool from the workpiece when the polishing process is over.

This operation of setting the contact force is critical in order to have a constant and known force on the piece.

Initially the pressed air system (NSK AIR LINE KIT: AL-0201 for the pressure and NORGREN B07-101-A1EG for the back pressure) showed some problems due to a not negligible

decrease (1 out of 10 N) of the applied force after about 100 seconds. This result was not acceptable and the pressed air system was modified in order to get a more stable force.

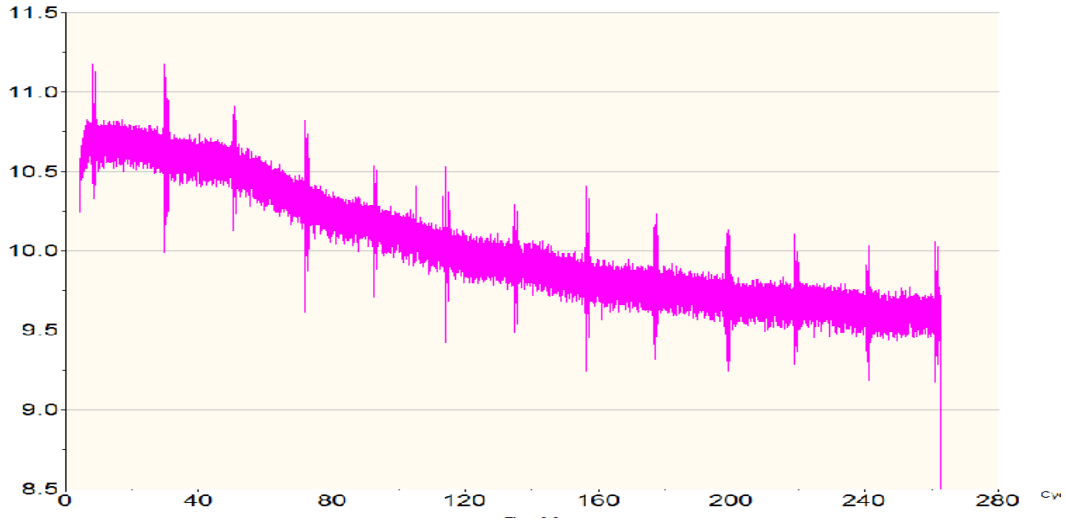

FIGURE 4.11 Pressure behavior with air filter

A filter on the pressed air tube that was feeding the system was then removed, this modification induced a very noticeable change in the force profile; the decrease became an increase and a periodical waviness (period 40 seconds) appeared. Even this times the result in not suitable for the final tests. A constant force is needed during the whole process and with this profile of force all the data acquired would be influenced by this inaccuracy and the results would inevitably be compromised.

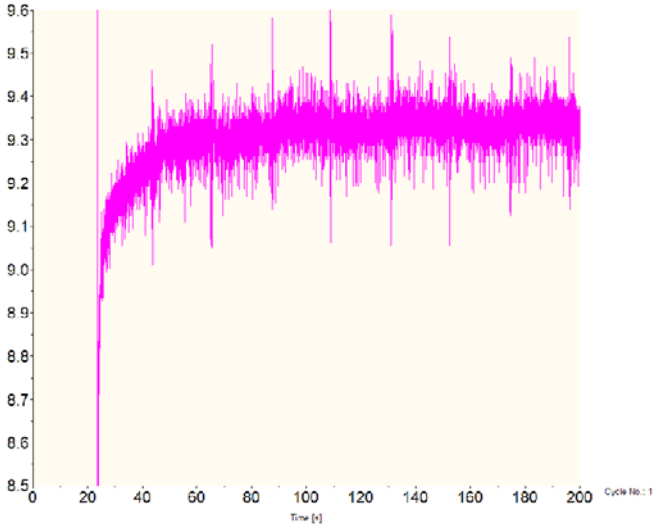

FIGURE 4.12 Pressure behavior without air filter

Studying the system was understood that these problems could derive from pressure waves that are going to be created insides the tubes due to the backpressure.

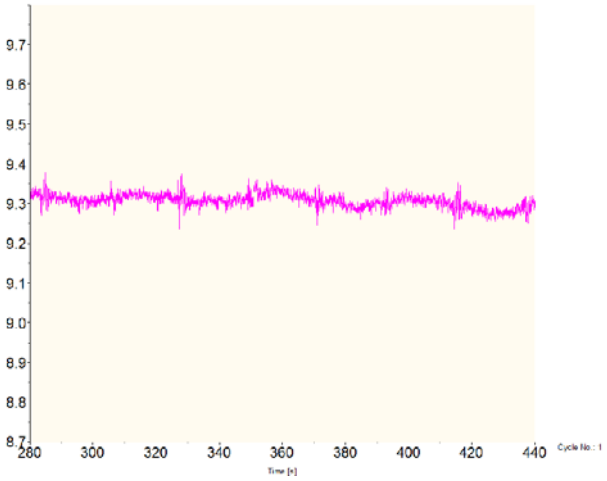

FIGURE 4.13 Waves in the pressure signal

In order to overcome this situation it was decided to apply an overflow valve (NORGREN V72G-2GK-NMN) on the back pressure system in order to keep the back pressure constant and avoid unwanted waves.

This solution showed very good results, the pressure was constant during the tests, short and long ones, and the waviness is no more visible. This set-up was chosen as the official one for this project.

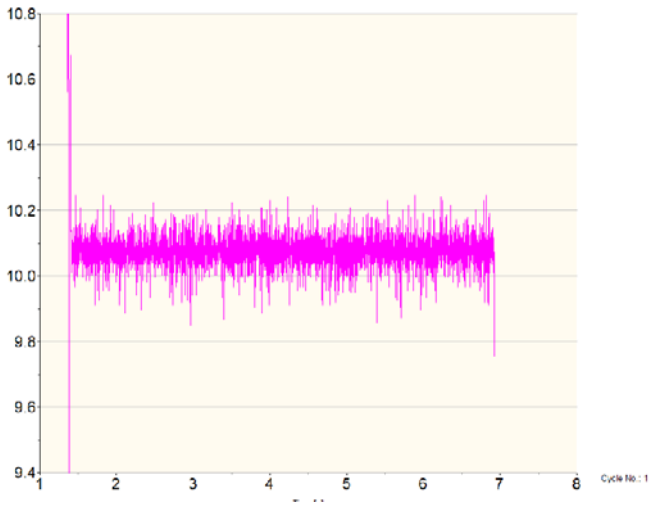

FIGURE 4.14 Pressure behavior with overflow valve

Another issue is to set the force value, or rather how many newtons need to be applied to get reasonable results. Polishing is a final process so the force used is definitely lower if compared to other machining processes; dealing within a range from 10 to 30 N.

It's easy to state that a higher force produces bigger friction forces on the workpiece and then a faster achievement of the desire surface roughness, saving time and money. On the other side the bigger is the force the bigger is the deformation that occurs on the polishing arm and in this way also the alignment is compromised.

Several tests were been carried to identify the best holding down pressure, analyzing the bending of the arm, the time elapsed for the process and the final results on the surface roughness. The variation of the force shows not a negligible difference between the final surface roughness and on the required time, on the other hand also a noticeable difference is evident in the arm's bending. This last factor is determinant for the success of the polishing process and has to be under control. A deformation too big could disable the tilting allowance of the pad and cause defects on the surface.

According to all gathered information and in order to prevent possible defects the force was set to 15 N.

4.2.2 Pad and Arm

Pad and arm are playing a fundamental role in the polishing process; find the best combination to achieve the best reachable surface is a not trivial challenge because of the multiple combinations available in commerce for these two elements. 3 types of arm were tested: a long flexible arm made of carbon fibers with tightly fixed pad by screw, a short and stiff arm made of aluminum with fixed pad and finally a long ball ended arm made of steel, allowing for tilting the pad due to spherical snap-fit interface.

The types of pad were definitely many more, differing in shape and material: PMMA having sharp edges, chamfered PMMA, rubber, PMMA + polishing cloth, rubber + polishing cloths, glass, felt, etc.

The first attempts were performed with the long flexible arm and a PMMA pad having sharp edges. Several tests were carried on but despite of the changes made in diamond paste size, down pressure and number of passes every time the results were very negative, since one could never get a uniform surface that is the first issue for the polishing success.

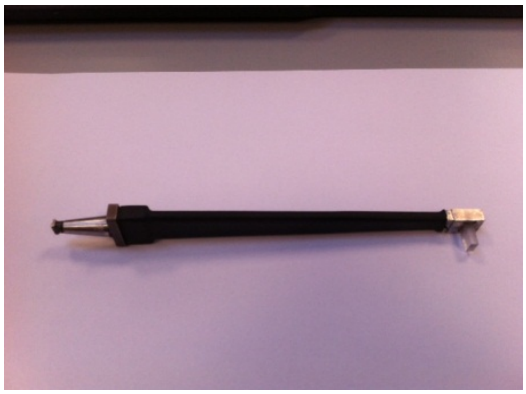

a b

FIGURE 4.15Stiff arm with PMMA pad(a) and the PMMA pad (b)

Assuming that this disparity was due to the edges of the pad or the not perfect flatness of it, it was decided to change pad opting for a chamfered one. In this way there should be no problems with sharp edges. Also this set-up brought rubbish results because another time some areas on the surface were not polished at all.

FIGURE 4.16 Chamfered PMMA pad

A change was made in the arm, using a shorter one;, that was originally built to facilitate heavy Montronix AE sensor mounting. Polishing some spots with this arm and the chamfered pad led, for the umpteenth time, to a not uniform surface. Even this set-up was then discarded.

It was argued that the main problem is because of the tight fixing of the pad by screw. Since there is no degree of freedom, arm deformation result in swinging movement of the pad on the surface, leading to contact are being limited to pad edges.

FIGURE 4.17 Short arm with chamfered PMMA pad

The solution found is a tilting pad, free to move around a support sphere. In this way one should have overcame all the problems related to the not perfect contact between pad and the surface to be machined because the ball snap fitting allows for rotational degree of freedom and thus compensating for the swinging movement creating edging problem.

This arm with tilting pad was definitely chosen as official for this project.

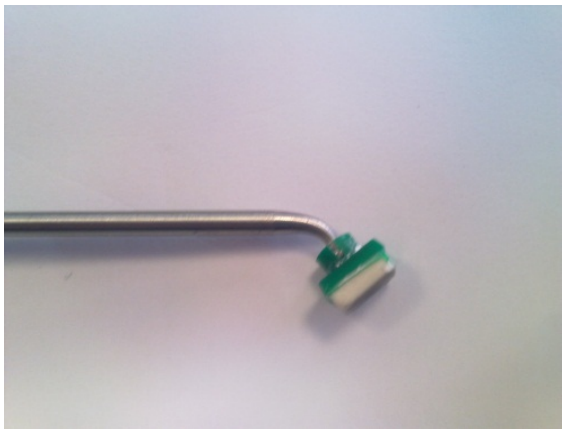

FIGURE 4.18 Arm with tilting pad

After choosing the arm, next step was to find a pad that let reach a uniform and mirror-like surface.

The first attempt has been done with PMMA, suddenly it was noticed that with this setting the surface was not uniform and it was decided to go for a softer pad, which could deform following the surface shape. Rubber looked perfect for the goals but after some tests it was noticed that the surface had some defects probably due to the bending of the edges of the pad caused by the friction forces and the nature of the material

a b

FIGURE 4.20 PMMA (a) and rubber pad (b)

Then it was tried a rubber pad on which a polishing cloth was stuck, usually adopted in the manual polishing process. In this case the results were very good. The surfaces looked uniform, shiny and visibly improved thanks to the double action of the rubber, that can fit the surface form, and the cloth that embeds the diamond paste and decreases friction.

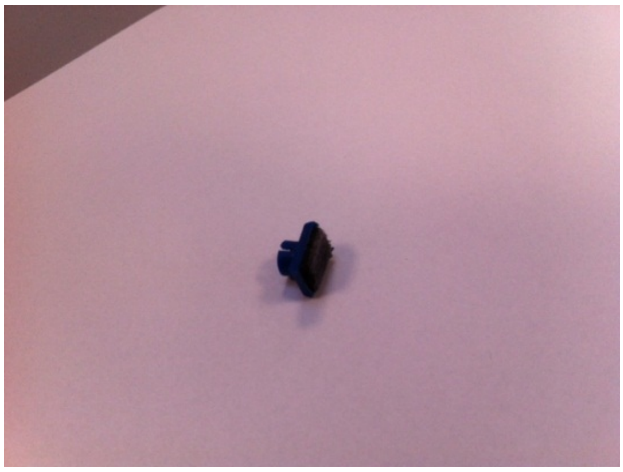

FIGURE 4.19 Rubber with polishing cloth glued on it

Then a pad made with PMMA base and polishing cloth stuck on it was tested, even in this case the results were good but worse; because the PMMA is not adoptable to the workpiece form. This option was discarded. From the general experience it was known that for final steps of polishing using diamond paste, felt is widely used in polishing industry,. However, the felt sheet used by slicking it to the pad was too little stiff and flaked under the pressure.

At the end a glass pad was tested to ensure that no particles were embedded in the pad with relatively good flatness of the pad surface, the full surface area was polished with this pad, however, the surface was definitely not shiny and also this option was discarded.

All the pads for the arm allowing the tilting movement were manually made from Joke's stone pad.

The procedures is at first extracting the stone inserted in the pad and then smooth the borders of the plastic support to get a flat surface, this was manually made using differ type of sand paper.

At this time a piece of rubber already cut by the right dimensions is glued on the support with quick-setting super glue, the polishing cloth is in turn glued on the rubber because the adhesive already present on the back side of the cloth is not so strong and could have brought a detachment. The polishing cloth used is DP-Mol by Struers.[42]

4.2.3 Alignment

A reliable procedure to align the arm, and therefore the pad to the workpiece is needed. The alignment is a fundamental issue because one of the most important parameter in the polishing process, the amplitude of the stroke, has to be kept know and constant. The oscillation movement has to be parallel to the surface. A tilted arm induces a different value of the stroke due the angle that is going to create between arm and surface.

During the preliminary tests it was noticed that the arm is bending under the pressure force applied on it, this bending will induce a little inclination in the arm and a possible misalignment. The first step was shortening the arm from about 150 mm to 100 mm. This shortening provided a lower but still considerable deformation.

Since it was impossible to prevent this bending in any way, the solution was the tilting pad mentioned before, mounted on a spherical support. In this way we have a pad free to move in a 53 degrees angle that compensates the bending of the arm.

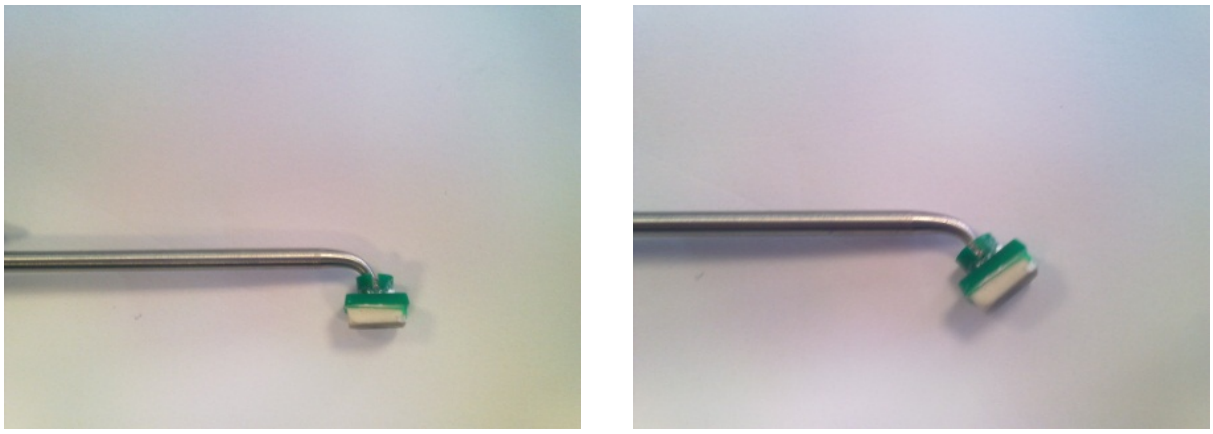

a b

FIGURE 4.21 Arm with the arm tilted (a),(b)

Not only the alignment with the workpiece is to be taken into account but also the alignment on the arm itself, due to the presence of two rods on the connection sphere. These two rods have to be parallel to the surface too. A possible misalignment brings defects on the surface even if they only constrain the rotation of the pad. This alignment of the rods is not so critical as the previous one and for the impossibility to absolutely define a procedure is done with the naked eye.

The proper procedure to align the arm with the workpiece is exposed below:

- The first step is to clamp carefully the work piece on dynamometer not allowing any movement.

- Afterwards a gauge block long enough to cover the whole length of the arm (in order to achieve better results) is positioned on the workpiece surface. Gauge blocks have a really strict tolerance of planarity between its faces so it's perfect as reference for two elements that have to be placed parallel.

- The spindle of the machine is moved down till the whole arm is touching the gauge block surface, a naked eye checking is performed using a white background and also a manual control of the force impressed in performed.

- Now arm and surface are parallel but there is a known offset due to the gauge block that has still to be compensated. This offset compensation has to deal with the dimension of the pad itself because is the pad that finally has to be aligned with the surface. In order to calculate the final offset we have subtract from the height of the gauge block the distance between the arm and the bottom of the sphere (4,825 mm) and the distance between the bottom of the cavity on the pad and the surface of the pad (3,706 mm based on a batch of 5 different pads). The machine position is recorded and the value of the offset is subtracted

- The gauge block is removed and the spindle is moved down to the final position.

4.2.4 Feed rate, oscillation and stroke of the pad

These parameters define the kinematics of the pad. They are really important and, in this project, were kept fixed not to introduce too many variables and keep most things under control.

The stroke, or rather the amplitude of the movement of the pad in the oscillation direction, could be set from 0,5 mm up to 1,5 mm. In this project it was set 1 mm. The oscillation rate, or rather the frequency of movement of the pad, has a very large setting interval; from 0 to 5000 RPM. The oscillation rate play an important role in the polishing process, previous studies showed that the higher it is the faster is the process, with limitation due to the capabilities of the module [32], [9], [11]. In this project it was fixed at 3000 RPM, a common value used by the company. The feed rate, or rather the speed in the orthogonal direction to the polishing movement, is a little less important parameter that affects the polishing required time but mostly when low down pressure is used. In this project the feed rate was set to 1 mm/sec. This setting led to an easy calculation of the polishing required time.

4.2.5 Polishing path

The polishing path is another important parameter. The path controls the polishing area and the uniformity of it. In order to get the surface as uniform as possible, the whole area has to be polished for the same total time and then the path of the pad assumes the role of protagonist.

Two paths were tested, a simple “back and forth” and a more complicated “trochoidal”.

Dealing with the first one, it has to be considered that a lot of the final surface has to be discarded because it has not polished for the total amount of time; the proper polished area results uniform and shiny with some stripes due to the embedding of grains in the pad. These stripes, noticeable with the microscope would disappear with the succeeding polishing step using a finer diamond paste. Dealing with the second one, the trochoidal movement should generate a larger uniform surface because of the combined movement of translation in two directions at the expense of the speed of the process. Also in this case some stripes, this time with a circular shape “Olympic rings type”, were seen by the microscope, demonstrating that even in this case the embedding of grains is not avoidable.

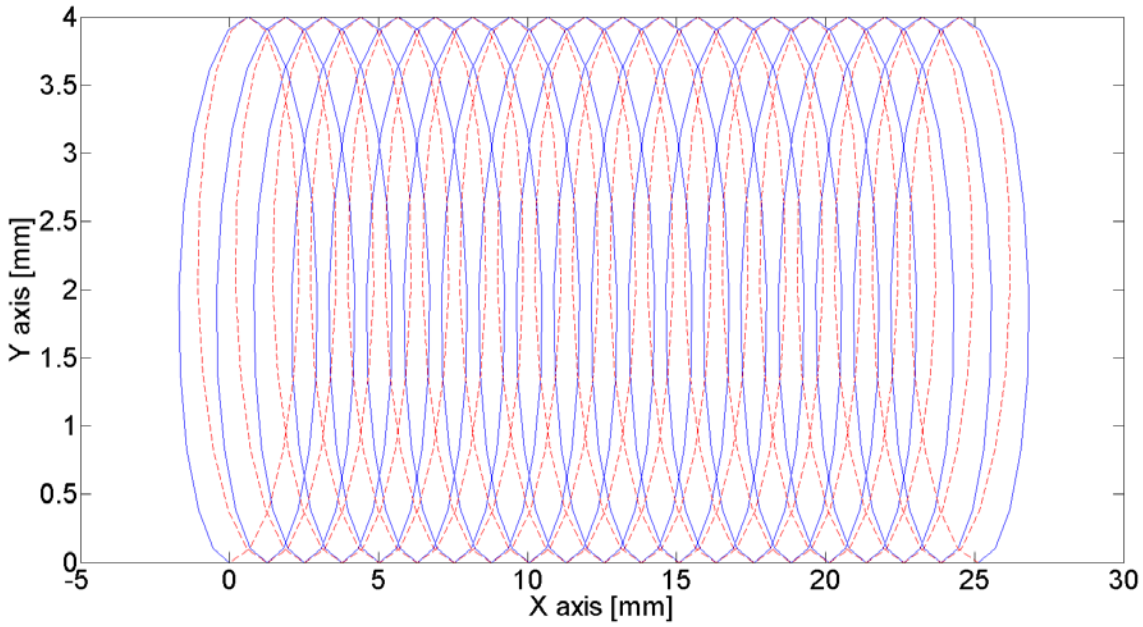

FIGURE 4.22 Trochoidal path

In conclusion a negligible difference in surfaces between the two paths was noticed and in order to simplify the analysis of the data and speed up the test campaign the “back and forth” path was chosen as official for this project.

4.2.6 Abrasives

The abrasive in the polishing process is fundamental, maybe the most important parameter. Using a wrong abrasive could bring a bad surface or could not reach the final roughness in an acceptable time. In this kind of polishing process the abrasive is a diamond paste.

Dealing with the diamond paste there are several variables that should be taken under control for example the mass ratio of abrasive to lubricant, the density of abrasives in the slurry, the main abrasive size. More the concentration of abrasives is high; more abrasive could scratch the surface reflecting on the time of polishing. Furthermore the nominal grain size of the diamond paste is not evincible and has to be taken as an absolute value. The size of the grains plays an important role to define which the final roughness reachable is.

FIGURE 4.23 Diamond gel

The very little control over this parameter has meant that an already mixed 8µm diamond gel by JOKE MAGIC proper for polishing was bought to carry on the tests in this project. In this way the ratio between diamond paste and lubricant is as constant as possible and the only variable for which one can have no certainty is the dimensions of the grains. [41]

4.2.7 Polishing time

The whole cost of the polishing process depends on this factor. The more the timing increases, the more the pad has time for polishing the interested part, but more the cost of the process increases and this is a great problem that has to be minimized. Then the

understanding of the optimal combination of parameters to obtain the shortest time to polish the piece and the understanding when the process has to be stopped because the final roughness value has been reached are two important purposes to improve the polishing process itself.

4.2.8 Couplant for AE sensor

The removal of air from the interface between a measurement surface and an AE sensor is crucial to the transmission of ultrasonic energy. The acoustic impedance of air is around 5 orders of magnitude lower than that of the two contacting surfaces, allowing for very little transmission of acoustic energy at the frequencies typical of acoustic emission (AE). The use of a couplant can greatly improve this transmission. A poor choice of couplant could significantly reduce signal-to-noise ratio in broadband or high-frequency AE measurements and could lead to distortion of the waveform being measured [15]. In this project five types of coulplant were tested to verify which one could bring better signals. The couplants tested were: grease, oil, silicon, silicon grease and ultrasonic gel.

The tests performed with these different types of couplant bring good results for oil and ultrasonic gel. In fact using grease, silicon and silicon grease the sensors couldn't acquire any signal except from the noise.

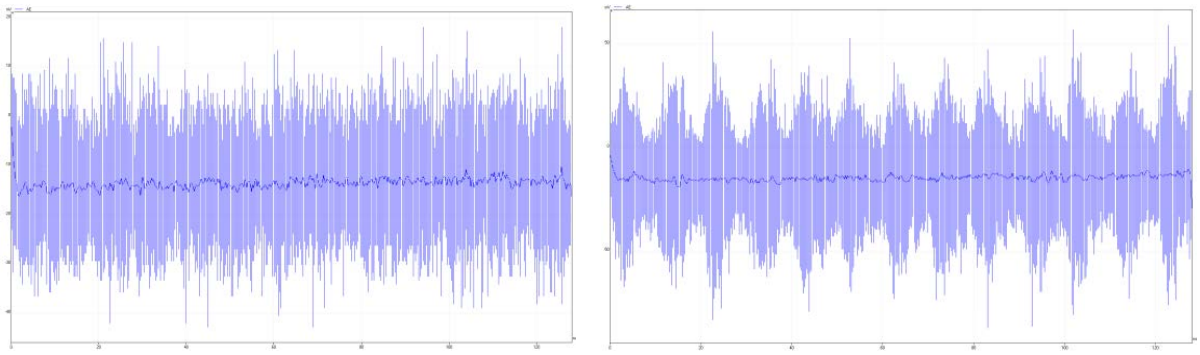

a b

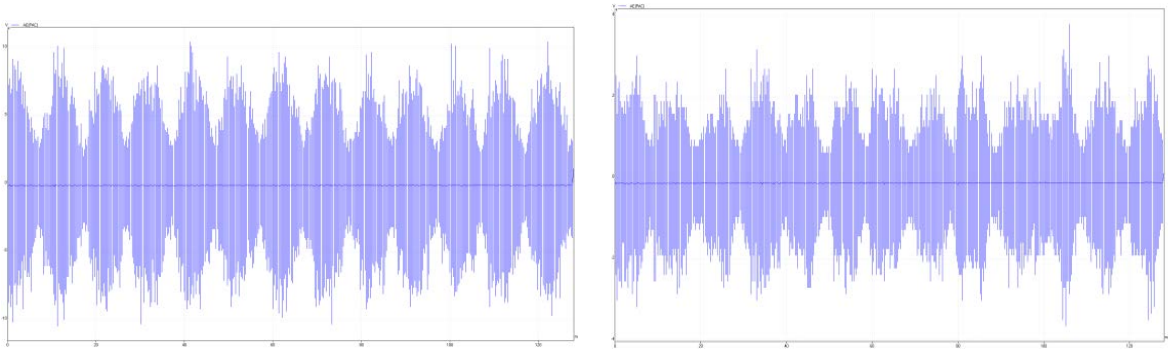

C d

FIGURE 4.24 Acoustic emission signals: background noise (amplitude 0,4V) (a); diamond polishing with Ultrasonic gel couplant (amplitude 0,9V) (b); stone polishing with oil couplant in the beginning of the process (amplitude 13V) (c); stone polishing with oil couplant at the end of the process (amplitude 4V) (d)

This is because the polishing process with diamond paste is a finishing process that involves really low signals, definitely lower then stone polishing where the AE emission is noticeable. Comparing the signal with oil and ultrasonic gel that were the only capable to have a proper acquisition, it was noticed that the ultrasonic gel allows the acquisition of a signal more clear and defined. For these reasons ultrasonic gel was chosen as official couplant for this project.

4.2.9 Hall sensors and resistors

During the preliminary tests of the power consumption of the polishing module a very inconsistent behavior was shown in the graphs of the signals acquired with the Hall sensors. It was neither an increase nor a decrease but a not regular fluctuation. At this point a verification of the Hall sensors had to be done to clarify if that trend was due to the irregularities of oscillation module power consumption or to the sensors themselves.

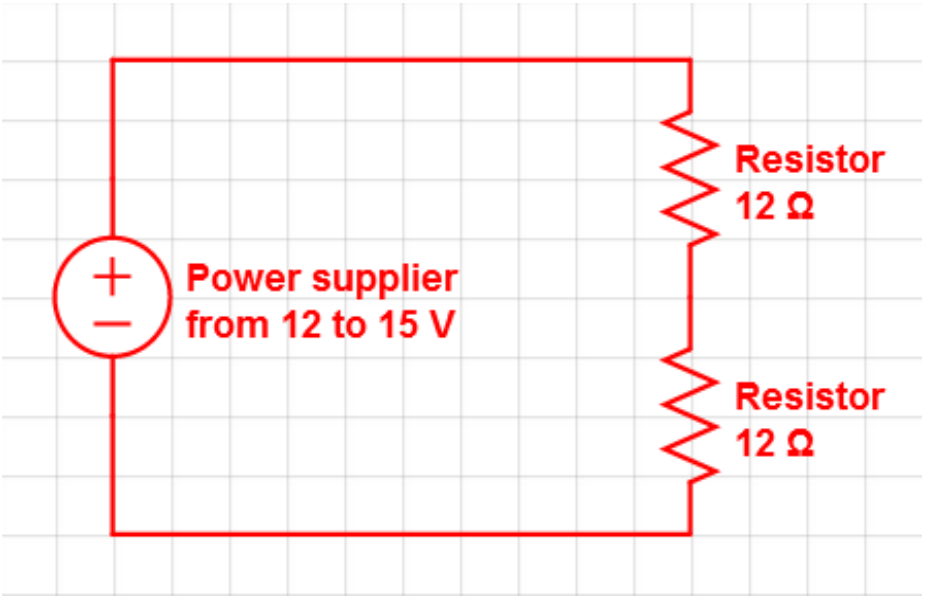

FIGURE 4.25 Circuit with resistors

The verification was made using two resistors (12 Ohm) connected in series ($R_{tot} = R_1 + R_2 = 24$ Ohm) and powered with a voltage from 12 to 15 V in order to cover the power range of the oscillation module (7- 8 Watts). [43]

V(V)	I(A)	W= V x I
12	0,5	6
13	0,542	7,042
14	0,583	8,17
15	0,625	9,375

TABLE 4.13 Voltage, current and power

The acquisition made with the Hall sensors of the resistors power consumption brought really good results showing a steps diagram as expected. This means that the sensors work

properly and the behavior of the signals acquired from the oscillation module are due to bearing or other internal parts that contribute to power consumption. More detailed information will be provided by the final test campaign.

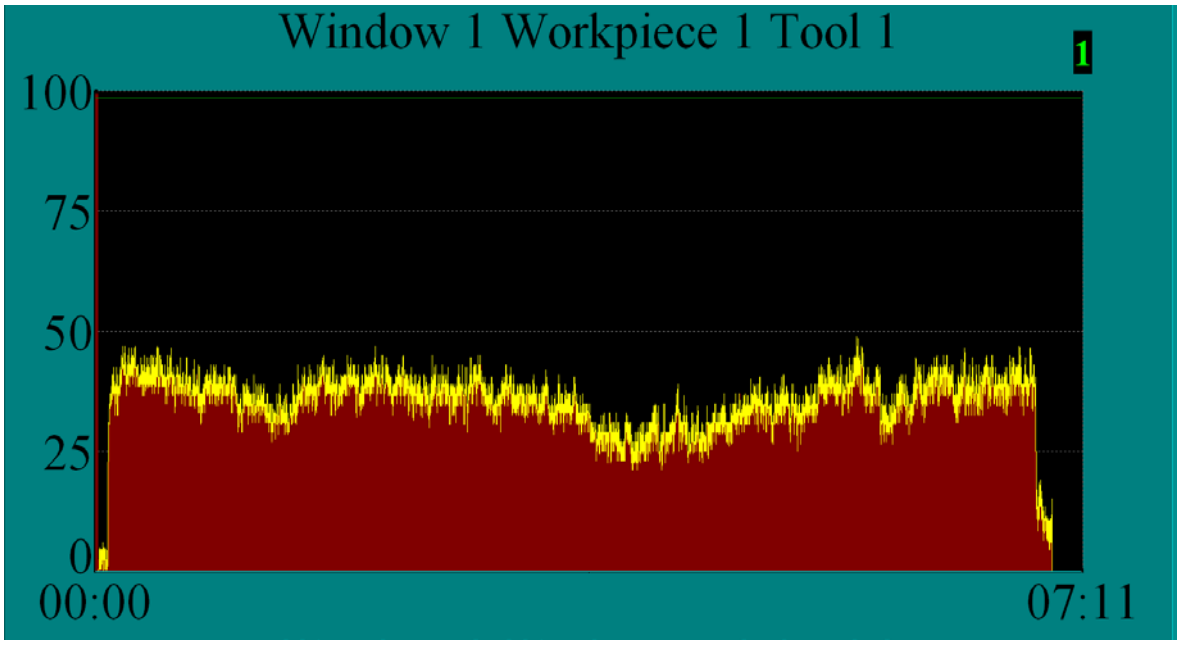

FIGURE 4.26 Measured power consumption in time domain

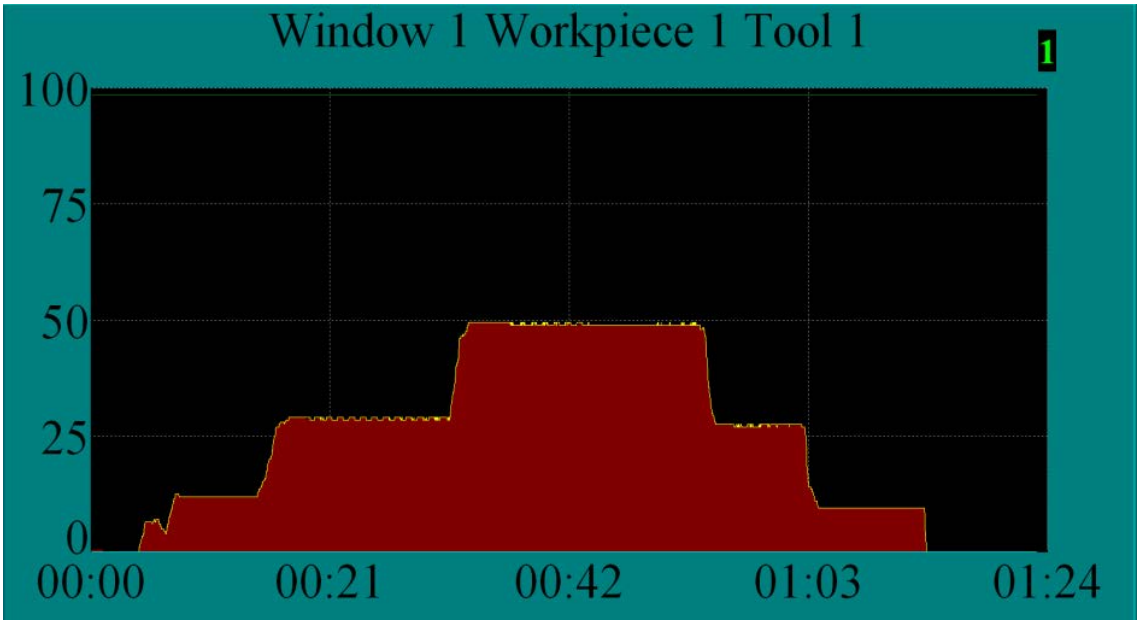

FIGURE 4.27 Resistors power in time domain

4.2.10 Polishing procedure

During the preliminary tests it was noticed that polishing with diamond paste directly on a grounded surface is not suitable. Several tests were performed on Ra 0,2 µm surface for different passes and with different diamond pastes. The results showed that the improvement on the surface roughness is very slow and the grinding marks are never completely removed by the diamond paste that is too fine to delete that kind of scratches.

Long test of 300 passes with a 25 µm diamond paste, the most coarse available, showed a roughness improvement from 0.25 µm down only to 0,08 µm and still the presence of grinding marks. Usage of 8 µm diamond paste for this roughness range is entirely inappropriate, not a noticeable improvement could be seen after numerous passes and the grinding marks are more visible. The measurements in this phase are made with a touching profilometer FTS that will not be used for the validation roughness measurements.

For these reasons it was decided to follow the proper polishing procedure in these tests and pre-polish all the surfaces with a stone, common procedure in industrial processes.[21]

4.2.10.1 Stone pre-polishing

Polishing with stone presents a lot of variables as polishing with diamond paste and finding the proper way to get uniform and well-polished surfaces is, another time, definitely not easy.

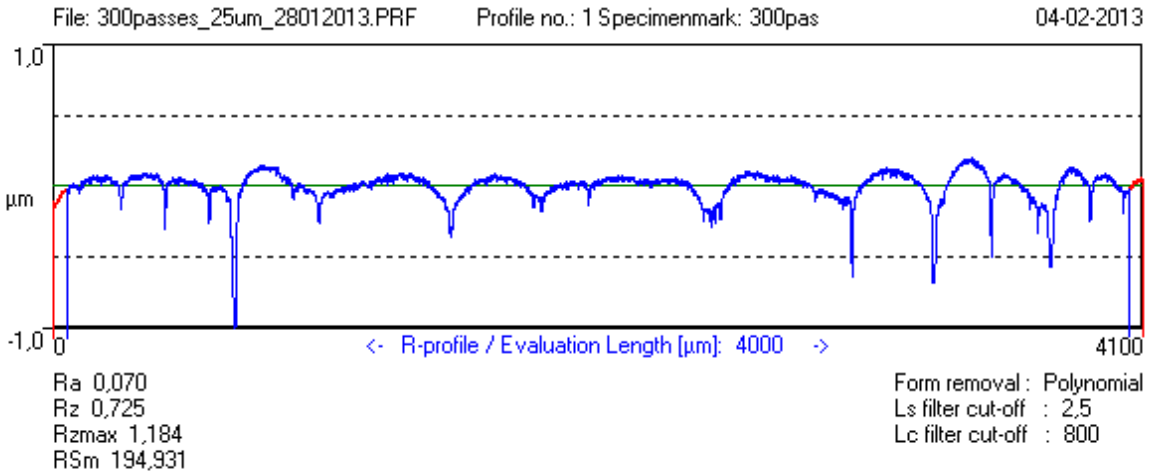

FIGURE 4.28 Surfce profile after 300 passes with 25 µm diamond paste

First problems arise from the stones themselves that are not all equally well produced, some of them present missing corner and holes on the surface that can result on defects on the processed surfaces.

Despite these problems it was noticed that this operation improves a lot the surface and the next step with diamond paste benefits greatly. Measurements showed roughness values, just after 10 passes of stone polishing, about 0.045 µm, almost the same achieved after 300 passes with 25 µm diamond paste, and the almost complete disappearance of grinding marks. The subsequent polishing process, on the prepared surface, with 8 µm diamond paste has then reached a final surface roughness about 0.01µm, typical of the processes of polishing.

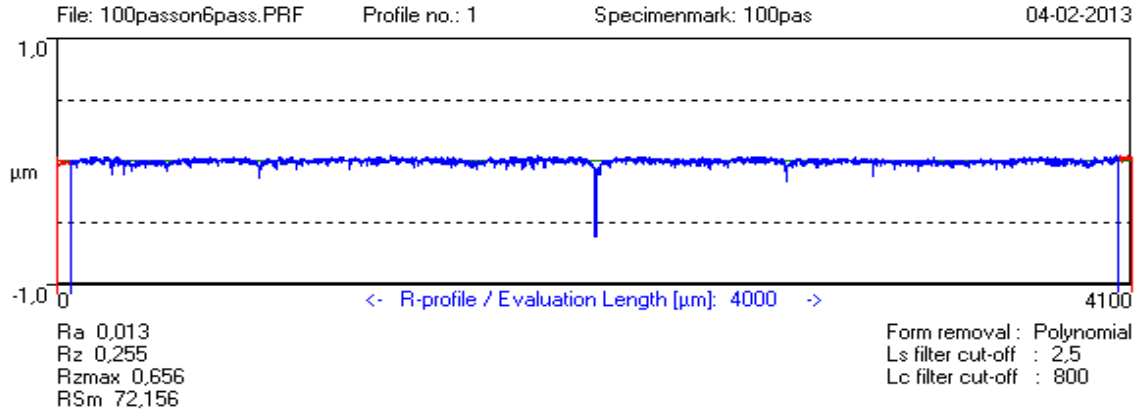

FIGURE 4.29 Surface profile after 100 passes with 8 µm diamond paste on a surface pre-polished with stone

Before reaching these results a lot of preliminary tests on stone polishing have had to carry on. First of all it was necessary to define the use of lubricant, in terms of type and presence.

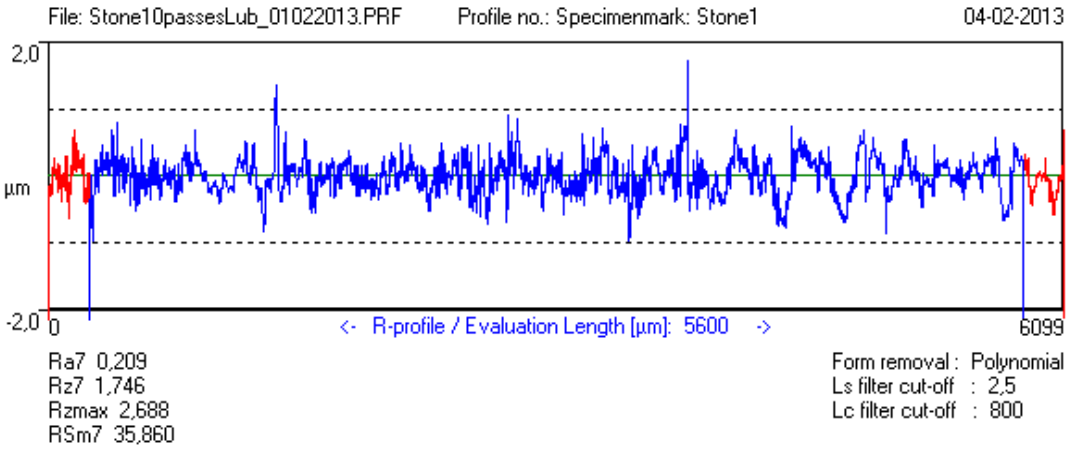

FIGURE 4.30 Surface profile after 10 passes with stone and lubricant

Stone polishing with proper lubricants brought bad surfaces; they were not uniform and slightly improved with a surface roughness around 0,2 µm starting from 0,25 µm. Forces behavior in stone polishing with lubricant is weird, characterized by a trend that would seem to indicate that the pad is hopping.

Water was then used as lubricant for other tests, but also in this case the results were awful. The surface was polished only on sides and in this case the forces behavior showed a trend that would seem to indicate that the pad is tilting during its movement, leaving the center of the surface not polished.

At last no lubricant was used and the surface was polished dry. This solution brought the results mentioned before with an adequately uniform surface and a good behavior in forces that shows that this mode of polishing is the best.

Another issue is the repeatability of the process, or how to deal with the stone; how to shape it, how often one has to change it and how to clean it.

The shaping was initially made using sandpaper and “polishing” on it, but this way did not give good results. It is then decided to shape the stone directly on the workpiece for a congruous amount of passes until it was noticeable that the surface was uniform and complete. This second way brought really good results.

Cleaning the stone is critical for the surfaces because the residues from the process clog the stone and do not allow it to work properly; above all in the middle of the surface where a not polished stripe could be seen.

It was decided to clean the stone after every surface, but also how to clean plays an important role. Sandpaper was again the first choice but the poor accuracy and repeatability due to the fact that the process is manual has led to bad surfaces, not uniform but mostly smaller due to the different action of the sand paper on the edges of the stone.

To be less aggressive and change less the shape of the stone it was tried to clean it with a common thick cloth used for household cleaning; this solution though somewhat trivial, led to very good results and definitely to repeatable surfaces even after many passages.

CHAPTER 5

Experimental Validation Of Monitoring Solutions for RAP Process

The study of the polishing process and the equipment owned brought to the definition of all the parameters playing a foundamental role within this project.
Now the final tests are carried on for the validation of correlation between CHPV (Critical Hidden process Variables – forces, AE, power) and VQC (Vital Quality Characteristics – surface roughness) and validation of the feasibility of on machine surface roughness measurements by light scattering technique. This is to provide robust monitoring techniques for industrial application in RAP (robot assisted polishing) machine. The experimental setup used for the final campaign is the same used for the preliminary tests, improved with the information gathered and presented in the previous chapter.

5.1 Experimental Plan

5.1.1 Timing interval and number of repetition

The steady state in the polishing process, where the variation in surface roughness over a certain number of polishing passes is negligible and there is no longer improvement adding value to the surface, represent the right moment for process stop and tool change. Such moment is designated by T_7 number of polishing passes in Figure 5.1.

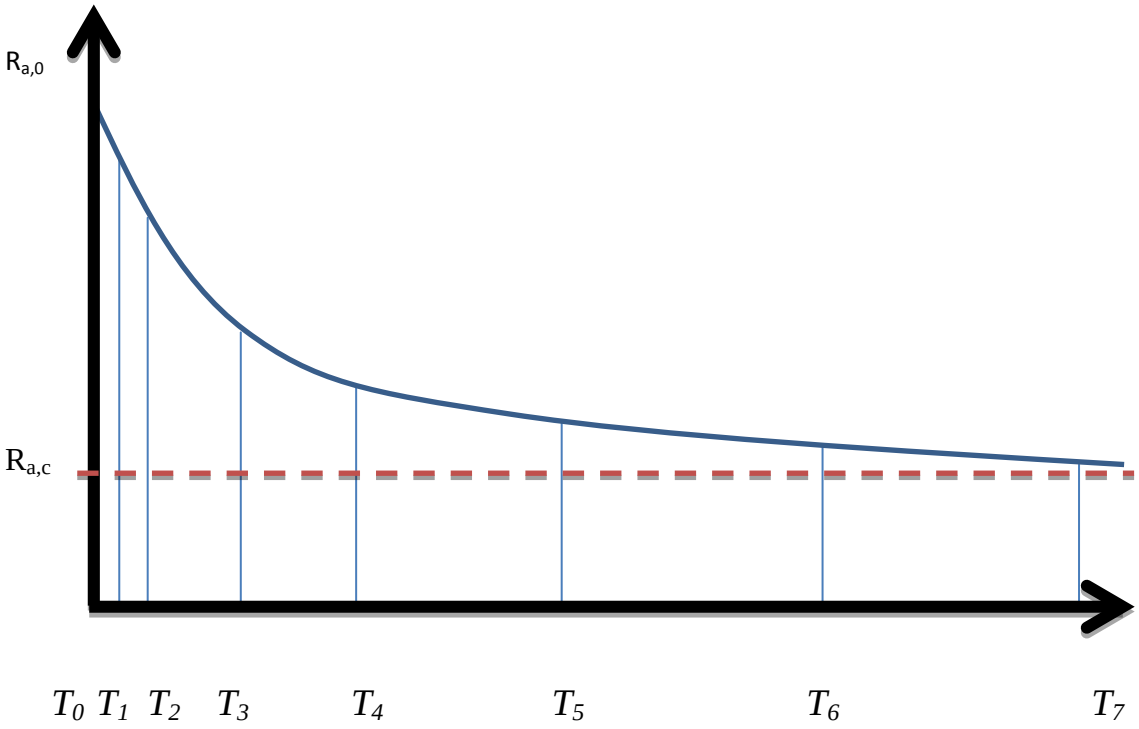

FIGURA 5.1 Expected roughness behaviour

Regarding the timing intervals, these are important to understand how the roughness behavior varies with processing time and 7 points have been chosen to evaluate this. From the literature survey, it is expected that the roughness curve is steep in the beginning when the polishing process has just started, and almost flat when the convergence roughness value is close to be reached. [10]
In this thesis, surface quality will be evaluated with reference to roughness amplitude parameter Ra. Although this parameter does not give a complete understanding of the surface characteristics, it allows a meaningful representation of the progress of the process condition ij this specific case. Obtained data files can be analyzed later with respect to other characteristics of the surface roughness.

In the figure, the seven timing intervals are T_1, T_2, T_3, T_4, T_5, T_6, T_7; whereas T_0 is the starting moment when the polishing surface is in the initial condition. The employed methodology to define the seven intervals is simple; first of all T_7 has to be found; it is the required time for the process to reach the convergence roughness value.

Once this time is determined the other are defined as a percentage of the total time according to Table 5.1.

Step	Percentage	Number of passes
1	5 %	8
2	10 %	16
3	20 %	32
4	30 %	48
5	50 %	80
6	75 %	120
7	100 %	160

TABLE 5.1 Polishing intervals

This choice has been made because the variation of the roughness is more important in the starting phase of the polishing process.

In order to detect the final point different surfaces were polished using the final procedure for different passes, the final roughness was finally measured and when the improvement was negligible that was chose as final point for the final tests.
From the graph below it can be seen that the stabilization, noticeable also in the forces is approximately 1500 seconds that in terms of passes means 120 passes, for this reason 160 passes was chosen as T_7.

At this point two were the options for the final tests campaign, an incremental or an absolute one.

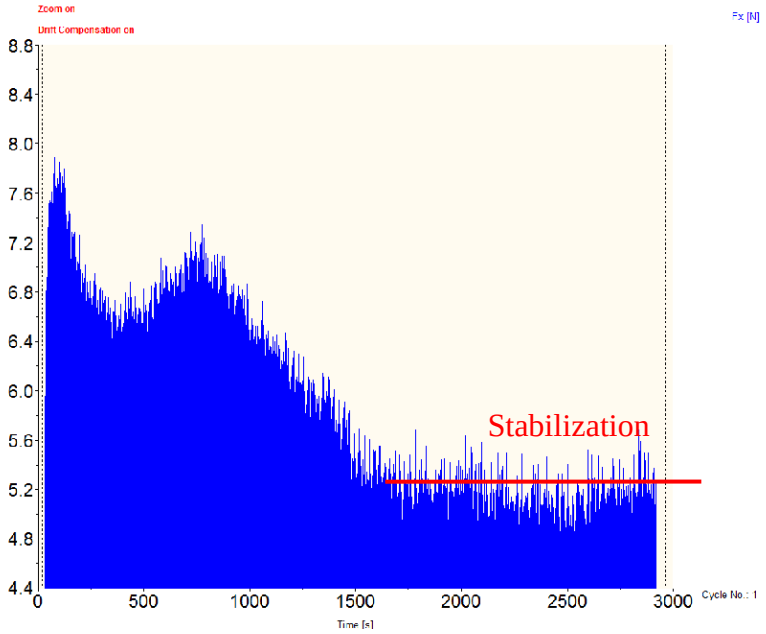

FIGURA 5.2 The stabilization of the signal is noticeable in force measurement

The main difference between the methods is that in the first case a given area is polished in incremental steps, that implies less samples needed and less time required; in the second case every timing interval has its own surface that increase the number of samples needed and especially the time required. On the other hand the second method allows having, at the end of the tests, all the surfaces with the different timing that could be measured off-line.
In the first case only measurements inline are applicable because it would be not manageable to carry the piece after each interval to the metrology laboratory and taking the negative of the surface using Replica method was not suitable for those levels of roughness. [23]
Such method consists in the application of a double component paste on the interested area that will be duplicated in negative when the paste will be hard. This is very useful to store several surfaces without the need of the entire workpiece. [35]

For all these reasons it has been chosen in order to use an off-line measurement instrument as reference.

Regarding the number of repetitions it has been decided that 5 were sufficient from a statistical point of view, considering required effort to perform the test campaign. In this way reliable results could be achieved.

At the end the total amount of surfaces to polish is equal to 5 X 7 = 35.

5.1.2 Workpiece

The workpiece was designed in order to have one entire test repetition thus 7 polished areas, plus some free windows for possible errors, on it. Furthermore the need of some extra space to clamp the sensors for the acoustic emission has been taken into account.
The main dimensions fit the piezoelectric dynamometer used for the acquisition of forces. There are 4 holes of 3,5 mm in diameter to screw the piece on the dynamometer using M# screws and a threaded hole M6 to screw the Montronix AE sensor.

The polishing areas are positioned as shown in Figure 5.5, to be as close as possible to the sensors. Their dimensions are driven by the pad ones that are 9 x 7 mm. The final nominal dimensions of the area would be 20 x 10 mm. A large part of this surface has to be discarded for the measurements because it didn't receive the same "polishing time"; at the end the final area suitable for measurement is 5 x 8 mm in the centre, enough for the purposes of this project.

The starting roughness of the workpieces was requested to be 0,3 µm but all the samples have been measured before starting to check if the specifications were followeds (see Paragraph 5.2.5).

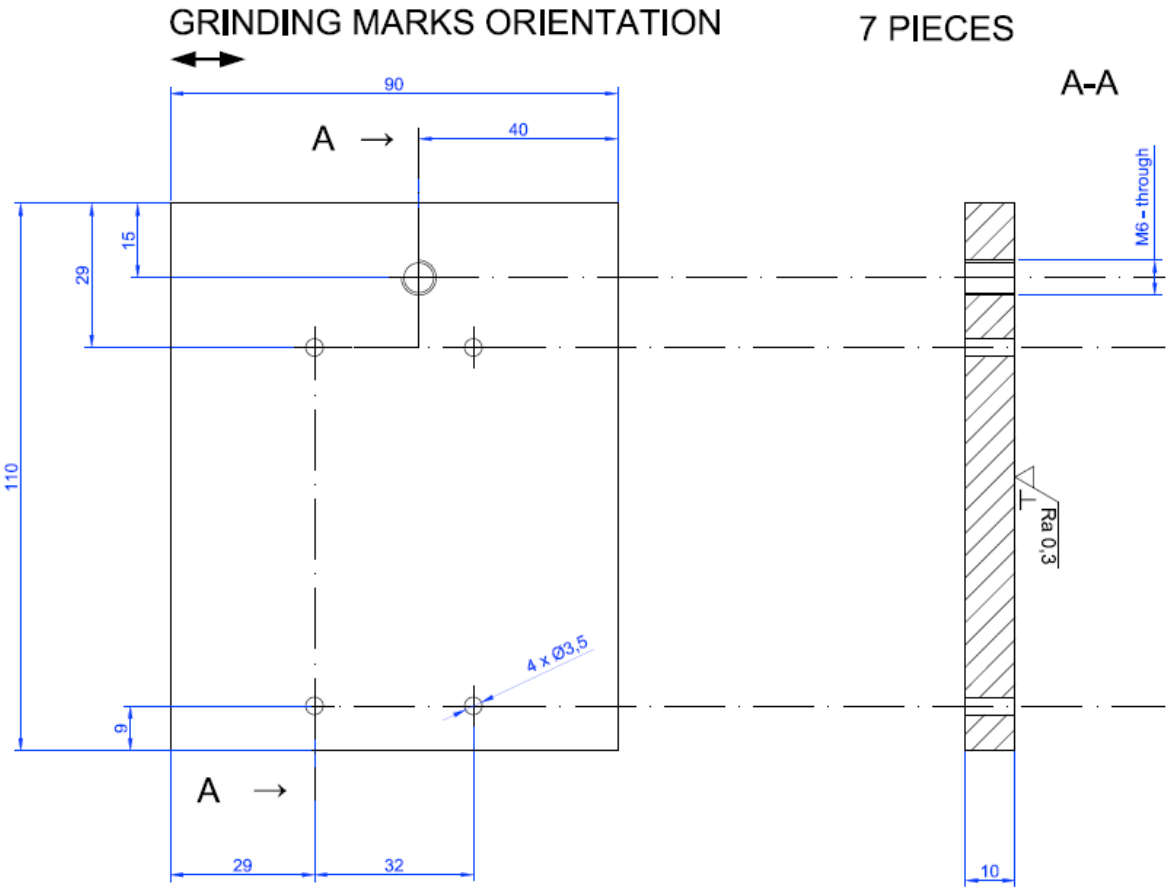

FIGURA 5.3 The workpiece drawing

FIGURA 5.4 The workpiece

5.2 Experimental strategy and procedure

The polishing modeule was mounted on a CNC milling machine. A dedicated part program was generated to carry out the experiments. All the movement during the process are assigned to the machine, in this way all the samples have perfectly the same appearance and also the measurement campaign is easier because even in this case a CNC programming strategy could be used.
The human help is needed only for the first alignment in order to define the origin of the reference on the workpiece. This strategy definitely speeds up the campaign and also means less possibility of errors.

The program starts from the first surface and then moves the module following the path showed in Figure 5.3, at every step the program stops and allows the operator to act on the piece for the necessary operations, it will start again after a manual input.

Polishing sequence :

- Polish Surface 1 (S1) for 8 passes back and forth (12mm)
- Move in Y direction 30 mm
- Polish Surface 2 (S2) for 16 passes back and forth (12mm)

- Move in Y direction 30 mm
- Polish Surface 3 (S3) for 32 passes back and forth (12mm)
- Move in X direction -20 mm
- Move in Y direction -60 mm
- Polish Surface 4 (S4) for 48 passes back and forth (12mm)
- Move in y direction 30 mm
- Polish Surface 5 (S5) for 80 passes back and forth (12mm)
- Move in Y direction 30 mm
- Polish Surface 6 (S6) for 120 passes back and forth (12mm)
- Move in X direction -20 mm
- Move in Y direction- 60 mm
- Polish Surface 7 (S7) for 160 passes back and forth (12mm)

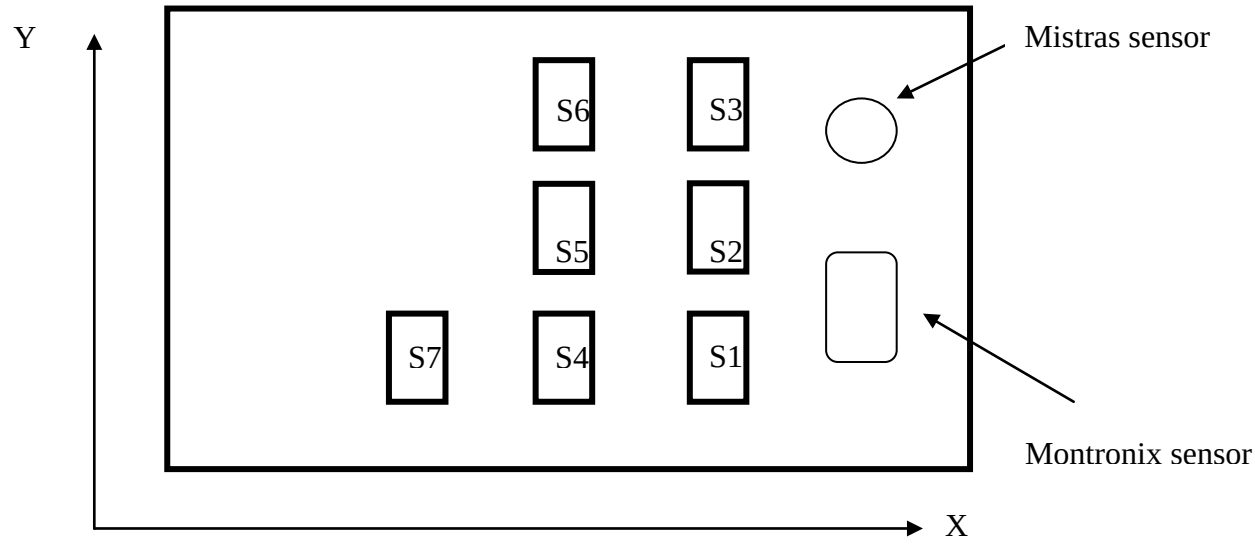

FIGURA 5.5 Polishing strategy

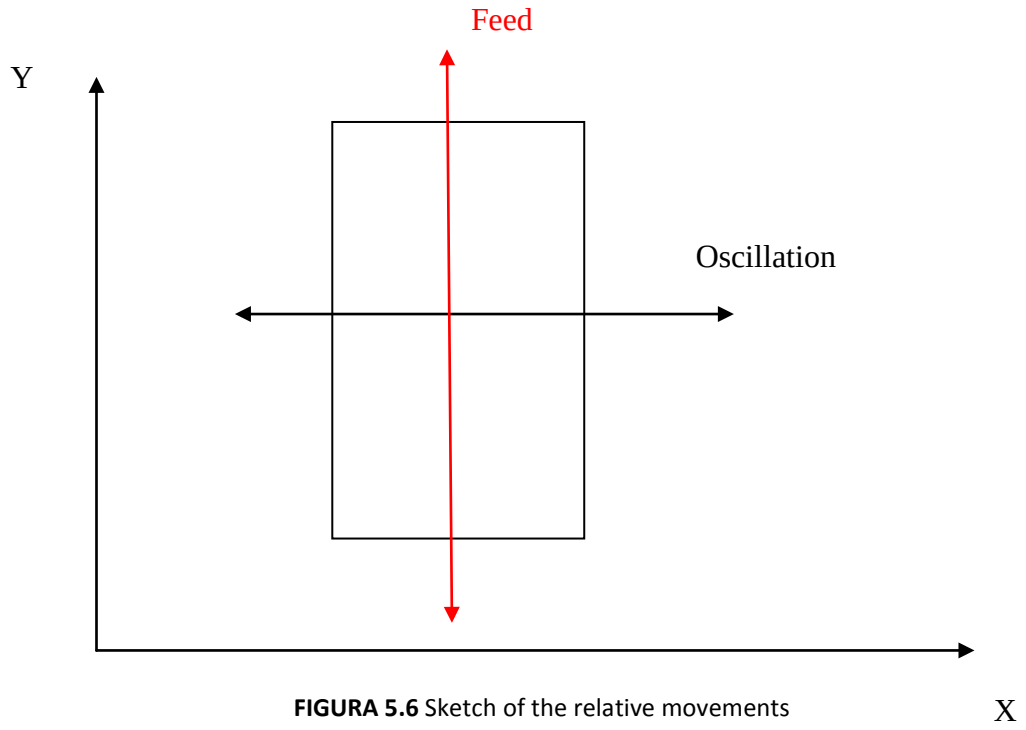

FIGURA 5.6 Sketch of the relative movements

After the positioning of the module in the right spot one drop of 8 micron diamond gel is put on the surface where there will be the first contact between the pad and the surface. The oscillation module in then started, the acquisition of the signals from the sensors begins. After a proper amount of time is elapsed, in order to correct the drift “a posteriori”, the down pressure is applied and the machine starts its movement back and forth. When the machine ends the pad is suddenly raised from the surface and after few seconds all the acquisition stopped. The machine then, after a manual input, moves to the next polishing spot.

5.2.1 Pre-polishing with stone

As discussed in Chapter 3 all the surfaces were pre-polished with stone. The stone was grit size 600 by Joke (dimensions 9x7) initially shaped to get the full contact area on a scrap workpiece. Then the shaped stone is used to polish the surfaces for 10 passes back and forth for 14 mm, following the same strategy of the final polishing process, in order to prepare the surface for the subsequent polishing with diamond paste. Every sample is polished with a different stone, which means that each stone polishes 9 surfaces for a total of 90 steps. After every surface the stone is cleaned using a cloth. No lubricant is added, neither on the stone nor on the sample. The stone polished surfaces were measured with FTS and the results are reported below.

Numb	Ra10	Rz10	Rzmax	RSm10
1	0,047	0,575	0,941	54,945
2	0,044	0,533	0,774	49,971
3	0,042	0,512	1,258	78,963
4	0,047	0,441	0,995	66,589
5	0,04	0,406	0,816	56,263
6	0,036	0,4	0,986	69,133
7	0,045	0,463	0,918	57,256
8	0,047	0,532	1,245	86,831
9	0,049	0,53	1,2	75,569
10	0,041	0,387	0,928	52,545
Avg	0,044	0,478	1,006	64,806
Std	0,004	0,067	0,172	12,565
Std%	9,2	14	17,1	19,4

TABLE 5.2 Starting surface roughnesses measured with FTS

FIGURA 5.7 Polishing stone pad

Table 5.2 shows which are the starting roughnesses after the stone polishing process measured with Form Talysurf profilometer (FTS).
It is noticeable that all the surfaces have almost the same Ra, calculated on 8 mm evaluating length, of approximately 40 nm.

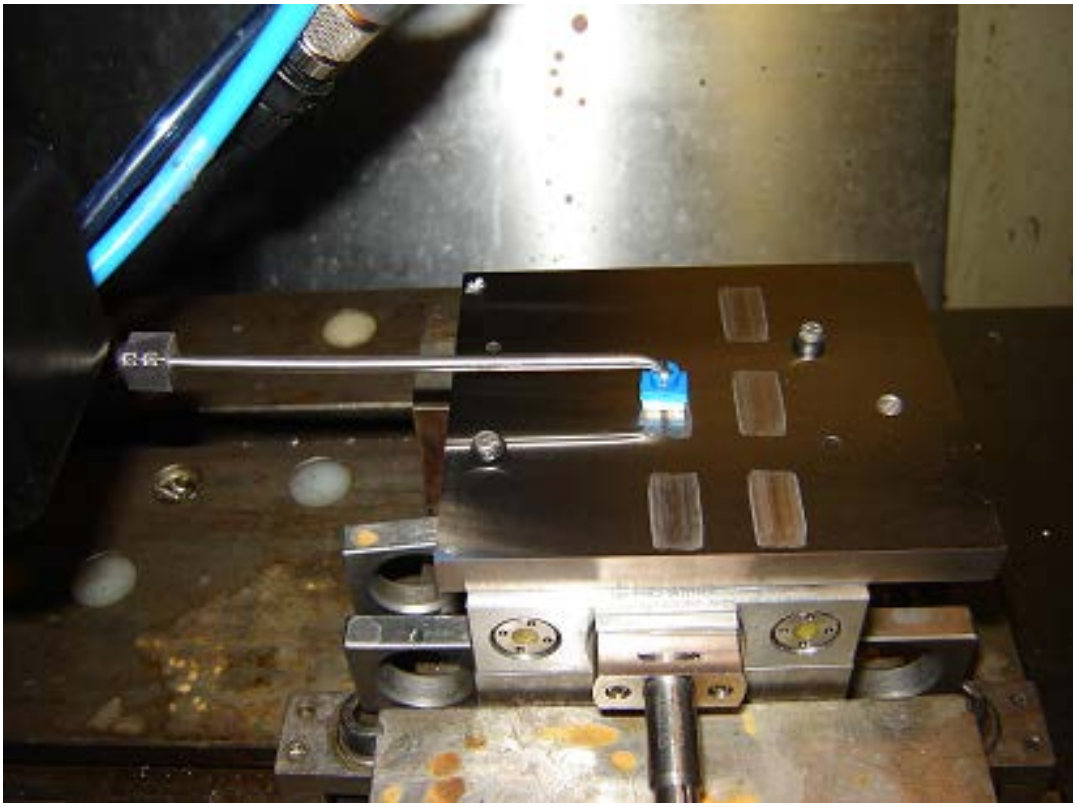

FIGURA 5.8 Polishing process with stone

5.2.2 Polishing with diamond paste

All the test were made with constant process parameter discussed in Chapter 4.
The diamond polishing process follows the procedure presented above; the pad is initially positioned 1mm inside the starting position of stone polishing to avoid problems due to polishing on the not pre-polished surface. The pad, handmade gluing the DP-Mol cloth from Strues on a piece of rubber made to replace the stone from a Joke stone pad, is wet with the lubricant and the diamond paste is applied directly on the workpiece where the pad will touch the surface for the first time. The dimensions of the pad are 9 x 7 mm.

Each workpiece is polished with a brand new pad that is also cleaned after every surface spot using alcohol and a toothbrush. This to remove particles trapped in the cloth and to keep the same condition of the pad.

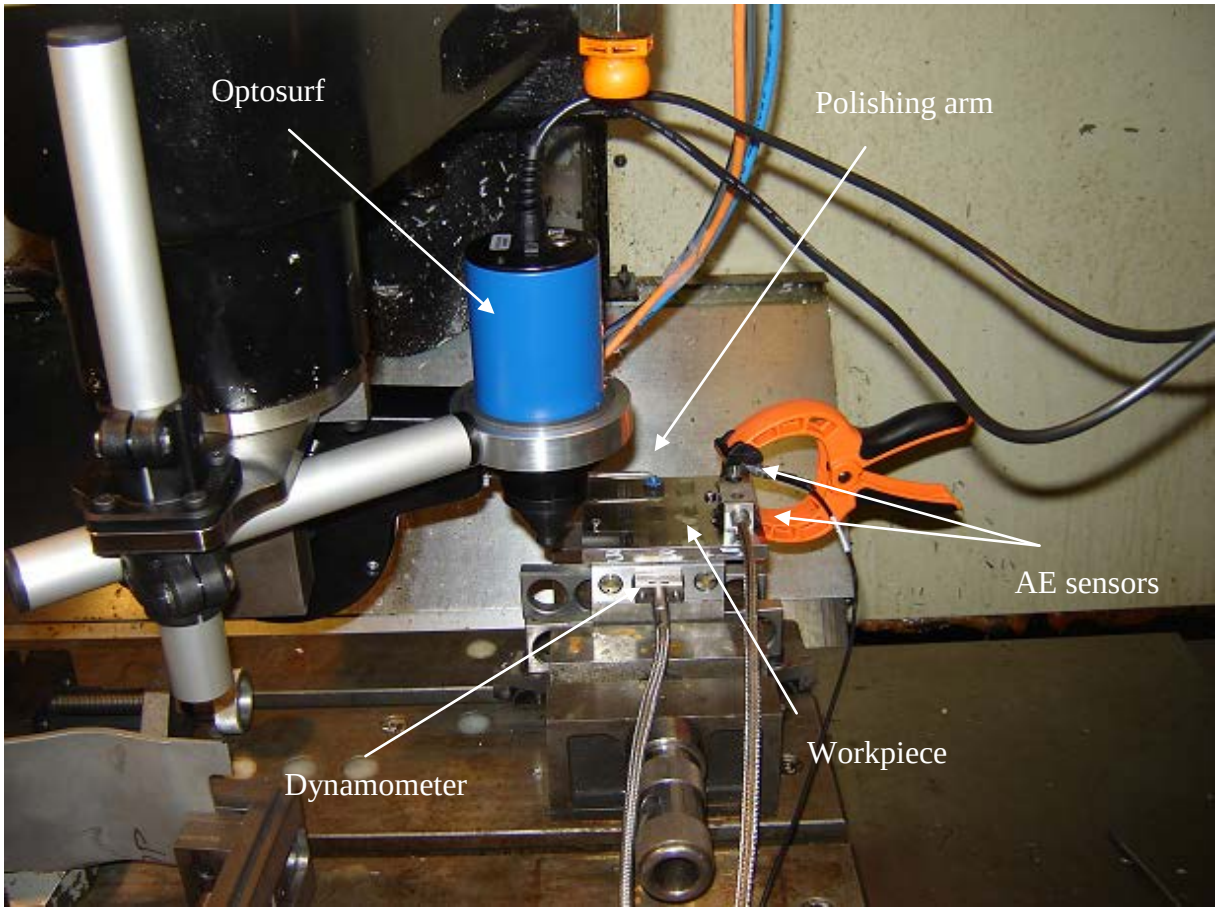

FIGURA 5.9 Final tests setup

The normal force applied was set to 15 N for all tests and the polishing path is back and forth for 12 mm in order to have enough uniform polished surface area to perform the measurements afterwards.
In order to be sure to acquire all the data from AE, force, and power consumption and have a reference zero value, all the sensors were started 30 seconds before the polishing process began and stopped 30 seconds after the process ended. In this way it is possible to correct the drift error and also evaluate the contribution due by the background noise in the signals.

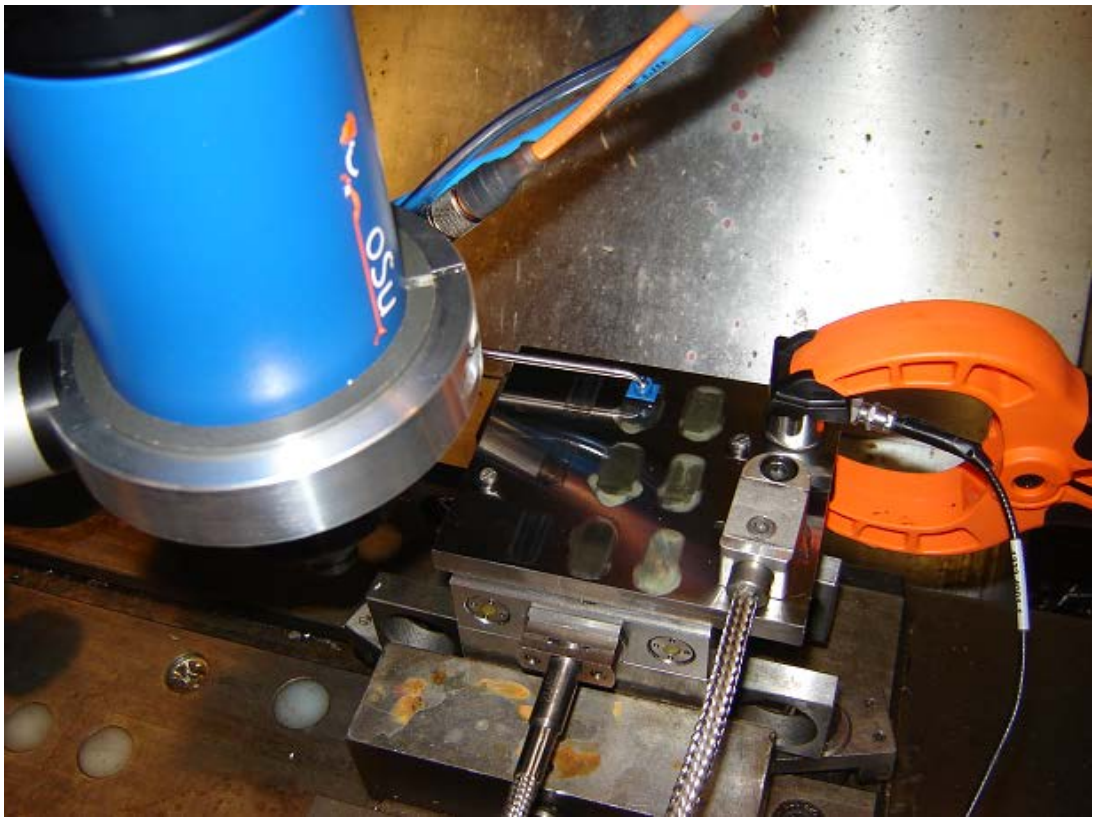

FIGURA 5.10 Polishing process

Process parameters	
Force	**15 N**
Pad	**Rubber +DP-Mol cloth**
Arm	**With tilting pad**
Feed	**1 mm/sec**
Oscillation	**3000 RPM**
Stroke	**1 mm**
Path	**Back and forth 12 mm**
Abrasives	**8 µm diamond gel**

TABLE 5.3 Summary of process parameters

5.2.3 Cleaning procedure

After all areas on a workpiecece are polished they need to be properly cleaned in order to measure the surface roughness. This process is critical and the smallest error or inaccuracy could compromise the surface because the minimal particles pressed too hard could scratch it making it inadequate for the measurements. Greater attention has to be paid with the most finished surfaces that are more vulnerable.
Using information gathered from a literature survey and direct connection with some companies a proper cleaning procedure has been defined. First of all the material deposited on the surface is blown away using a pressed air gun. The remains are then cleaned using alcohol and a wad of cotton applying the lowest possible pressure. It has to be pointed out that alcohol has to be well dried because it could bring rust quickly, even if the material is a stainless steel. [31], [39]

5.2.4 Protection procedure

The surfaces cleaned are ready to be measured, in order to protect them from possible damages, scratches or incoming rust during the period they are stored, the workpieces have to be properly treated and packed.
Another time communication with some companies led to kwon how usually they behave with finished surface and the same procedure is used in this project.
First of all a light mineral oil is sprayed on the sample and then is coated with a very resistant transparent film to prevent scratches. Finally everything is packed with Bubble wrap to prevent collisions and a layer of thick paper. [39]

5.2.5 Measuring strategy

The measuring strategy is very important to have a structured method to measure the roughness of the samples and get reliable results.

Optosurf is mounted on a Cincinnati CNC work-station, so one can program the machine to move from a surface to another very quickly and doesn’t have any problem due to wrong positioning.
In addition to the displacement program from a surface to another, a program for the measuring procedure itself is needed.

Every surface is measured in 6 different spots to cover the whole surface and have more reliable data. The 6 spots have to be in the centre of the surface where the action of the abrasive is uniform and there are no boundary effects that could influence the measurements.
The human help is needed only for the first alignment in order to define the origin of the coordinates that will be the workpiece coordinates for the whole project. This strategy definitely speeds up the campaign and also means less possibility of errors.
The program starts from the first surface and then moves the module following the path showed in Figure 6.5, at every step the program stops and allow the operator to act on the piece for the necessary operations, it will start again after a manual input.

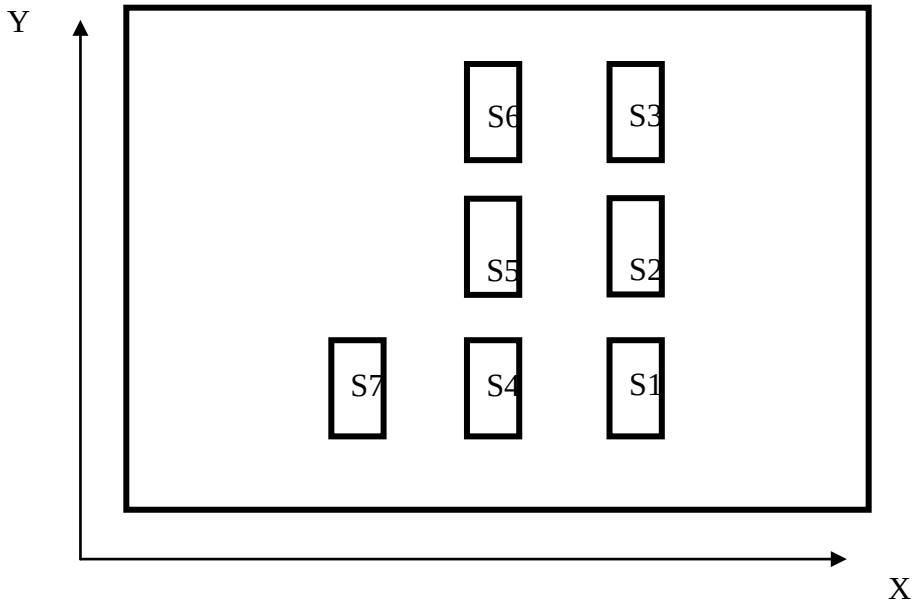

FIGURA 5.11 Measuring strategy (main plan)

The whole measuring procedure including the displacement and the actual measurement could be summarized is a set of instructions translated into machine language:

Measurement procedure (MP): 6 measurement/surface (measure – move in X direction -2,5mm – measure – move in X direction -2.5mm – measure – move in Y direction 2mm – measure – move in X direction 2,5mm – measure – move in X direction 2,5mm – measure – move in Y direction - 2mm)

- MP on Surface 1 (S1)
- Move in Y direction 30 mm

- MP on Surface 2 (S2)
- Move in Y direction 30 mm
- MP on Surface 3 (S3)
- Move in X direction -20 mm
- Move in Y direction -60 mm
- MP on Surface 4 (S4)
- Move in y direction 30 mm
- MP on Surface 5 (S5)
- Move in Y direction 30 mm
- MP on Surface 6 (S6)
- Move in X direction -20 mm
- Move in Y direction -60 mm
- MP on Surface 7 (S7)

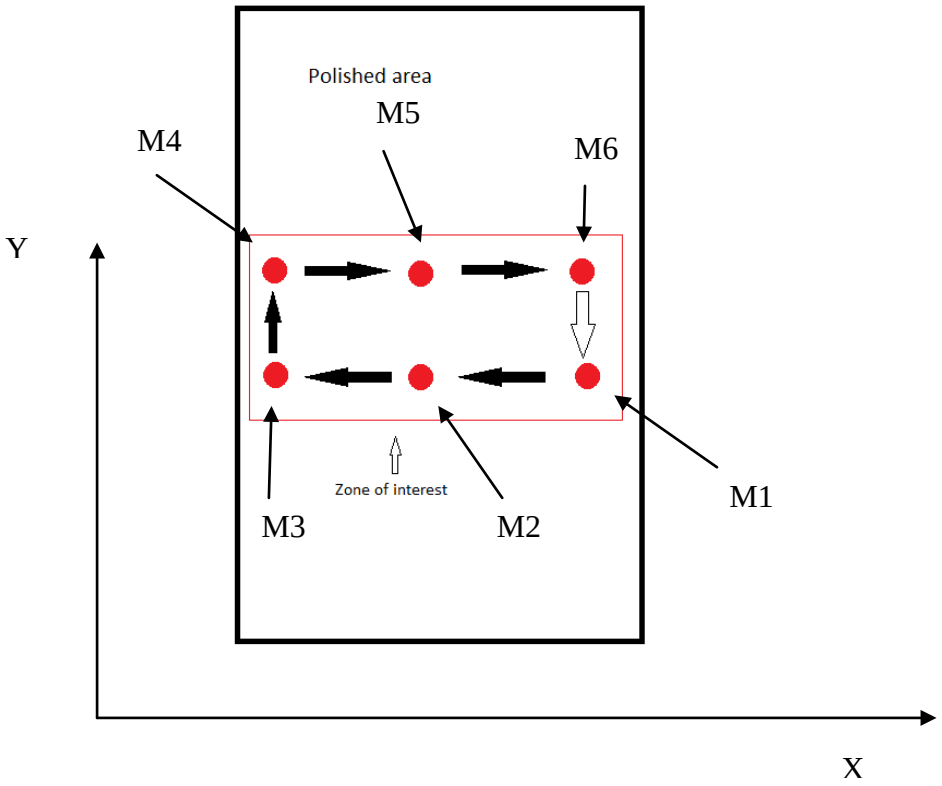

FIGURA 5.12 Measuring strategy (zoom on polished area)

5.2.6 Measurements of initial surface roughness

Before starting the test campaign all the samples were measured in order to know the starting roughness.
From a quick measurement process made with FTS on the workpieces it was noticed that the surfaces presented a different roughness from 0,150 µm up to 0,300µm.

Sample	Side 1 (Ra [nm])	Side 2 (Ra [nm])
1	0,193	0,192
2	0,146	0,247
3	0,188	0,237
4	0,283	0,216
5	0,203	0,156
6	0,17	0,238
7	0,280	0,242

TABLE 5.4 Samples roughnesses measured with FTS

Then from the seven samples it was decided to use for the final tests the 5 ones that presented the most close roughness value that was around 0,200 µm (Samples number 1, 3, 4, 5, 6).

As example the Table for Workpiece 1 is shown, all the measurement performed on the 5 samples are in Appendix A.

Num	Ra (µm)	Rz (µm)	Rzmax (µm)	RSm (µm)
1	0,214	1,67	1,968	29,849
2	0,193	1,644	2,029	29,297
3	0,181	1,583	1,811	26,675
4	0,184	1,448	1,606	28,814
5	0,185	1,483	1,779	28,096
6	0,188	1,57	1,821	28,608
7	0,191	1,537	1,885	28,796
8	0,188	1,553	1,933	27,621
9	0,209	1,705	2,134	32,498

Num	Ra (µm)	Rz (µm)	Rzmax (µm)	RSm (µm)
10	0,201	1,548	1,917	29,989
Avg	0,193	1,574	1,888	29,024
Std	0,011	0,08	0,146	1,576
Std%	5,7	5,1	7,7	5,4

TABLE 5.5 Data for workpiece 1 from FTS

The 5 samples that would be used during the final tests were also measured with the Infinite focus Alicona showing the following average roughness, for the all measurements see Appendix B. On the workpieces a 3D scan was made also with the FTS showing the following average roughness, for the all measurements see Appendix C.

Workpiece 1	
Sa	184 nm
Sa	218 nm
Sa	220 nm
Avge Sa	207 nm

a

Workpiece 1	
Sa	199 nm
Sa	162 nm
Sa	211 nm
Ave Sa	190 nm

b

TABLE 5.6 Data for workpiece 1 from Alicona (a) and FTS (b)

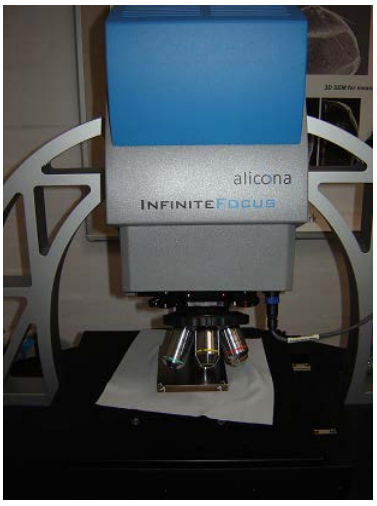

a

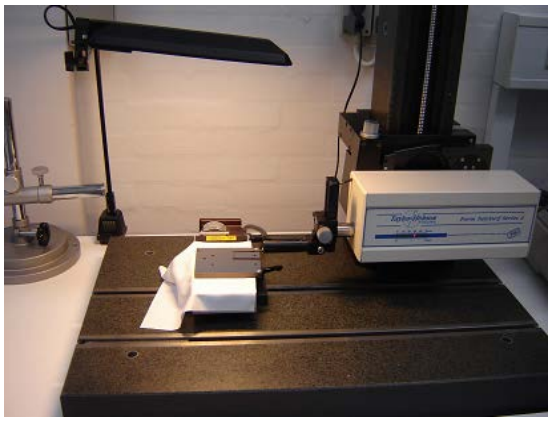

b

FIGURE 5.13 Infinite Focus Alicona (a), FTS (b)

5.2.7 Measurements of starting pre-polished surface roughness

After the stone polishing process all the surfaces were measured both with Optosurf and the WLI to know the starting roughness of the samples and generate, at the end of the project, the roughness progress curve.
The measurements were taken in 5 random points with the WLI and following the procedure showed before with Optosurf.

Below are shown the measurements for workpiece 1 performed with WLI and Optosurf, for the other workpieces see Appendix D and E.

Workpiece 1 (Ra in nm)						
Surface	meas1	meas2	meas3	meas4	meas5	**AVG**
1	41	31	36	37	42	37,4
2	35	33	33	38	48	37,4
3	34	32	39	46	41	38,4
4	37	45	34	36	38	38
5	39	36	35	34	38	36,4
6	56	54	52	56	57	55
7	35	36	39	40	39	37,8

TABLE 5.7 Workpiece 1 stone polished surfaces meaured with WLI (Ra in nm)

Is noticeable that the surface roughness for all the surface is almost the same (except for surface number 6 that presents a roughness 20 nm higher, that means that the stone polishing process and all the procedure connected to it were working well. The 5 measuring spots are random on the surface.

The measurements performed with Optosurf detected the same roughness behavior, all the surface present the same roughness value except for surface number 6 that has a Aq value definitely higher.

This is the first demonstration that Optosurf and WLI present a degree of correlation and that therefore Optosurf is a reliable instrument for this type of measurements.

Workpiece 1 (Aq [non-dimensional])							
Surface	meas1	meas2	meas3	meas4	meas5	meas6	**AVG**
1	45,28	42,55	56,09	59,45	47,75	42,13	48,88
2	43,01	40,83	39,26	39,39	38,24	43,3	40,67
3	43,54	42,76	45,93	40,29	41,3	40,01	42,31
4	38,87	54,19	34,69	39,5	52,38	32,87	42,08
5	41,77	54,98	34,686	30,28	53,41	44,38	43,25
6	63,89	71,5	60,38	60,5	67,79	60,1	64,03
7	37,12	36,2	56,23	56,67	48,26	39,5	45,66

TABLE 5.8 Workpiece 1 stone polished surfaces measured with Optosurf (Aq values)

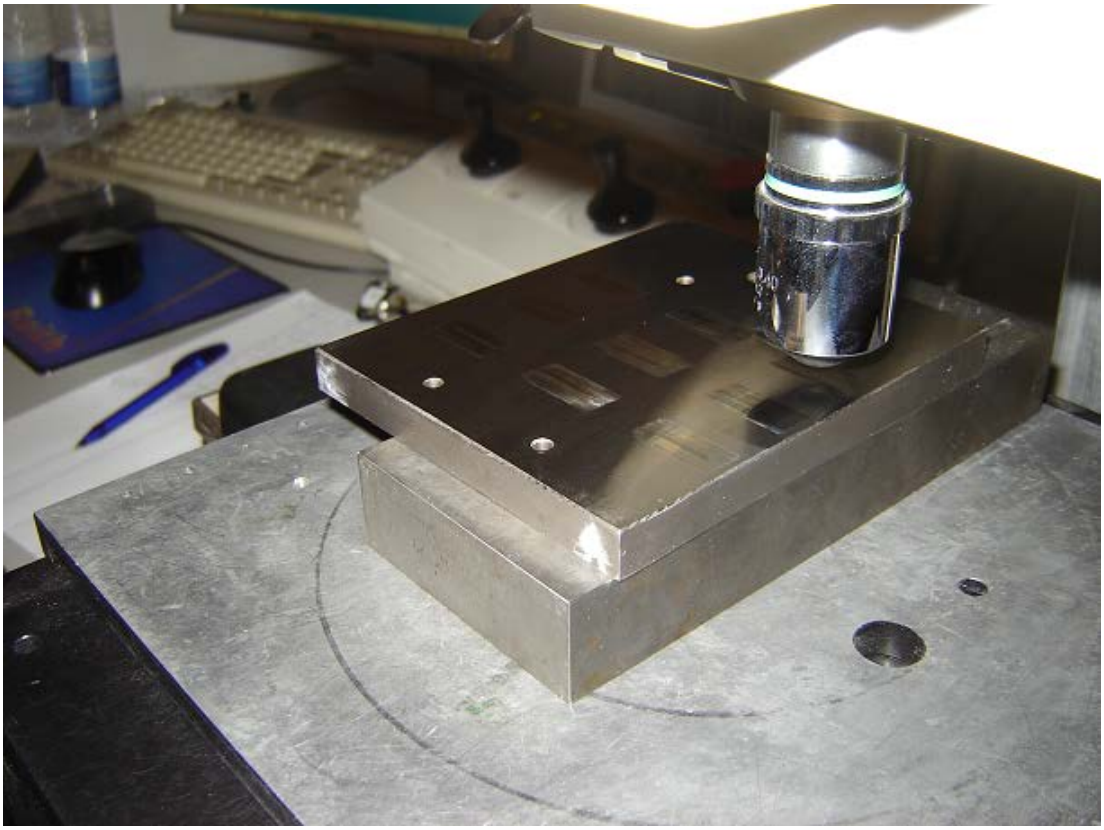

FIGURE 5.14 Measurements of polished surface with WLI

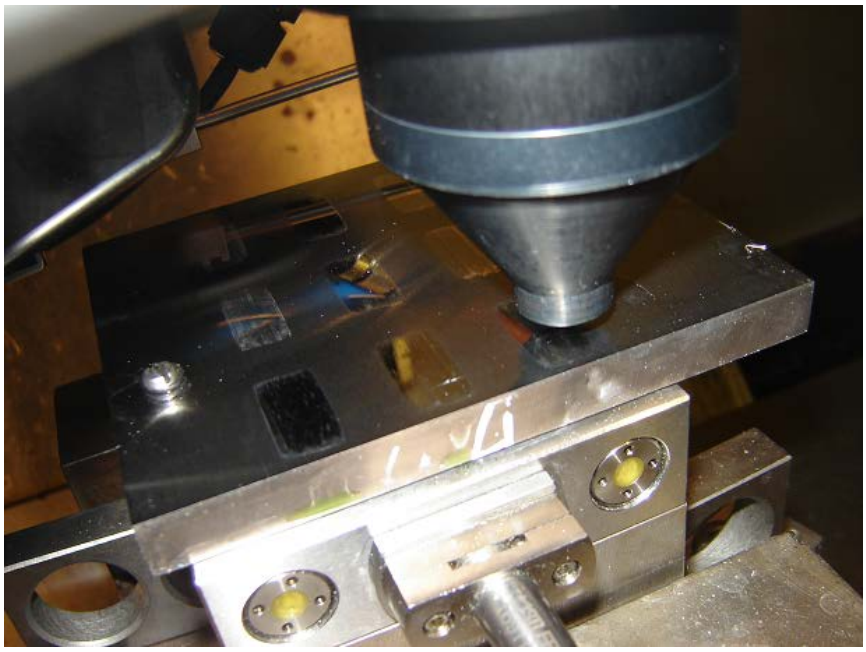

FIGURE 5.15 Measurements of polished surface with Optosurf

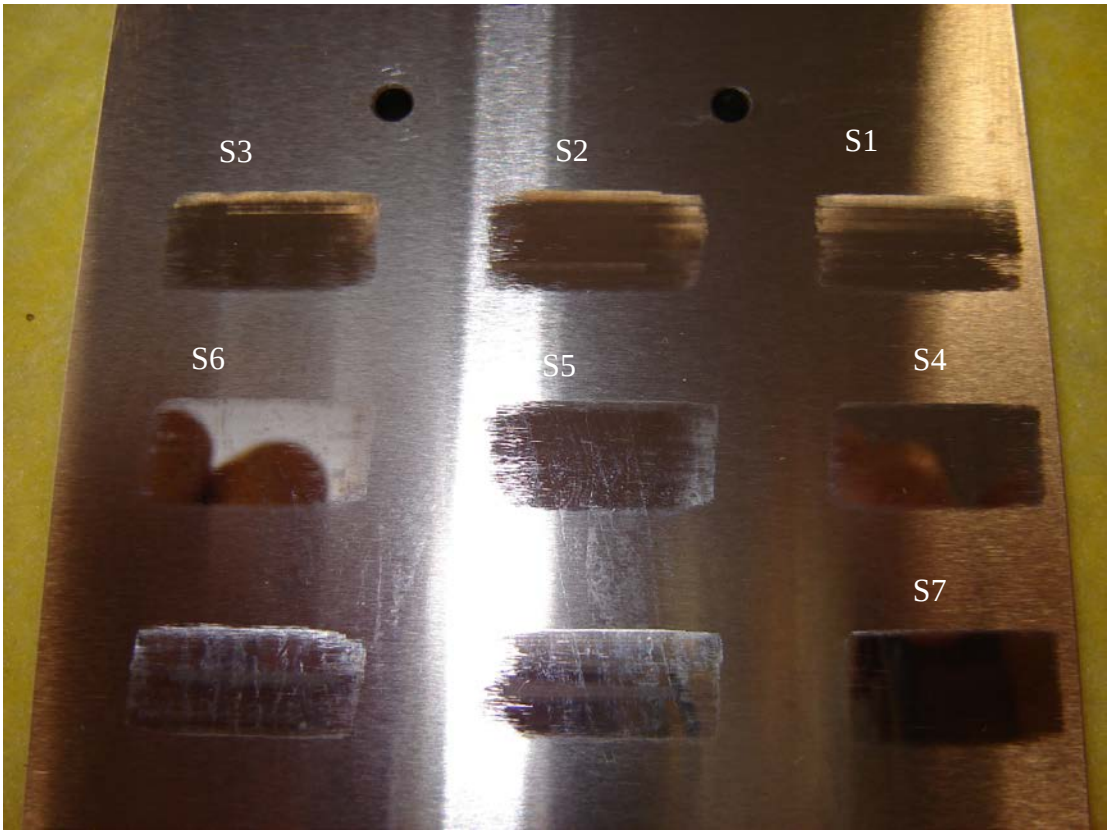

FIGURE 5.16 Final workpiece

CHAPTER 6

Results and Analysis

In this chapter the results from the final roughness measurements and the data from the different sensors are shown and discussed with the objective to verify if there is a correlation between them.

First of all the roughness values Ra measured with the White Light Interferometer (WLI) are analyzed in order to create a reference database for the subsequent analysis and to verify that the diamond polishing process had led to satisfactory results. Then the correlation between the Ra measured by the WLI and the Aq values measured with Optosurf are explained, this is also a validation of Optosurf in this range of surface roughness.

Afterwards the correlation with Forces, Acoustic emission and Power consumption is analyzed in this order, for the final validation of the sensor system used to monitor the process.

6.1 Roughness measurements

The first subchapter is about surface roughness and will show the results from the WLI and afterwards from Optosurf, studying the mutual correlation.

6.1.1 White light interferometer

Results of surface roughness measurements with the WLI are expressed in terms of Ra value. Each surface is measured 6 times following the procedure shown in Chapter 5, and then the average values and the standard deviations are calculated and considered as the reference Ra values.

Below the tables with the data and the graphs related to roughness against number of passes are represented for each workpiece.

On the X axis there is the number of passes and on the Y axis the Ra value in nanometers together with the standard deviation for each point.

Workpiece1 (Ra [nm])								
Surface	meas1	meas2	meas3	meas4	meas5	meas6	**AVG**	**StDev**
1	32	29	32	28	27	28	29,3	1,97
2	18	16,5	17,6	17	19	19	17,9	0,93
3	11	11	9,1	9,2	11	10,5	10,3	0,68
4	5,9	6,2	6	5,7	6,3	6	6,0	0,19
5	4,5	4	3,8	3,9	3,9	3,8	4,0	0,12
6	4,5	3,8	4	4,1	4,3	4,3	4,2	0,21
7	2,2	2,5	2,2	2	2	2	2,2	0,10

TABLE 6.1 Final roughness Ra for workpiece 1 (values in nm)

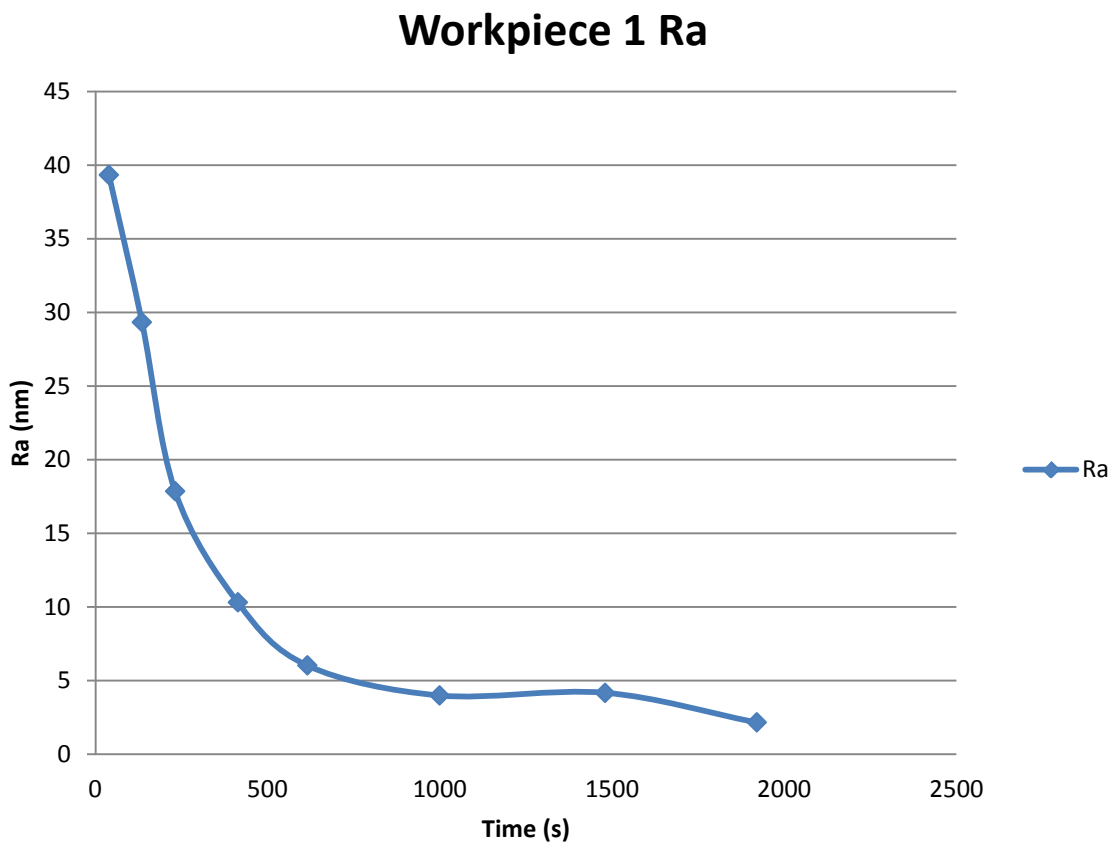

FIGURE 6.1 Final roughness curve Ra for 160 passes for workpiece 1 (values in nm)

Points represent the average of 6 measurements. Error bars are covered by the data markers

Workpiece3 (Ra [nm])								
surface	m1	m2	m3	m4	m5	m6	**AVG**	**StDev**
1	34	25	27	29	29	31	29,2	2,85
2	17	18	18	18	17	16	17,3	0,74
3	9	11	9	10	10	10	9,8	0,68
4	7	7,4	7,5	7,8	7	7	7,3	0,30
5	5	5	4,3	4,8	5	4,2	4,7	0,33
6	3	3,3	2,9	2,9	3,7	3,3	3,2	0,28
7	1,8	2,2	2,1	2	2,3	2,1	2,1	0,15

TABLE 6.2 Final roughness Ra for workpiece 3 (values in nm)

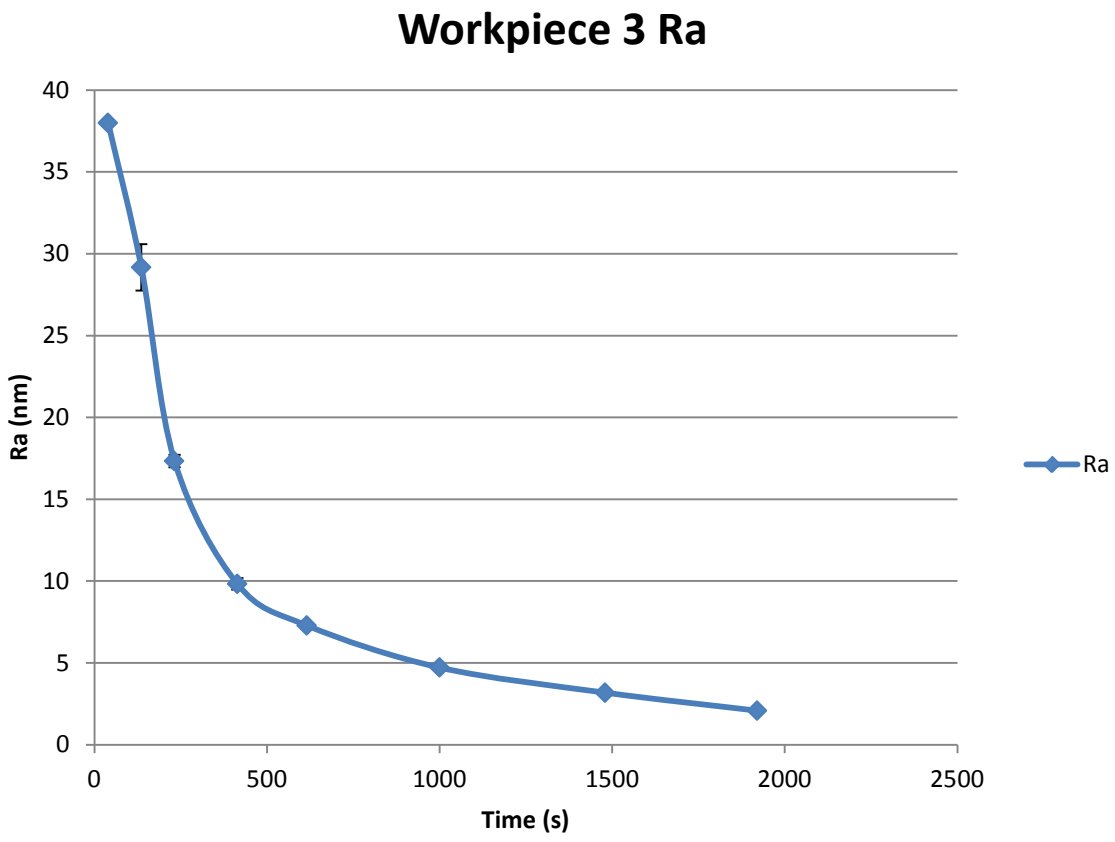

FIGURE 6.2 Final roughness curve Ra for 160 passes for workpiece 3 (values in nm)

Points represent the average of 6 measurements. Error bars are covered by the data markers

Workpiece4 (Ra [nm])								
surface	m1	m2	m3	m4	m5	m6	**AVG**	**StDev**
1	30	27	30	33	34	28	30,3	2,49
2	21	22	18	25	22	23	21,8	2,11
3	10,5	9,6	10	9	11	10,7	10,1	0,68
4	7	7,4	7,5	7,8	7	7	7,3	0,30
5	5	5,2	5,2	5,3	5,1	4,9	5,1	0,13
6	3,2	3,2	3,2	2,7	3,3	2,9	3,1	0,21
7	2,3	2,2	2,1	2	2	2,1	2,1	0,10

TABLE 6.3 Final roughness Ra for workpiece 4 (values in nm)

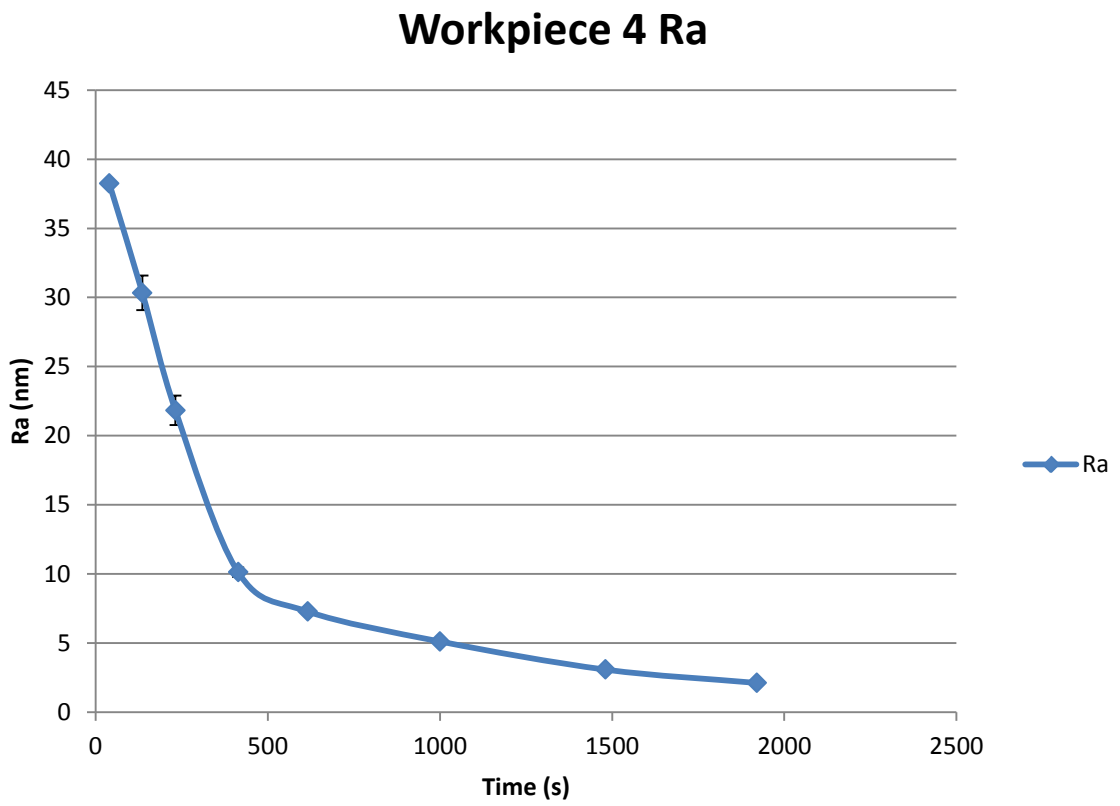

FIGURE 6.3 Final roughness curve Ra for 160 passes for workpiece 4 (values in nm)

Points represent the average of 6 measurements. Error bars are covered by the data markers

Workpiece5 (Ra [nm])								
surface	m1	m2	m3	m4	m5	m6	**AVG**	**St Dev**
1	28	27	26	25	26	29	26,8	1,34
2	17	18	21	17	18,5	18	18,3	1,34
3	8	10	8	9	8,5	11	9,1	1,09
4	6,1	6,9	7	5,7	6,4	7,1	6,5	0,51
5	3,7	4,2	3,4	4,3	4,5	4,4	4,1	0,39
6	3,2	2,6	3,3	3,5	3,2	3,1	3,2	0,27
7	1,7	2	1,6	1,8	1,8	1,8	1,8	0,12

TABLE 6.4 Final roughness Ra for workpiece 5 (values in nm)

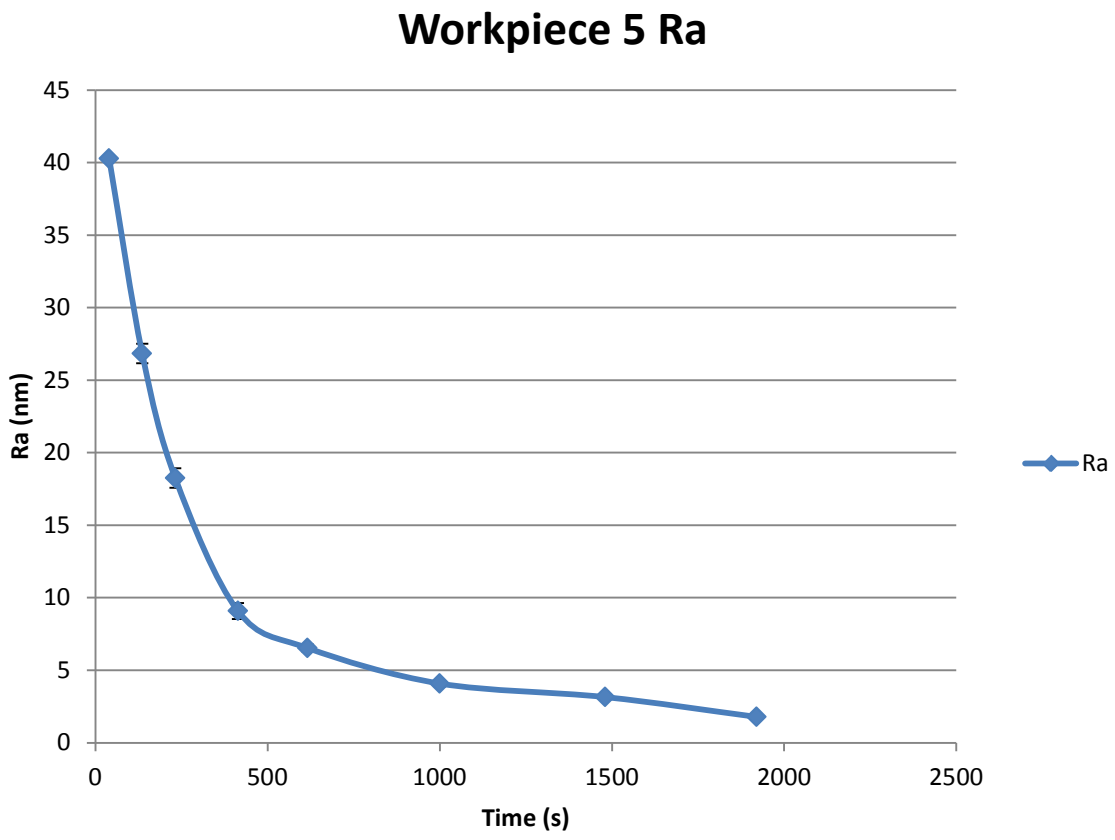

FIGURE 6.4 Final roughness curve Ra for 160 passes for workpiece 5 (values in nm)

Points represent the average of 6 measurements. Error bars are covered by the data markers

Workpiece6 (Ra [nm])								
surface	m1	m2	m3	m4	m5	m6	**AVG**	**StDev**
1	29	29	27	26	30	29	28,3	1,37
2	20	19	21	19	21	21	20,2	0,89
3	9	9	10	9	10	9,5	9,4	0,44
4	6,1	6,2	5,7	6,4	5,2	5,8	5,9	0,39
5	4,5	3,7	4,2	4,1	4,2	3,9	4,1	0,25
6	2,9	3,6	2,8	3,2	3,4	3,1	3,2	0,27
7	2,4	1,9	2,5	1,6	2,2	2,1	2,1	0,30

TABLE 6.5 Final roughness Ra for workpiece 6 (values in nm)

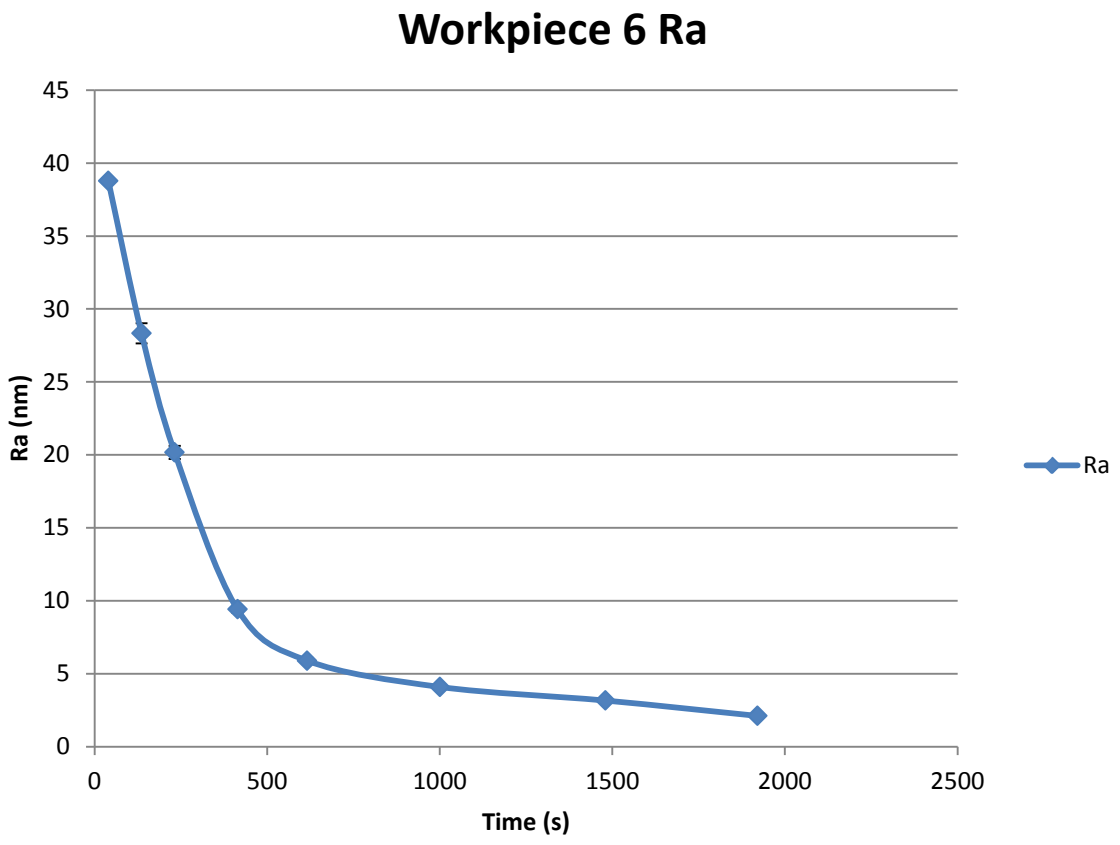

FIGURE 6.5 Final roughness curve Ra for 160 passes for workpiece 6 (values in nm)

Points represent the average of 6 measurements. Error bars are covered by the data markers

It´s noticeable that the Ra curve reflects very well the roughness behavior expected for a polished surface for every workpiece. There is a fast decrease of the surface roughness in the beginning and then stabilization when the process will not improve the surface roughness anymore. Furthermore the final Ra value around 2 nm is extremely good and it is also seen that the process is highly repeteable. It's possible to state that the beginning of the steady state is around 100 passes, continuing with the process over this threshold brings minimal improvement in the surface roughness compared to the required time.

Finally it's possible to state that the typical Ra curve is well reproduced by the data and that it's possible to go on with the analysis of the other parameters. These curves are then the reference ones.

An analysis using SPIP software was made on the images collected with WLI to check if the Ra value showed by the instrument is reliable for the characterization of an area, usually measured with the parameter Sa. In fact the WLI software gives has result from the roughness measurement already an Ra value that has been verified and compared with the Sa value.

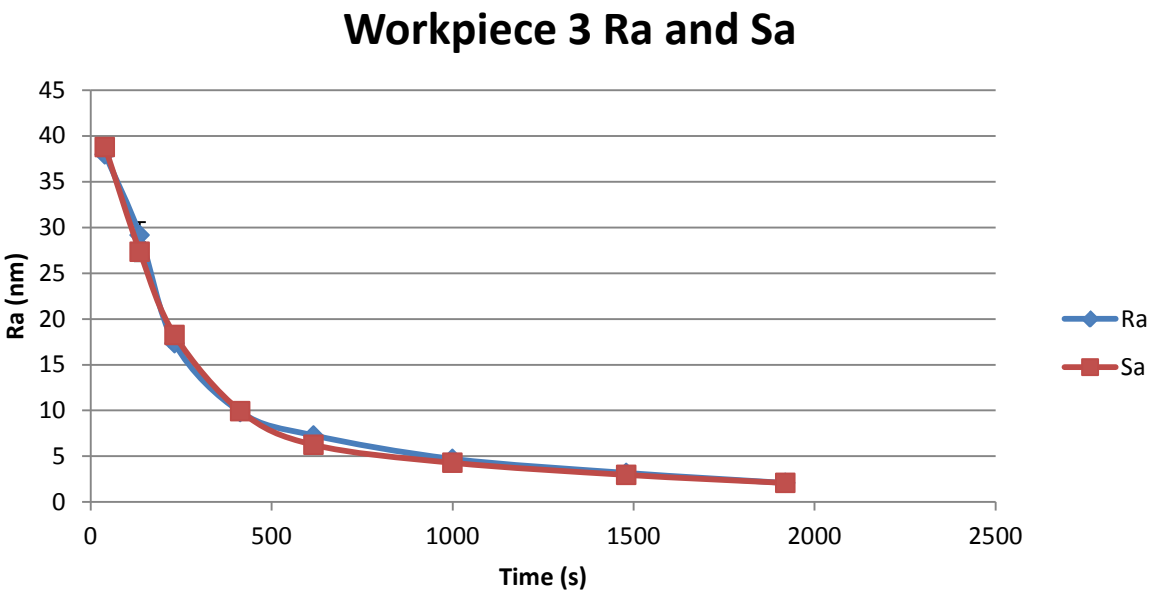

FIGURE 6.6 Correlation between Ra and Sa for 160 passes for workpiece 3 (values in nm)

Points represent the average of 6 measurements. Error bars are covered by the data markers

The graph above shows that there is not a noticeable difference between the Ra values calculated by the software instrument and the Sa values calculated with SPIP on the images caught.

All the correlation graph and tables are shown in Appendix F.

6.1.2 Optosurf

Now the results from the measurements performed with Optosurf are presented and afterwards correlated with the previous roughness measurements made with WLI. As introduced in Chapter 6 Optosurf is a very fast instrument and 500 measurements were taken for every measuring spot because the amount of time required was just half a second for every spot and in this way a better value is calculated, that is already an average of several measurements.

Optosurf was aligned just once per workpiece on the first surface and kept in that position for the entire measuring campaign. It started measuring exactly on the same absolute position, aided by the CNC, for every workpiece. This position is kept for the measurements before and after the polishing process. In this way the same points were measured before and after showing the real local improvement of the surface.

Optosurf was positioned with the sensor along the starting grinding marks because after the stone polishing the main scratches were in the oscillation direction and a higher Aq was noticeable.

The vertical distance was set manually to be as close as possible to 5 mm from the surface as suggested by the user manual.

Below the tables with the data are shown for each workpiece.

Workpiece 1 (Aq [non-dimensional])								
surface	m1	m2	m3	m4	m5	m6	**AVG**	**StDev**
1	16,03	15,19	25,50	26,02	15,14	14,82	18,78	4,94
2	6,87	5,34	7,03	10,15	5,22	7,30	6,99	1,62
3	4,44	5,84	2,77	3,48	11,22	5,21	5,49	2,475
4	3,17	3,06	2,19	2,39	3,11	3,24	2,86	0,41
5	2,65	2,15	1,94	1,93	2,17	2,72	2,26	0,31
6	4,60	3,38	3,95	4,66	3,39	3,76	3,96	0,51
7	2,20	1,87	1,82	1,82	1,86	2,24	1,97	0,17

TABLE 6.6 Final roughnesses Aq for workpiece 1

Workpiece 3 (Aq [non-dimensional])								
surface	m1	m2	m3	m4	m5	m6	**AVG**	**StDev**
1	19,62	15,56	27,10	16,95	17,14	13,51	18,31	4,33
2	7,16	6,67	13,23	7,00	6,53	8,52	8,18	2,34
3	3,95	5,41	10,26	6,90	6,73	4,62	6,31	2,05
4	7,34	5,02	6,45	4,73	4,16	4,26	5,33	1,17
5	7,43	2,59	5,32	3,40	3,09	7,88	4,95	20,9
6	3,82	3,30	4,29	4,15	3,71	3,67	3,82	0,32
7	3,05	2,86	3,78	3,89	2,99	2,97	3,26	0,41

TABLE 6.7 Final roughnesses Aq for workpiece 3

Workpiece 4 (Aq [non-dimensional])								
surface	m1	m2	m3	m4	m5	m6	**AVG**	**StDev**
1	8,63	10,12	23,00	22,58	9,16	8,59	13,68	6,46
2	9,86	11,29	11,86	10,31	7,39	9,90	10,10	1,41
3	3,08	6,94	3,97	3,71	6,83	2,87	4,57	1,67
4	2,81	2,37	3,12	3,16	2,23	2,61	2,72	0,35
5	2,31	1,93	2,08	2,34	1,95	2,87	2,25	0,32
6	2,19	2,15	1,82	1,80	2,22	2,20	2,06	0,14
7	2,06	1,79	1,81	1,88	1,79	1,90	1,87	0,09

TABLE 6.8 Final roughnesses Aq for workpiece 4

Workpiece 5 (Aq [non-dimensional])								
surface	m1	m2	m3	m4	m5	m6	**AVG**	**StDev**
1	24,09	35,74	25,61	24,38	33,26	23,50	27,76	4,85
2	8,42	16,78	36,65	35,27	17,50	9,70	20,72	11,28
3	10,67	5,98	9,25	11,54	5,32	11,18	8,99	2,47
4	7,00	5,85	13,06	13,07	5,71	6,61	8,55	3,22
5	2,95	2,63	3,42	3,51	2,91	2,85	3,05	0,31
6	3,66	3,90	3,33	2,83	3,72	3,36	3,47	0,34
7	2,11	2,14	1,89	1,85	1,86	1,86	1,95	0,12

TABLE 6.9 Final roughnesses Aq for workpiece 5

Workpiece 6 (Aq [non-dimensional])								
surface	m1	m2	m3	m4	m5	m6	**AVG**	**StDev**
1	11,28	18,27	21,64	18,29	15,31	13,38	16,36	3,44
2	7,57	8,35	5,95	5,49	5,90	5,24	6,42	1,13
3	9,49	2,30	2,21	2,09	2,31	11,02	4,90	3,81
4	2,38	2,06	2,15	3,02	2,00	2,44	2,34	0,34
5	2,20	1,92	1,81	1,89	1,95	2,14	1,98	0,13
6	1,93	2,05	1,78	1,81	1,88	1,92	1,90	0,108
7	1,89	1,79	1,80	1,79	1,90	1,83	1,83	0,04

TABLE 6.10 Final roughnesses Aq for workpiece 6

It is noticeable that the Aq values are almost the same for every workpiece, except for workpiece 5 that shows higher values in the beginning of the process but presents the same final roughness after 160 passes. This is probably influenced by the starting roughness of workpiece 5 that resulted a bit higher when measured with Optosurf compared to the other workpieces. A higher final roughness is, instead, present in workpiece 3. In this second case there is not any relationship with the starting roughness.

Below a comparison between the results obtained with WLI and Optosurf is presented showing on the same graph both the curves for the roughness behavior in Ra and Aq as the range of the values are similar, a single Y axis is used both Ra and Aq.

On the X axis there is the number of passes and on the Y axis there are the Ra value in nanometers and the Aq value together with the standard deviation for each point.

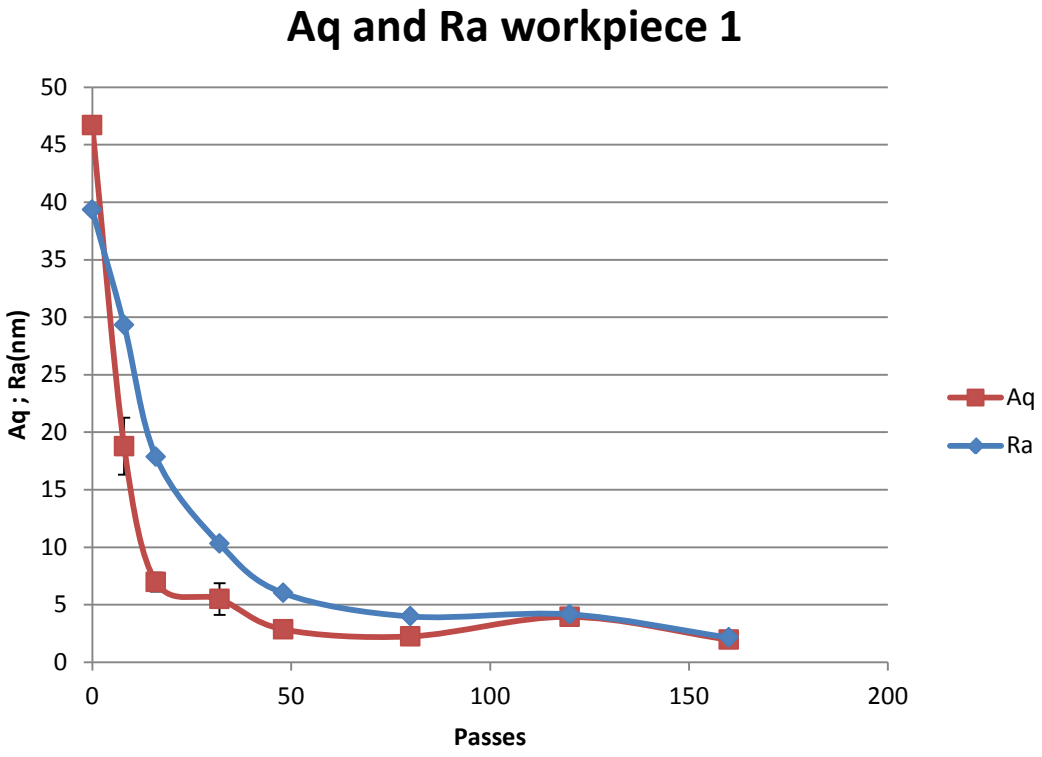

FIGURE 6.6 Comparison between Optosurf measurements and WLI for 160 passes for workpiece 1

Points represent the average of 6 measurements. Error bars are covered by the data markers

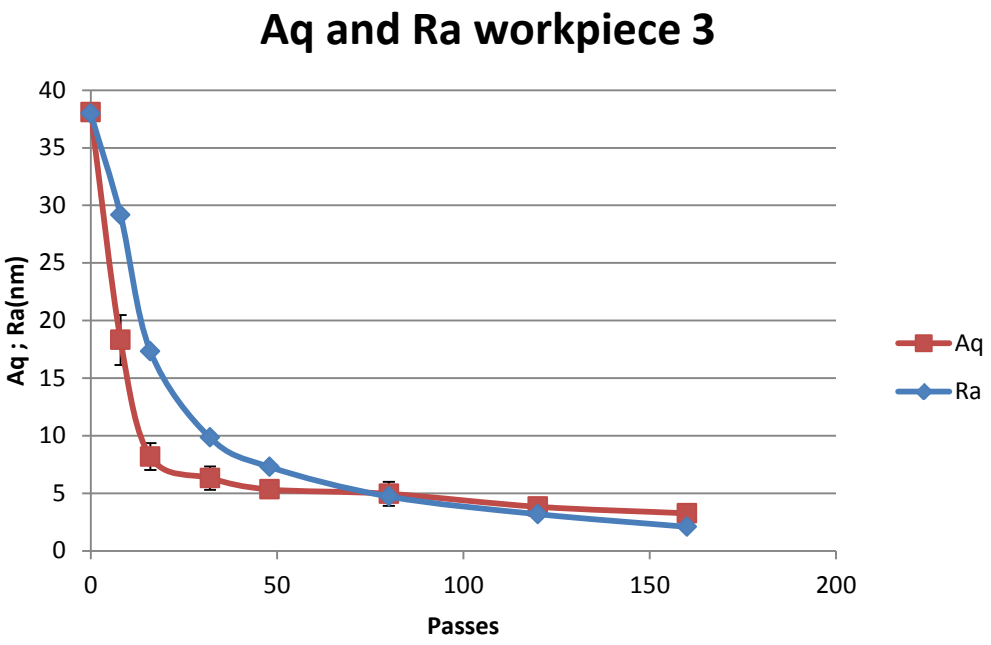

FIGURE 6.7 Comparison between Optosurf measurements and WLI for 160 passes for workpiece 3

Points represent the average of 6 measurements. Error bars are covered by the data markers

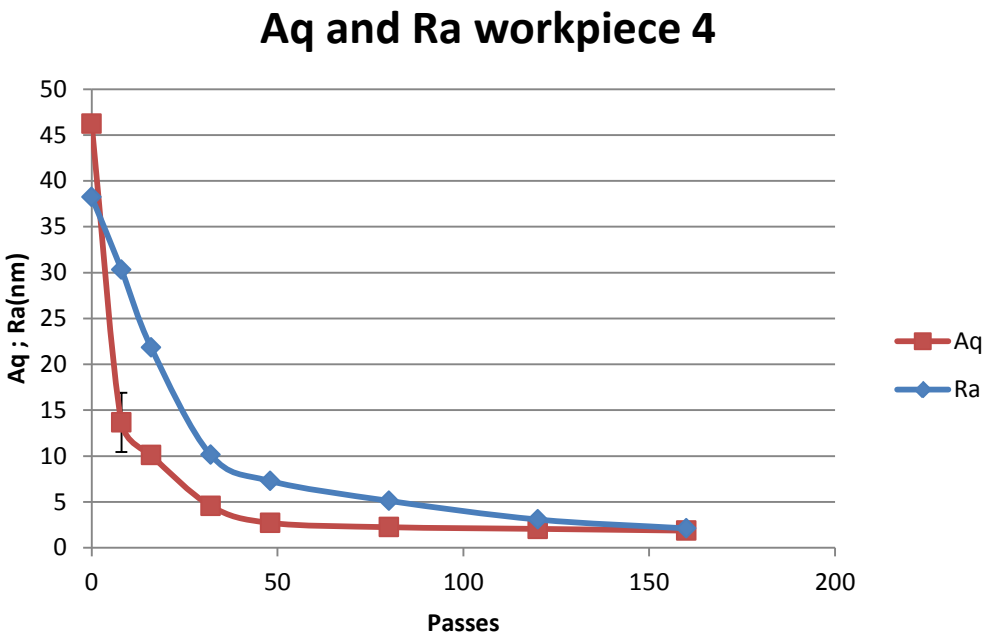

FIGURE 6.8 Comparison between Optosurf measurements and WLI for 160 passes for workpiece 4

Points represent the average of 6 measurements. Error bars are covered by the data markers

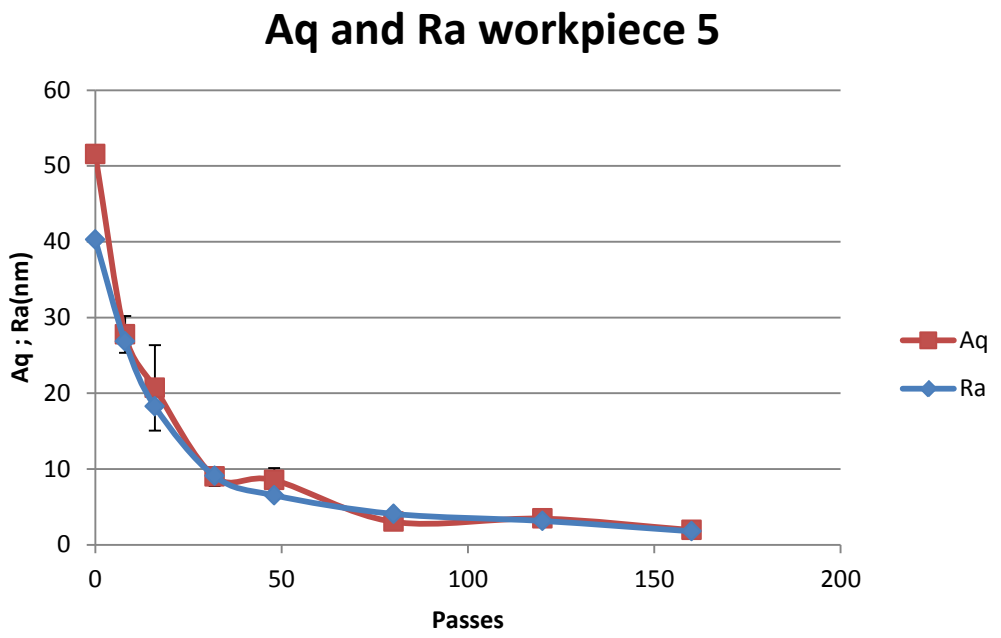

FIGURE 6.9 Comparison between Optosurf measurements and WLI for 160 passes for workpiece 5

Points represent the average of 6 measurements. Error bars are covered by the data markers

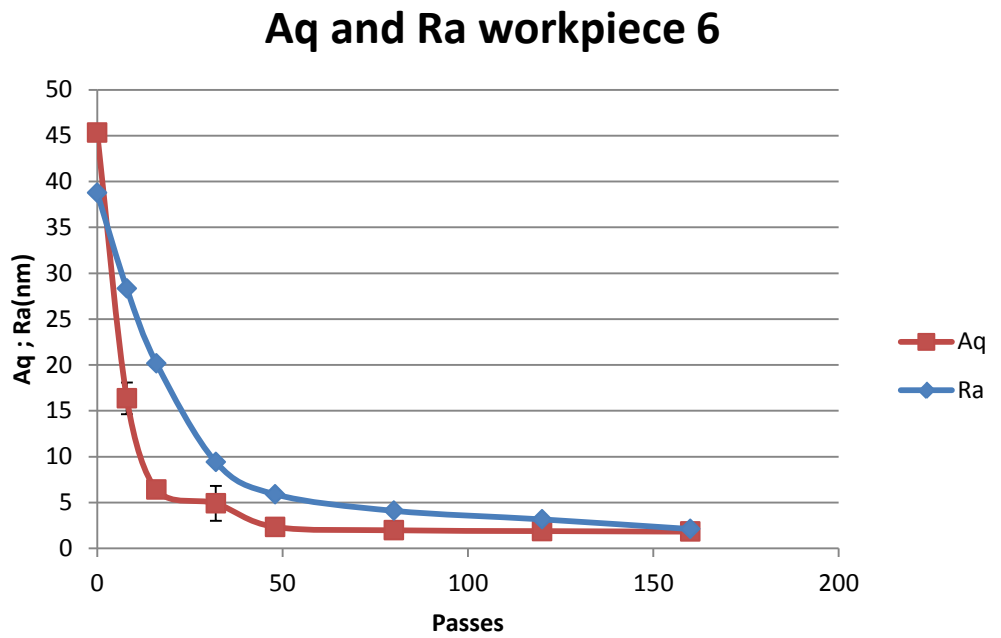

FIGURE 6.10 Comparison between Optosurf measurements and WLI for 160 passes for workpiece 6

Points represent the average of 6 measurements. Error bars are covered by the data markers

From the graphs above it is clear that there is a strong correlation between the Ra values measured with WLI and the Aq values measured with Optosurf.

Even if there is not a 1:1 ratio between Ra and Aq it is possible to state that the behavior of Aq parameter is extremely connected with the Ra parameter for the definition of the surface roughness in this range of values and for this type of surfaces..

For almost all the curves, except for workpiece 3, one can see that the point where the slope changes in a clear manner is almost in the same position for both the curves, around 40 passes. This means that both the instruments have detected the same improvement ratio if the slope of the curve is taken as index of the speed of improvement of the surface roughness. It is noticeable that the Aq tends to drop earlier, in the “rougher” part of the process.

Below are showed the graph that correlate directly the Ra values and the Aq values, with a trend line and the Correlation factor value for each workpiece.

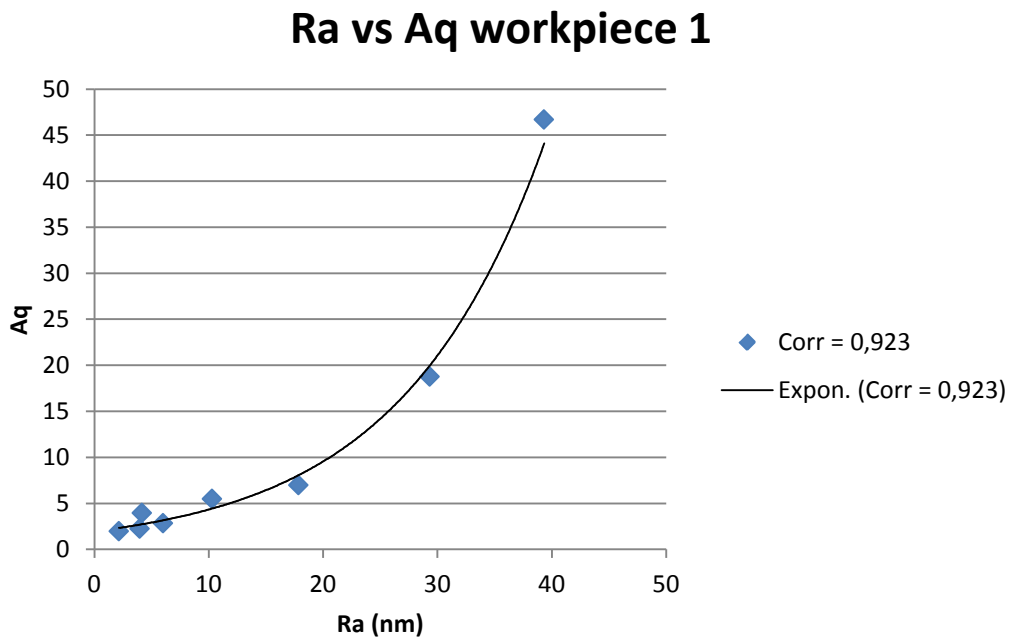

FIGURE 6.11 Correlation between Ra and Aq for workpiece 1

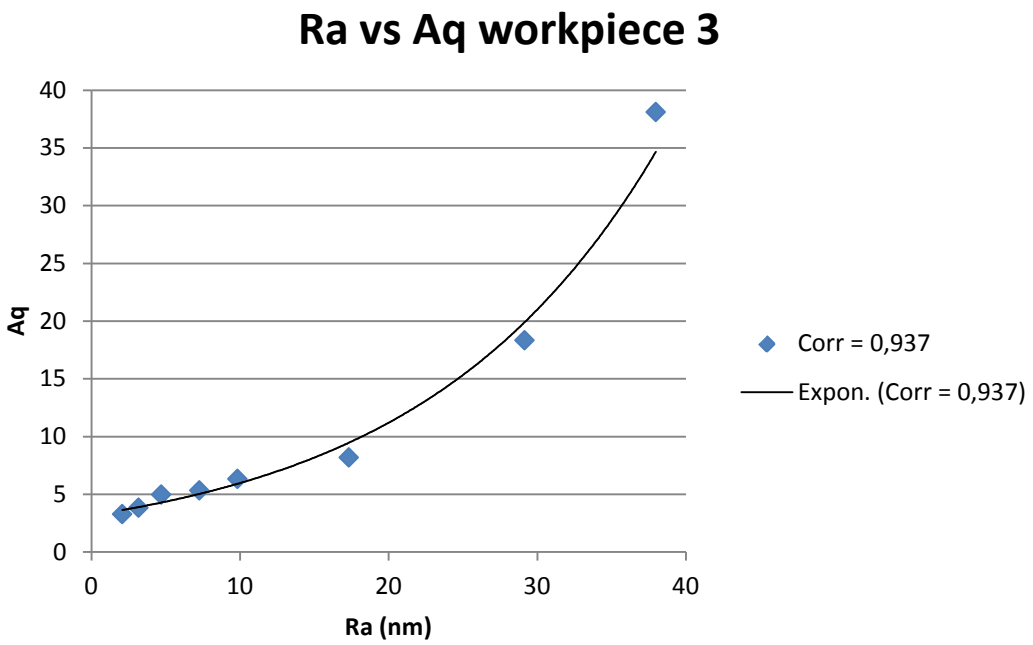

FIGURE 6.12 Correlation between Ra and Aq for workpiece 3

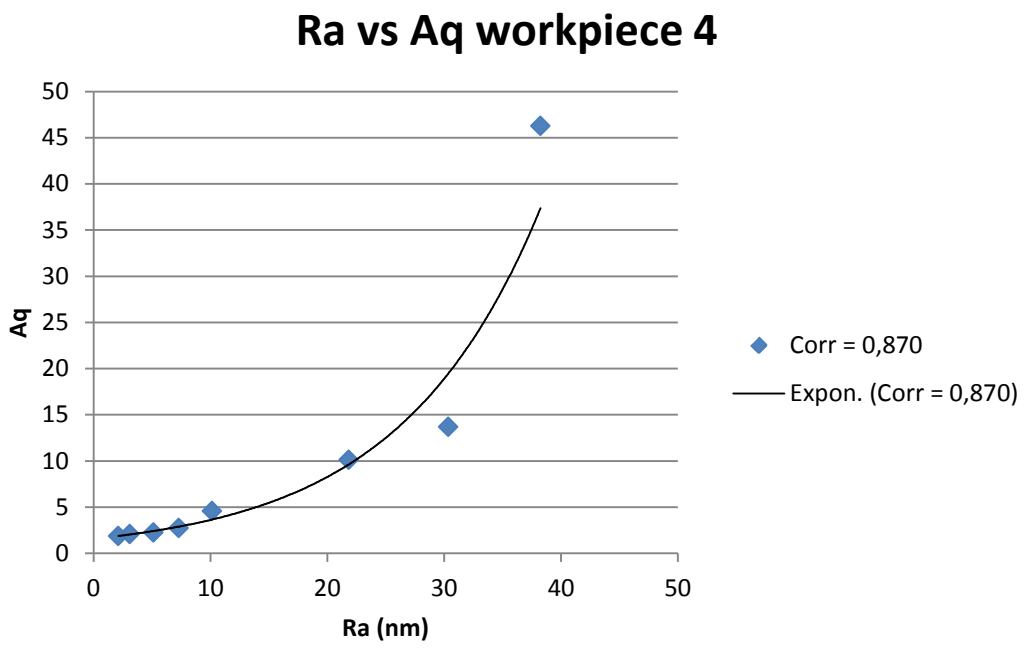

FIGURE 6.13 Correlation between Ra and Aq for workpiece 4

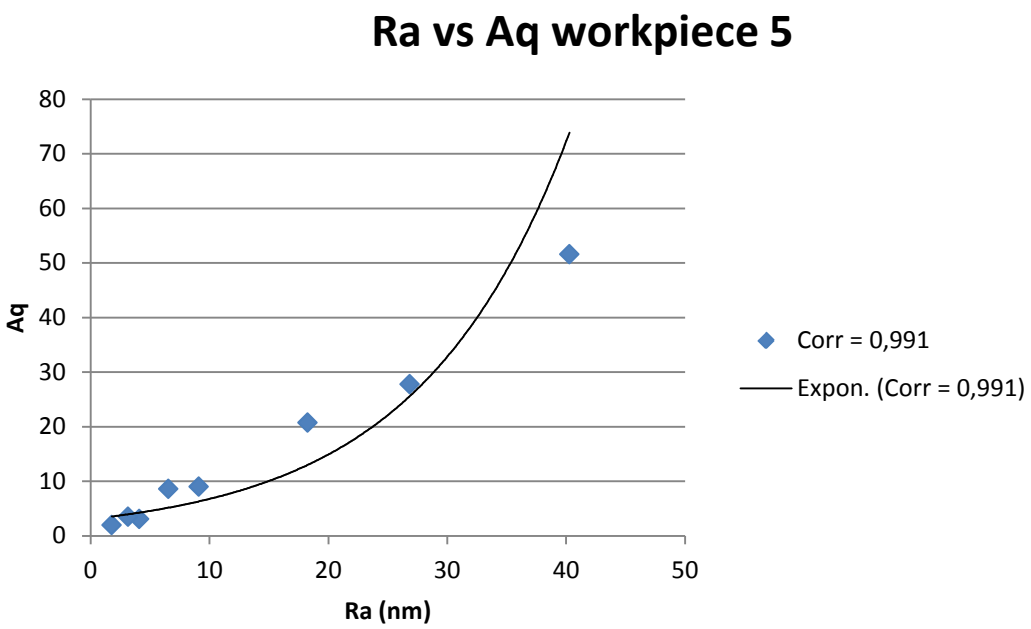

FIGURE 6.14 Correlation between Ra and Aq for workpiece 5

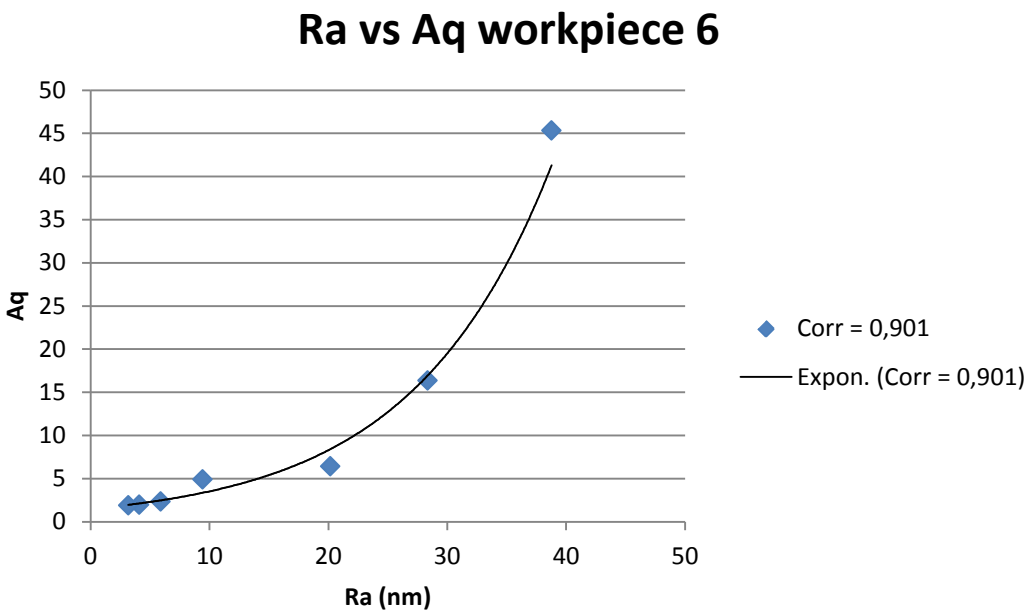

FIGURE 6.15 Correlation between Ra and Aq for workpiece 6

In conclusion it is possible to say that the process itself is validated by the White Light Interferometer showing the typical roughness behavior expected for a polished surface and that Optosurf is validated as well as instrument to measure the surface roughness in this range of values (average correlation factor 0,925) and its repeatability even in less controlled conditions compared to the preliminary tests. It must be remembered that the alignment of Optosurf was made manually.

6.2 Forces

The correlation between the force signals and the roughness values measured with WLI are now presented for the total polishing work of 160 passes, corresponding to 2000 seconds.

The force, acquired in the direction of the oscillation with a sampling rate of 3 kHz, present a rough behavior shown in Figure 6.16.

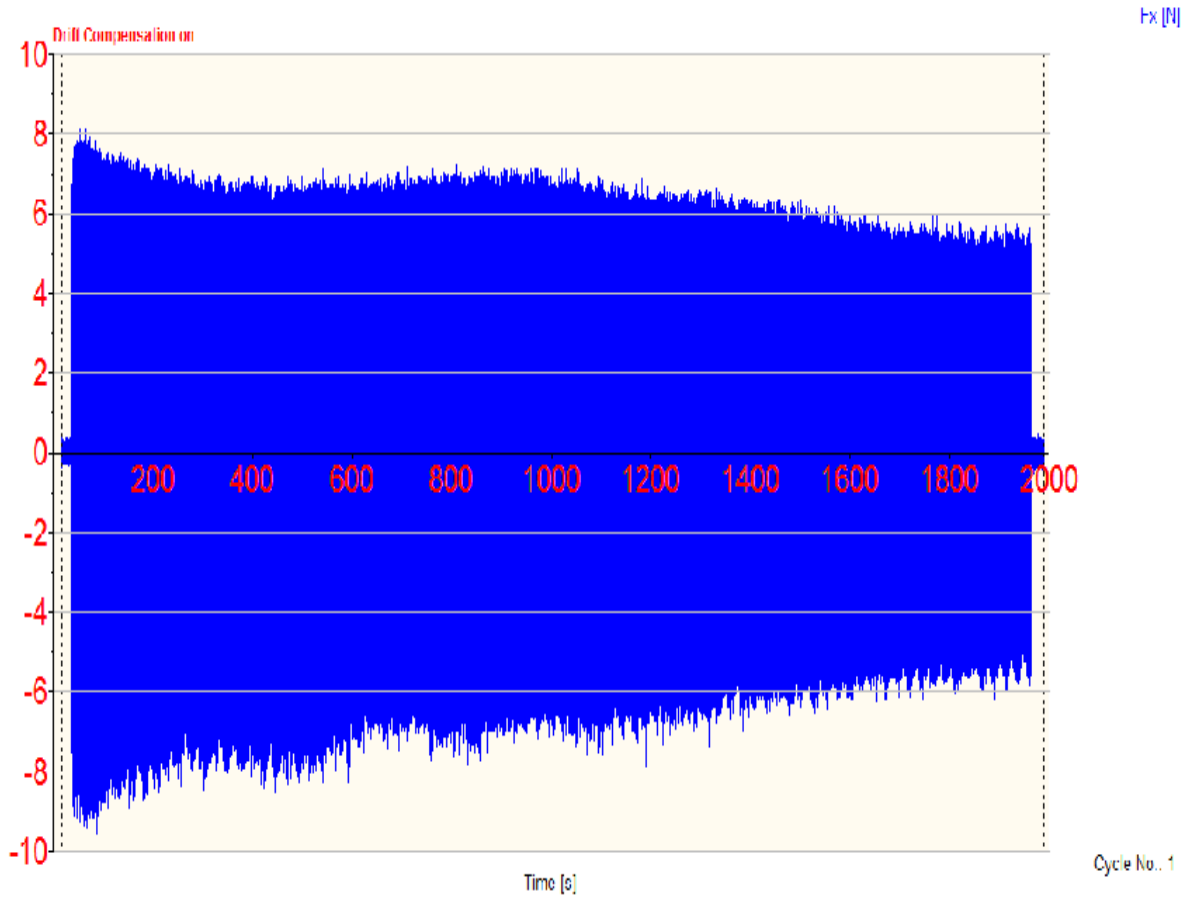

FIGURE 6.16 Rough signal from force for 160 passes for workpiece 3

It’s noticeable a decrease of the signal amplitude from the beginning of the process to the end of it from about 7 N down to 4N. This behavior makes sense that a correlation is actually present.

In order to better understand if the trend in force signal corresponds with the one in surface roughness some post processing was made on these rough data to find out the envelope of the curve and compare it with the curve of the Ra.

Using MATLAB from the bare signal the absolute value was calculated. Data smoothing by means of moving average with window size of 1000 data samples was applied to the acquired force signal . [22], [34]

The application of moving average system provides smooth approximation of the process trend reflected in forces data which can be directly correlated with the polishing process progression.

A trend reflecting the surface progression in polishing process is highlighted by spline fitting of measured average surface roughness Ra for direct evaluation of a relative correlation with the trend in Force data.

Below a comparison between the results obtained with WLI and Forces are presented showing on the same graph both the curves for the roughness behavior in Ra and the forces.

On the X axis there is the time in seconds and on the Y axis there are the Ra value in nanometers and the force in Newton.

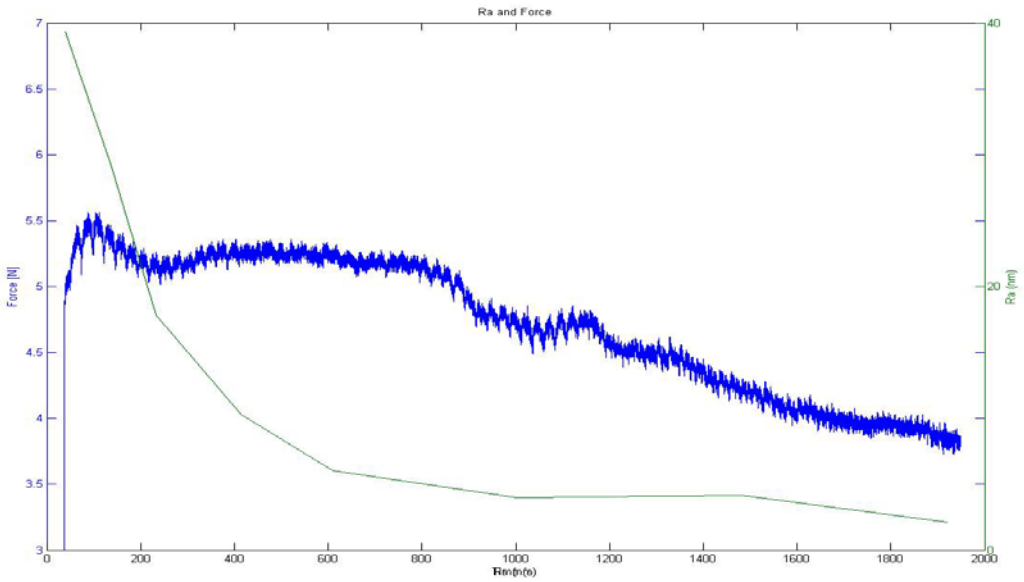

FIGURE 6.18 Correlation between forces and Ra for 160 passes for workpiece 1

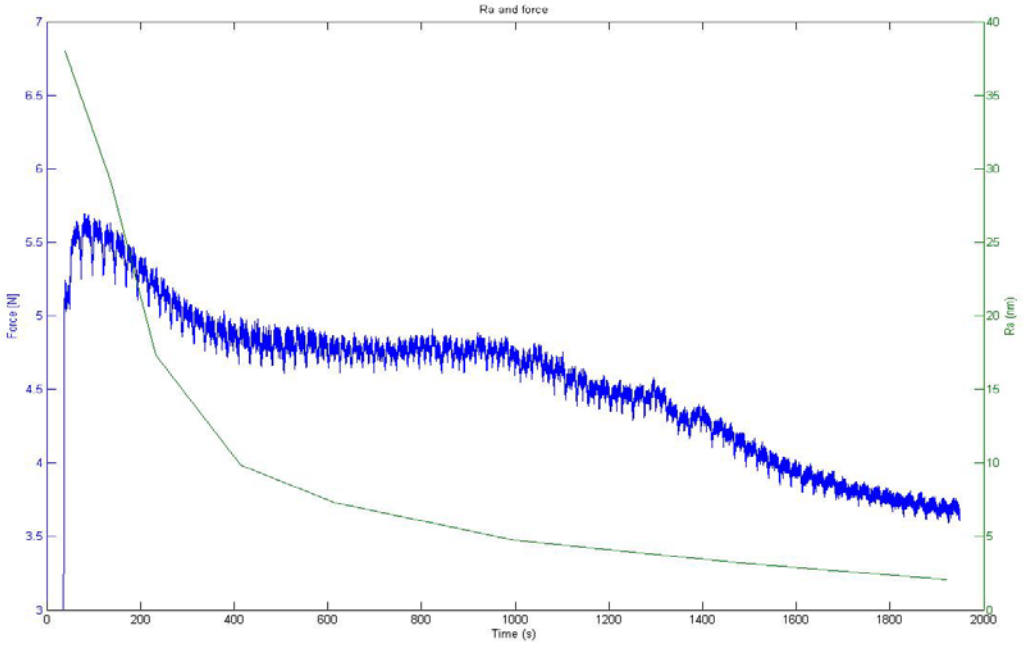

FIGURE 6.19 Correlation between forces and Ra for 160 passes for workpiece 3

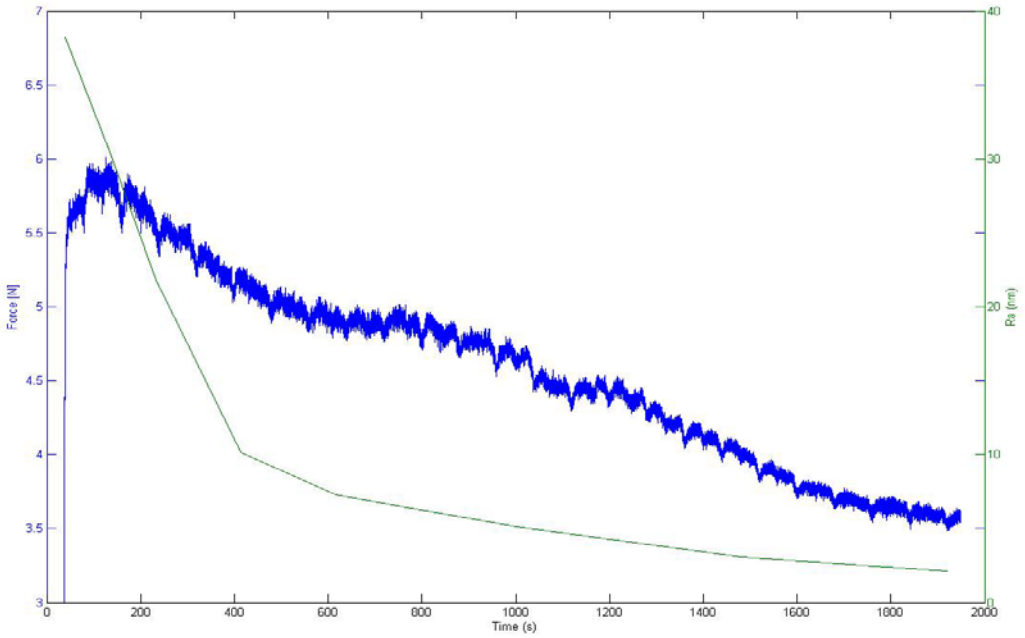

FIGURE 6.20 Correlation between forces and Ra for 160 passes for workpiece 4

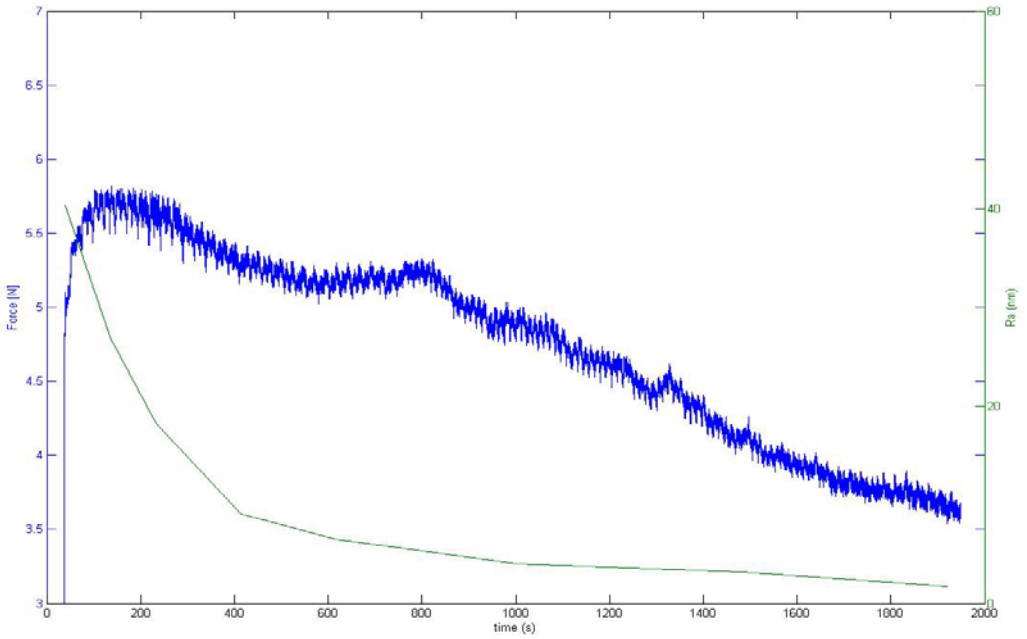

FIGURE 6.21 Correlation between forces and Ra for 160 passes for workpiece 5

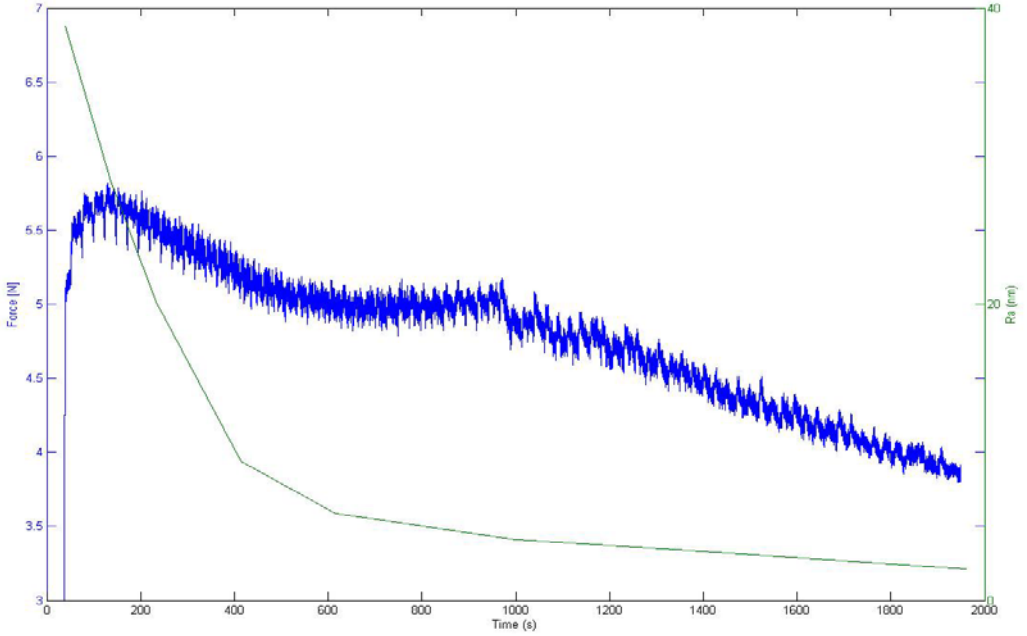

FIGURE 6.22 Correlation between forces and Ra for 160 passes for workpiece 6

For workpiece 1 it is noticeable that the forces follow the Ra curve in the beginning and in the end of the polishing process. The middle part from about 250 seconds to 1600 second doesn't follow at all the surface roughness curve.

For workpieces 3, 4 and 6 the situation is better, the force curve is closer to the Ra curve,specially for workpiece 4. Workpiece 5 shows a behavior similar to workpiece 1.

It is possible to state that the intensity of forces decrease significantly from the beginning of the process to the end of it, but the curve does not follow the behavior of the roughness of the surface.

Below are showed the graphs that correlate directly the Ra values and forces, with a trend line and the correlation factor value for each workpiece.

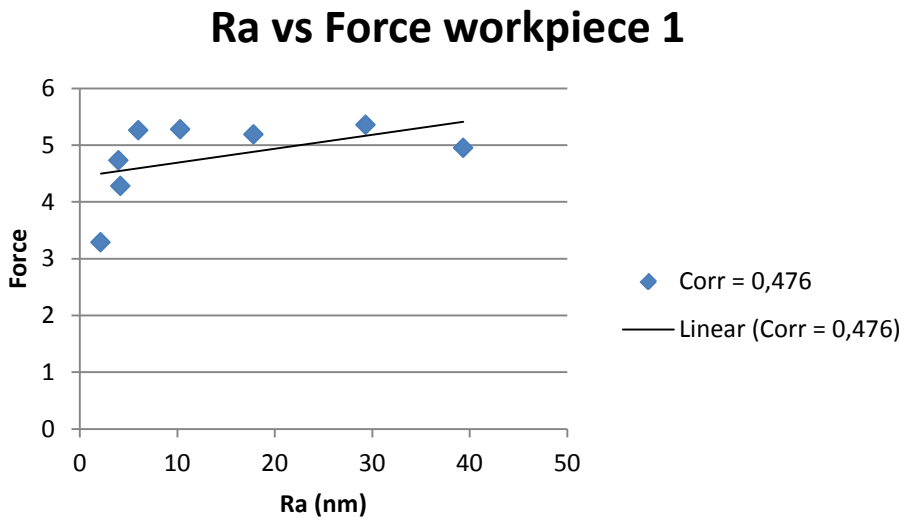

FIGURE 6.23 Correlation between Ra and forces for workpiece 1

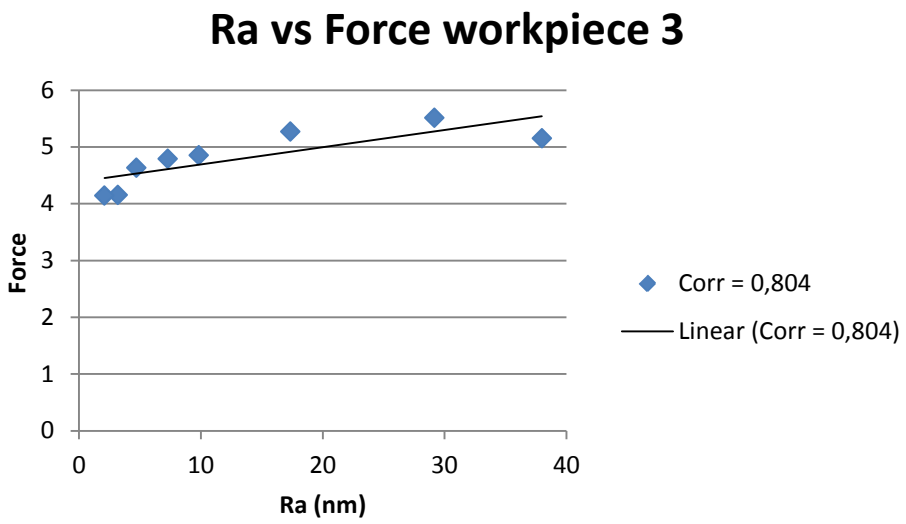

FIGURE 6.24 Correlation between Ra and forces for workpiece 3

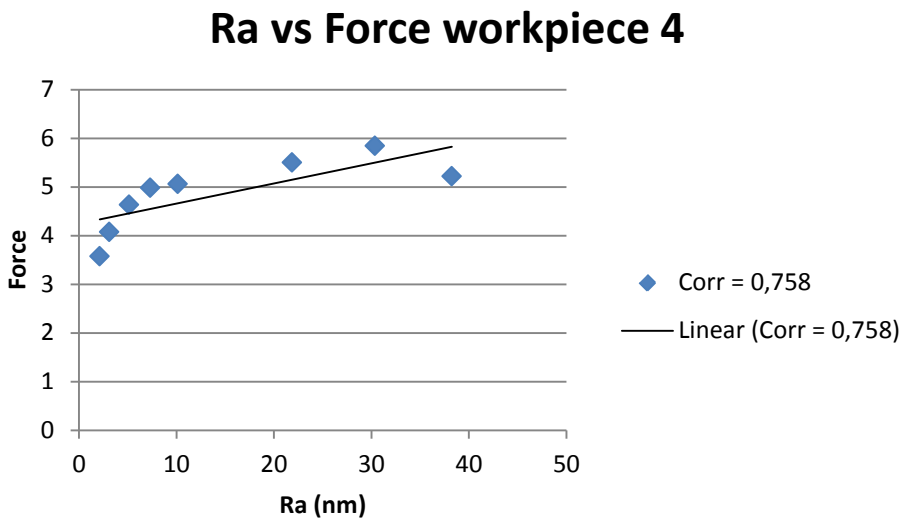

FIGURE 6.25 Correlation between Ra and forces for workpiece 4

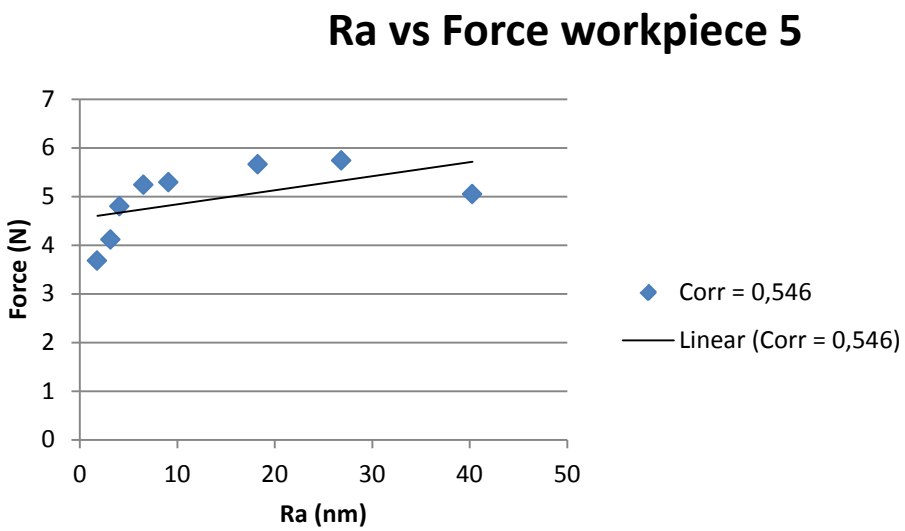

FIGURE 6.26 Correlation between Ra and forces for workpiece 5

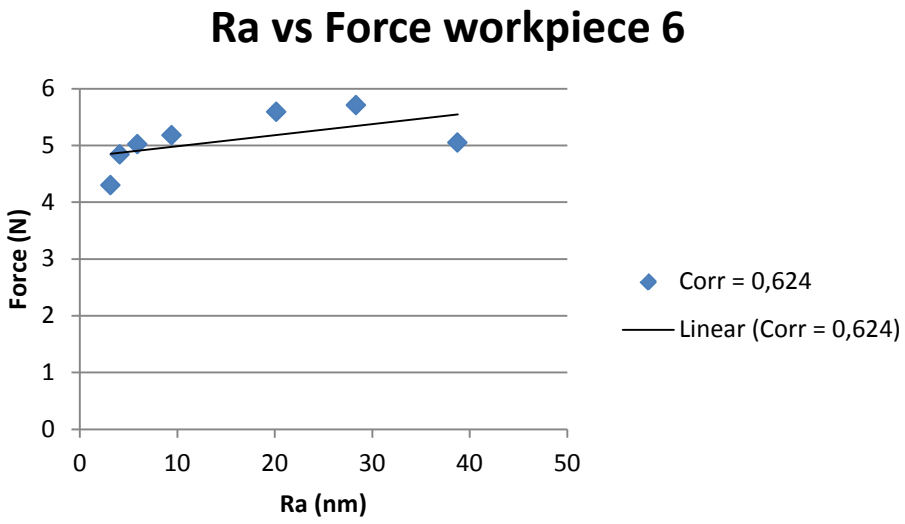

FIGURE 6.27 Correlation between Ra and forces for workpiece 6

The repeatability of the measurement is really good but one cannot then define a direct 1:1 correlation between the curve of forces and roughness curve. The curve of forces presents a more linear trend, different from the one noticeable in the Ra curve. It is not noticeable a stabilization in the end of the process. The average correlation factor is 0,642.

Graph with the correlation between forces and Ra for different amount of passes are in Appendix G.

6.3 Acoustic Emission

The correlation between the Acoustic emission signals and the roughness values measured with WLI are now presented for the total polishing work of 160 passes.

The AE is acquired using a sampling interval of 640 ns resulting in a sampling rate of 1,5625 MHz. The signal is acquired for both the sensors by intermittent sampling every 6 seconds for 10^5 points, because a continuous acquisition would have been too heavy and not manageable in post processing. AE is according to literature in ultrasound frequency range, AE sensor used measures frequency up to 0,5 Mhz. Taking into account Nyqist theorem 1,562 MHz sampling frequency was chosen to avoid signal aliasing and loss of signal amplitude.

The AE sensor R15 from Mistras is connected with an analogue signal preamplifier 20/40/60 C (PAC) with built-in band-pass filtering in a range of 20 kHz to 1.2 MHz using 60 dB signal gain. Then it was connected with Picoscope 3206 oscilloscope. The BV100 was, instead, directly connected with Picoscope 3206 Oscillocope without any analogue filtering.

During the post processing all the different acquisitions segments were merged together to create continuous signal using a MATLAB function ad hoc.

Due to computational limits the signal was imported subsampling the original signal by factor ten.

Using MATLAB from the bare signal, the power was calculated, this elevating it to the square. Then was applied a function that finds the peaks in the signal using a window of 1000 samples. This width of the window was set crosschecking the rough signal and evaluating how many samples were needed to enclose an acoustic emission burst.

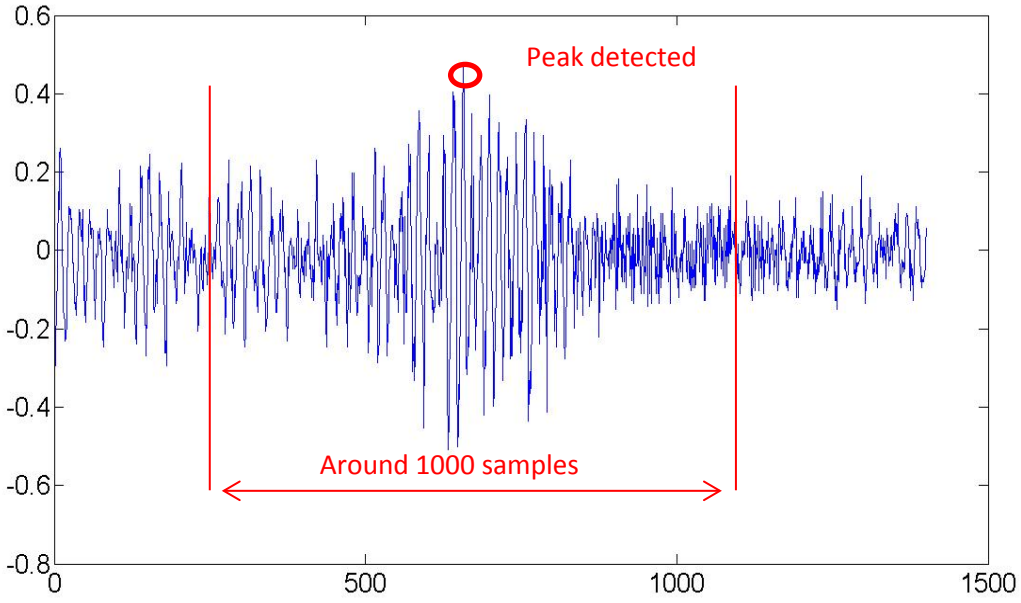

FIGURE 6.28 A burst presents in acoustic emission signal

Data smoothing by means of moving average system with window size of 1000 data samples was applied to the acquired AE signal power. The application of moving average system provides smooth approximation of the process trend reflected in forces data which can be directly correlated with the polishing process progression.[22], [34]

A trend reflecting the surface progression in polishing process is highlighted by spline fitting of measured average surface roughness Ra for direct evaluation of a relative correlation with the trend in AE data.

Below a comparison between the results obtained with WLI and Acoustic emission are presented showing on the same graph both the curves for the roughness behavior in Ra and the AE. First will be displayed charts dealing with R15 Mistras sensor and then the ones dealing with BV100 Montronix sensor.

6.3.1 R15 by Mistras

On the X axis there is a samples counter with respect to which the values of the time were normalized and on the Y axis there are the Ra value in nanometers and the AE power in V^2.

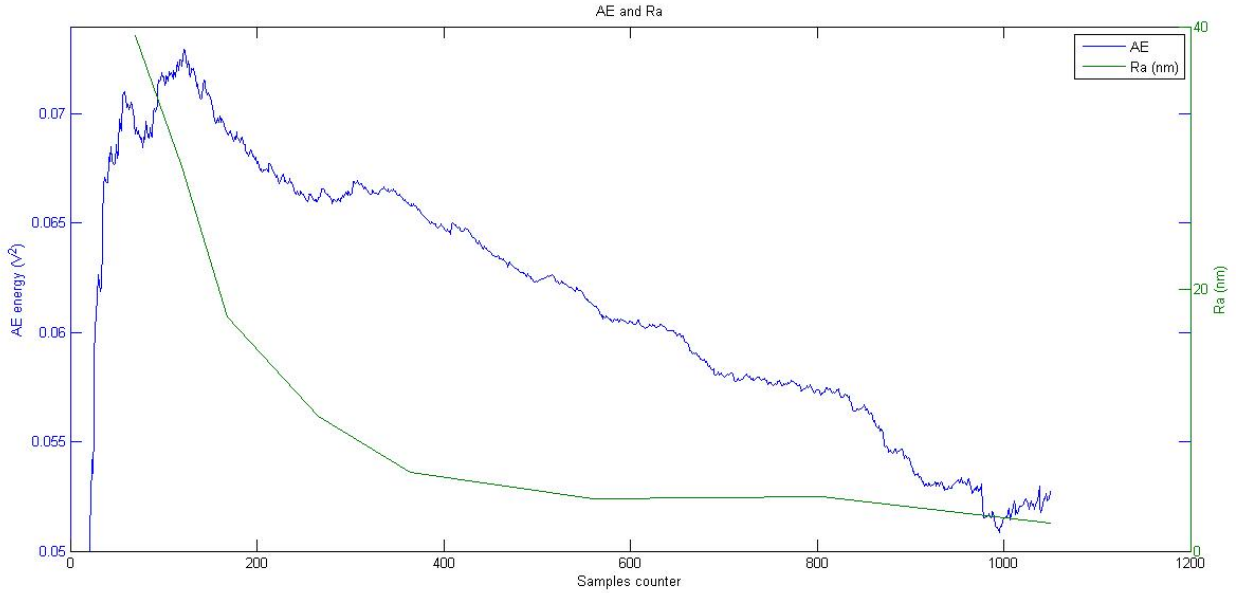

FIGURE 6.29 Correlation between AE and Ra for 160 passes for workpiece 1 (R15 Mistras sensor)

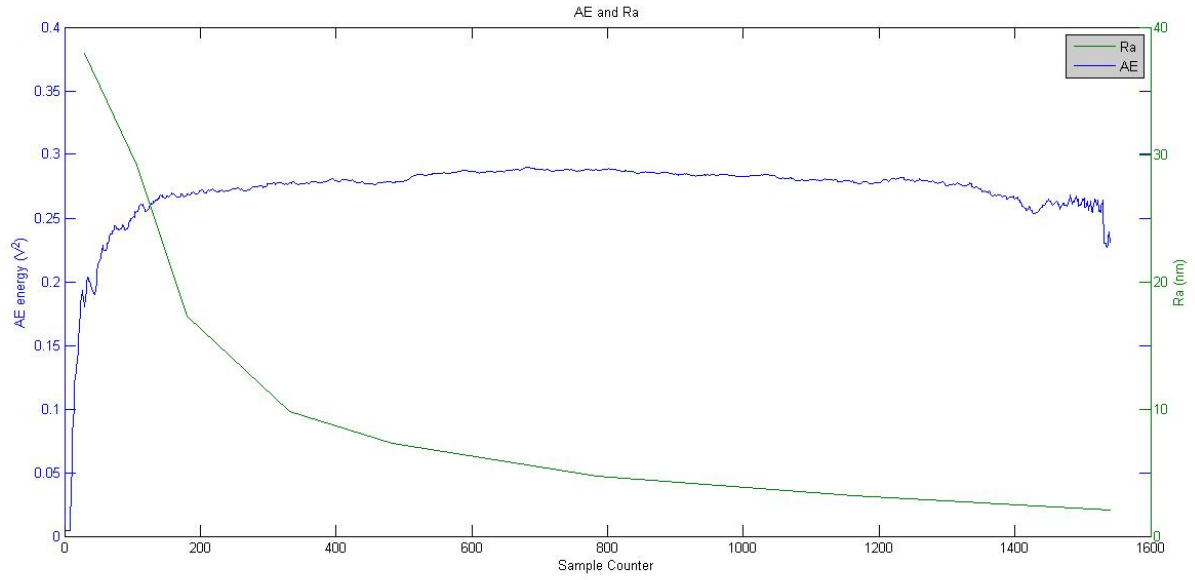

FIGURE 6.30 Correlation between AE and Ra for 160 passes for workpiece 3 (R15 Mistras sensor)

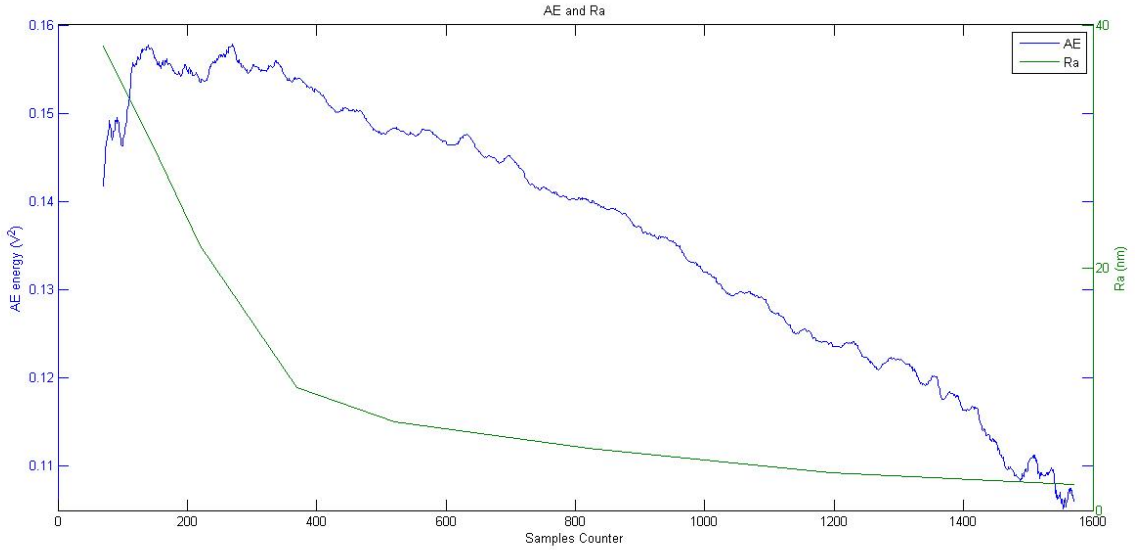

FIGURE 6.31 Correlation between AE and Ra for 160 passes for workpiece 4 (R15 Mistras sensor)

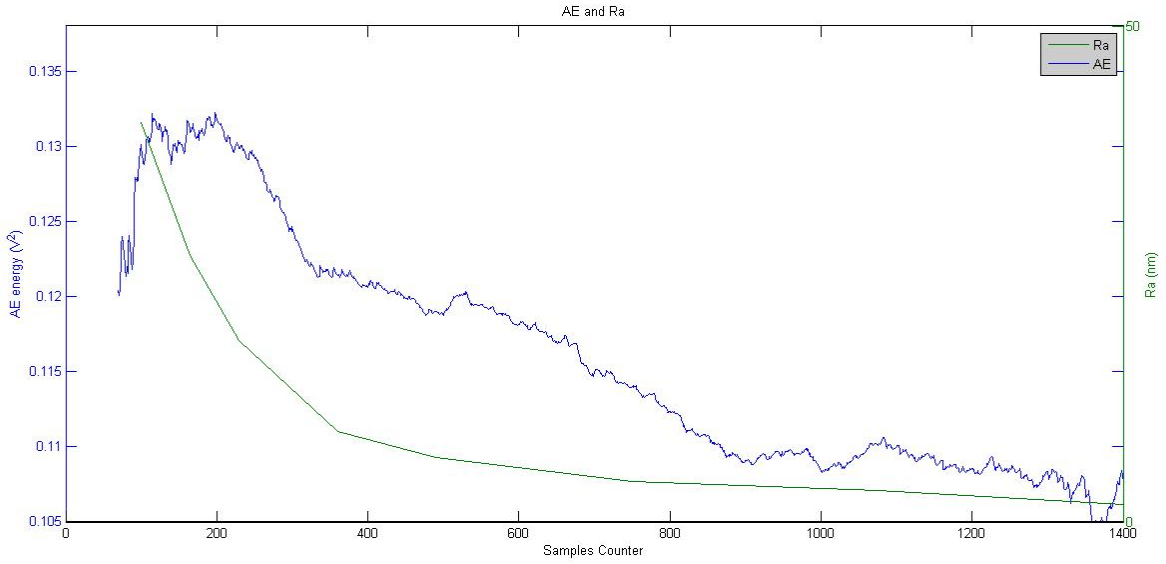

FIGURE 6.32 Correlation between AE and Ra for 160 passes for workpiece 5 (R15 Mistras sensor)

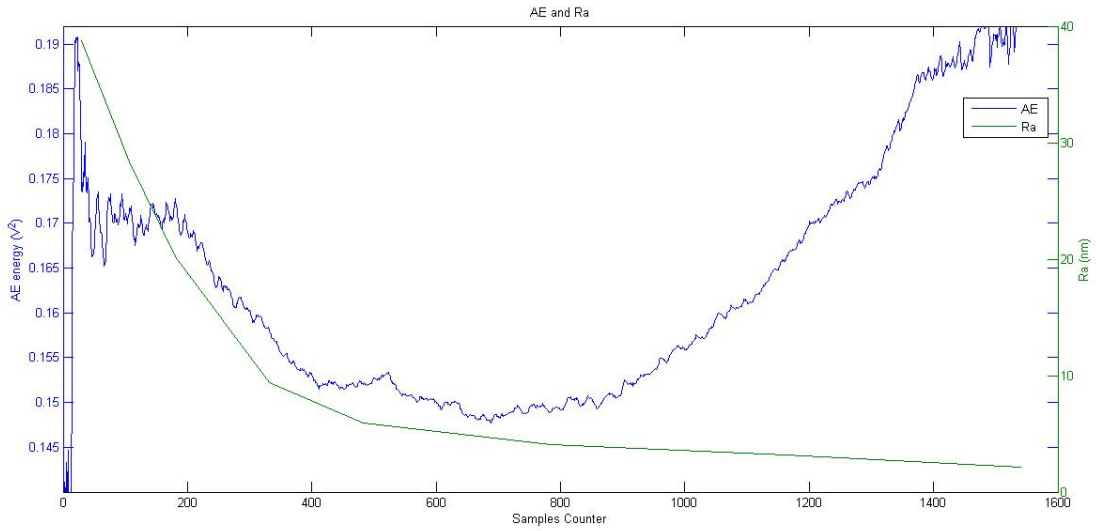

FIGURE 6.33 Correlation between AE and Ra for 160 passes for workpiece 6 (R15 Mistras sensor)

It is noticeable that there is not a constant behavior of the acoustic emission signal for all the workpieces. Workpieces 1, 4 and 5 present a similar trend with a linear decrease from the beginning of the process to the end of it. On the other hand workpiece 3 presents a behavior completely different underlining a constant signal throughout the whole process. At last workpiece 6 shows a decrease until the middle of the process and then an increase where the signal at the end of the process presents almost the same values compared to the beginning.

Below are showed the graphs that correlate directly the Ra values and the AE power in V^2, with a trend line and the correlation factor value for each workpiece.

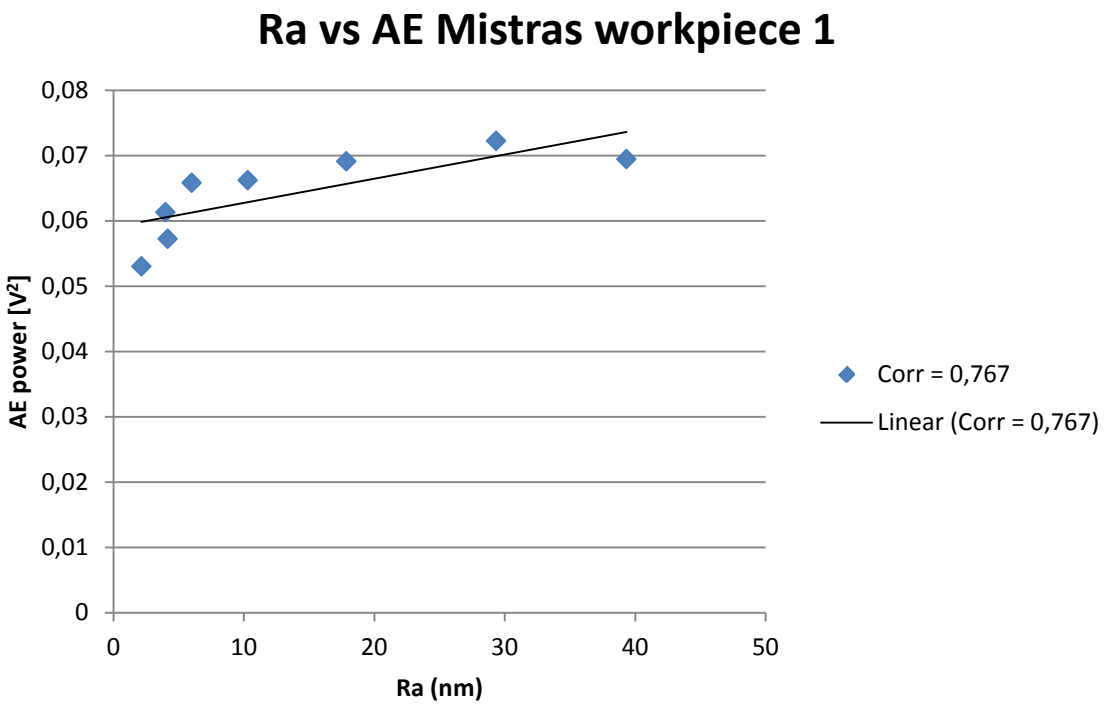

FIGURE 6.34 Correlation between Ra and AE for workpiece 1

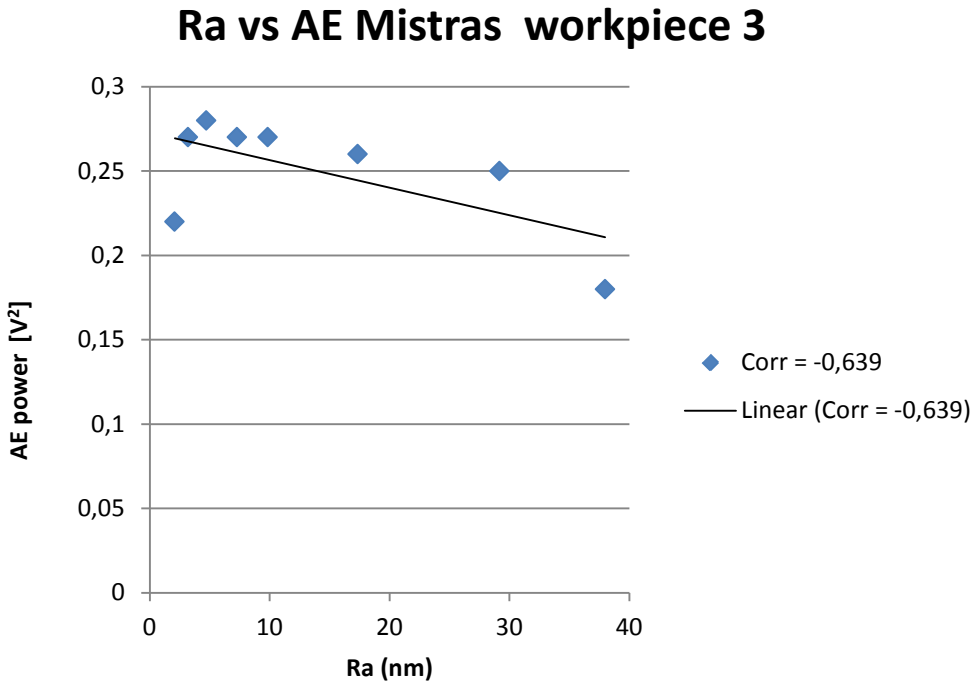

FIGURE 6.35 Correlation between Ra and AE for workpiece 3

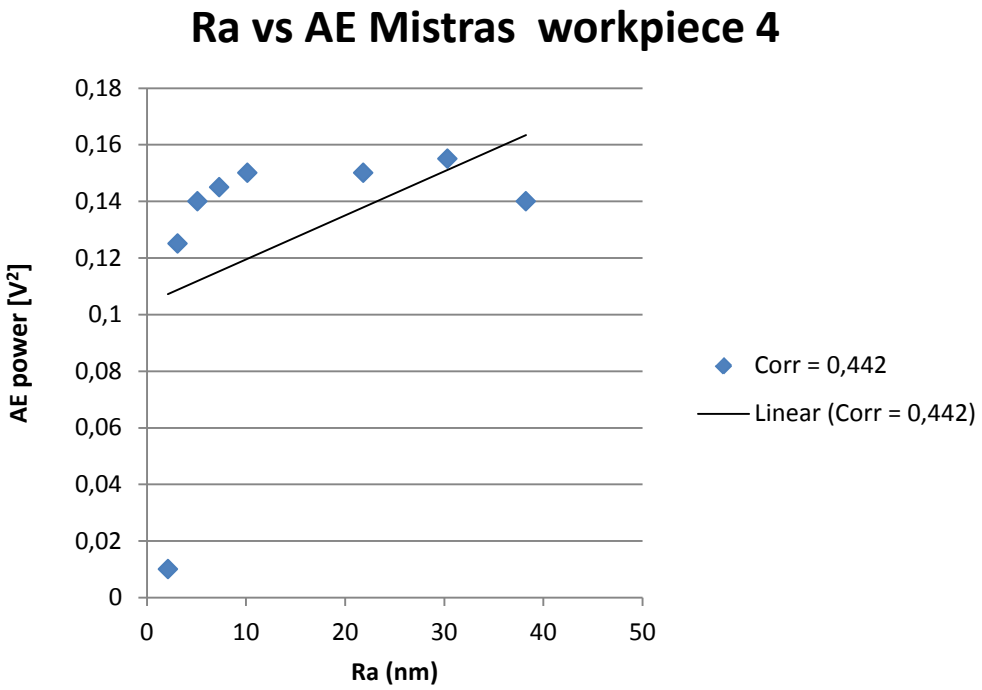

FIGURE 6.36 Correlation between Ra and AE for workpiece 4

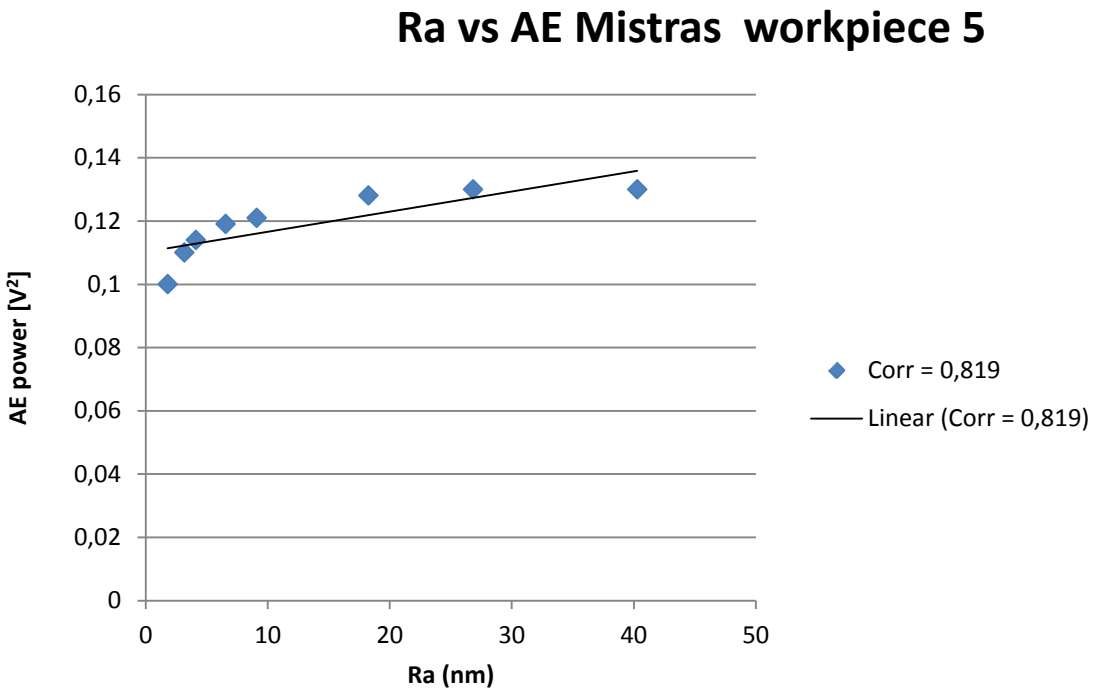

FIGURE 6.37 Correlation between Ra and AE for workpiece 5

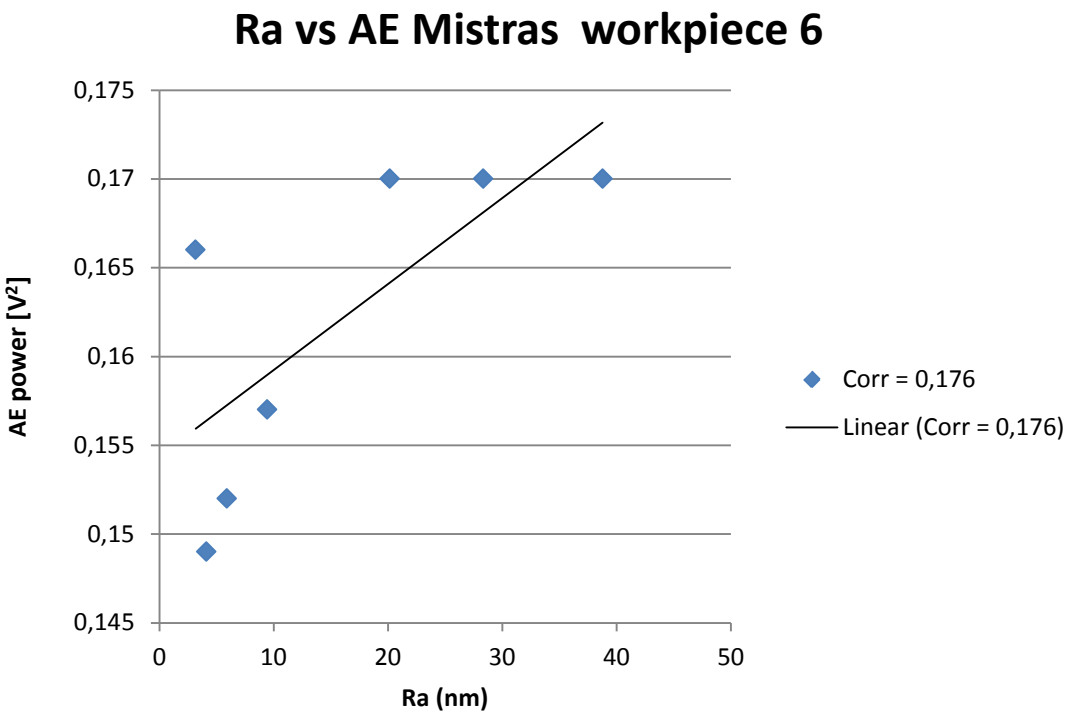

FIGURE 6.38 Correlation between Ra and AE for workpiece 6

This non repeatable behavior of the AE does not allow defining a reliable correlation to monitor the diamond polishing process with this sensor. Average correlation factor is 0,313.

6.3.2 BV100 by Montronix

From a quick view of the signal acquired with the Montronix sensor it is noticeable that in this case the signal looks to increase with the progression of the process.

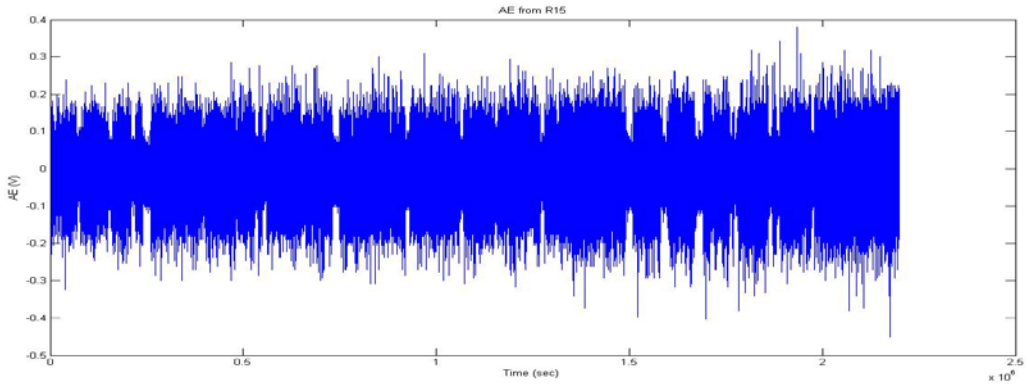

FIGURE 6.39 Rough signal from BV100 for 160 passes sub-sampled

Following the same analysis performed for the signal acquired with R15, the results collected from BV100 are now shown below. On the X axis there is a samples counter with respect to which the values of the time were normalized and on the Y axis there are the Ra value in nanometers and the AE.

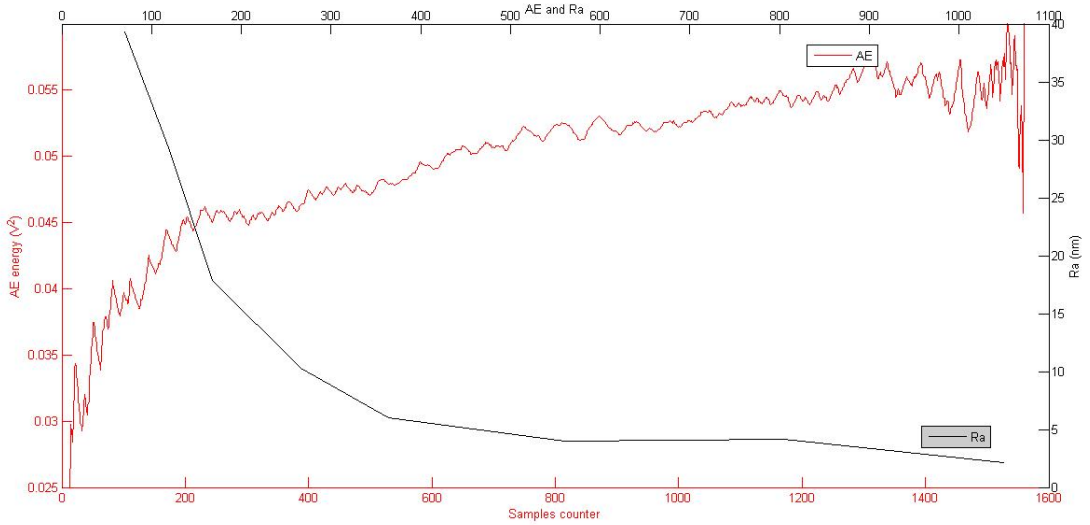

FIGURE 6.40 Correlation between AE and Ra for 160 passes for workpiece 1 (BV100 Montronix sensor)

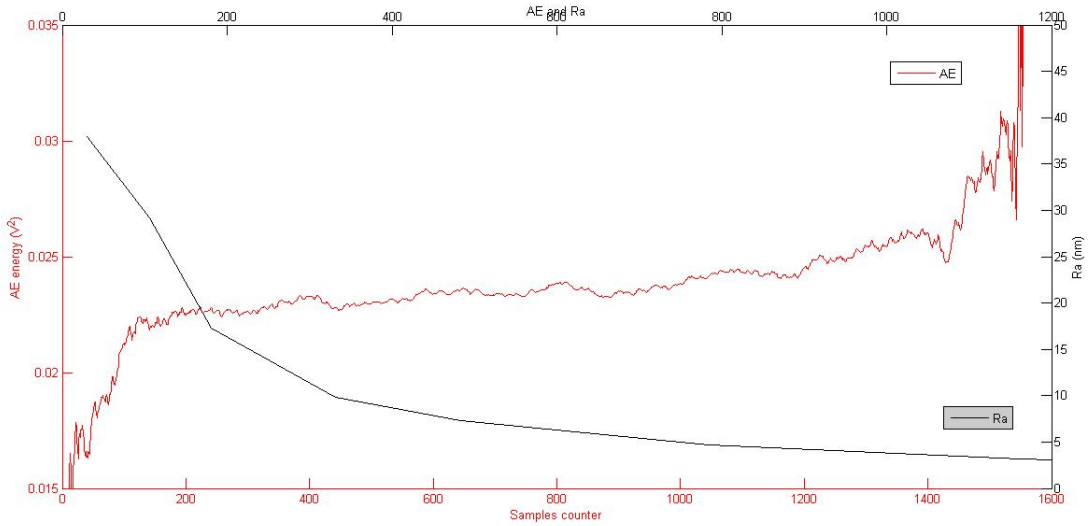

FIGURE 6.41 Correlation between AE and Ra for 160 passes for workpiece 3 (BV100 Montronix sensor)

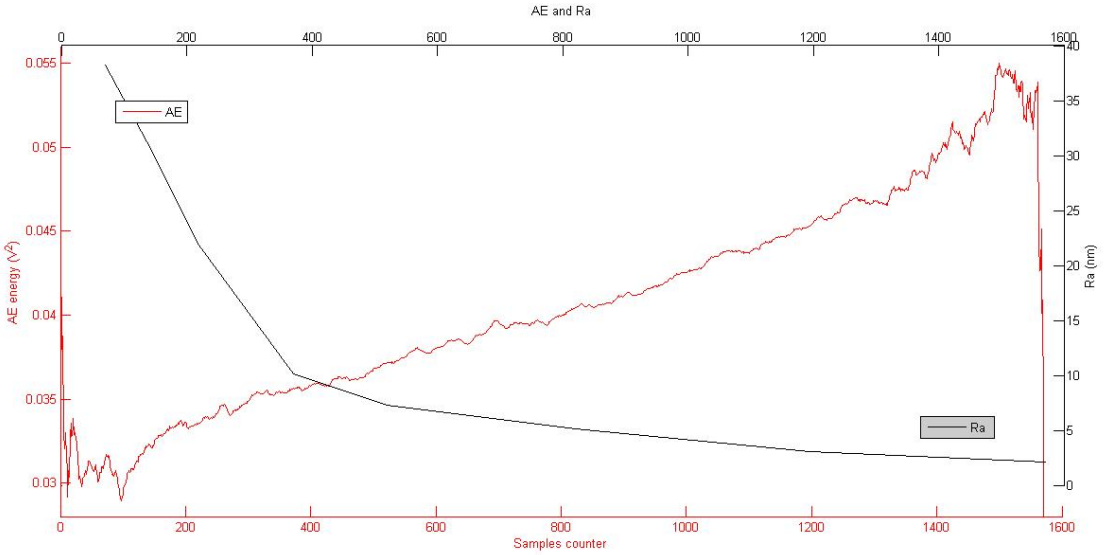

FIGURE 6.42 Correlation between AE and Ra for 160 passes for workpiece 4 (BV100 Montronix sensor)

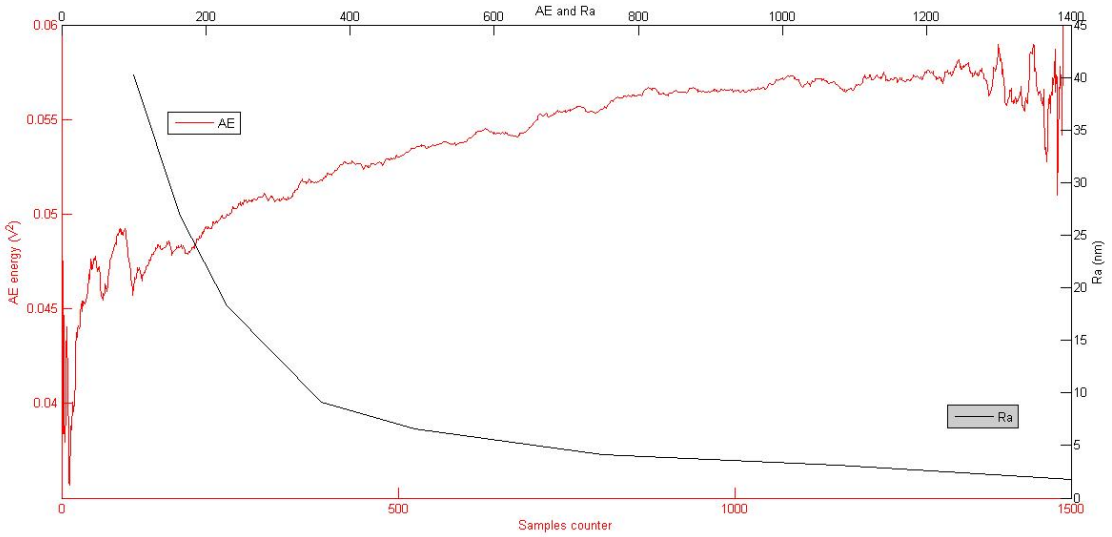

IGURE 6.43 Correlation between AE and Ra for 160 passes for workpiece 5 (BV100 Montronix sensor)

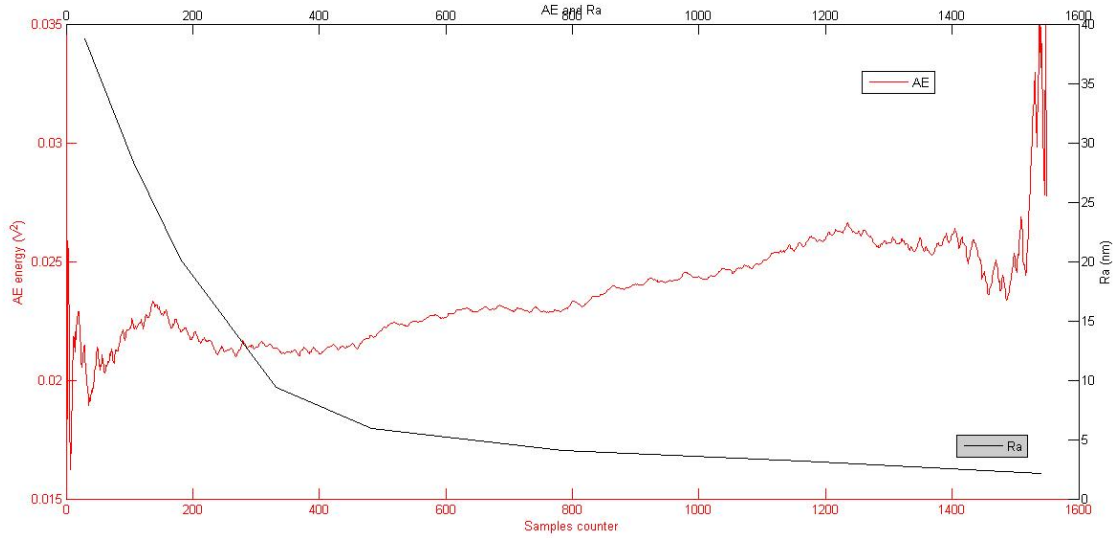

FIGURE 6.44 Correlation between AE and Ra for 160 passes for workpiece 6 (BV100 Montronix sensor)

It is noticeable that even in this case the behavior of the AE curve is not repeatable over the different workpieces and above all the trend is completely the opposite, showing a clear and deep increment in the signal acquired.

Below are showed the graphs that correlate directly the Ra values and the AE power, with a trend line and the correlation factor value for each workpiece.

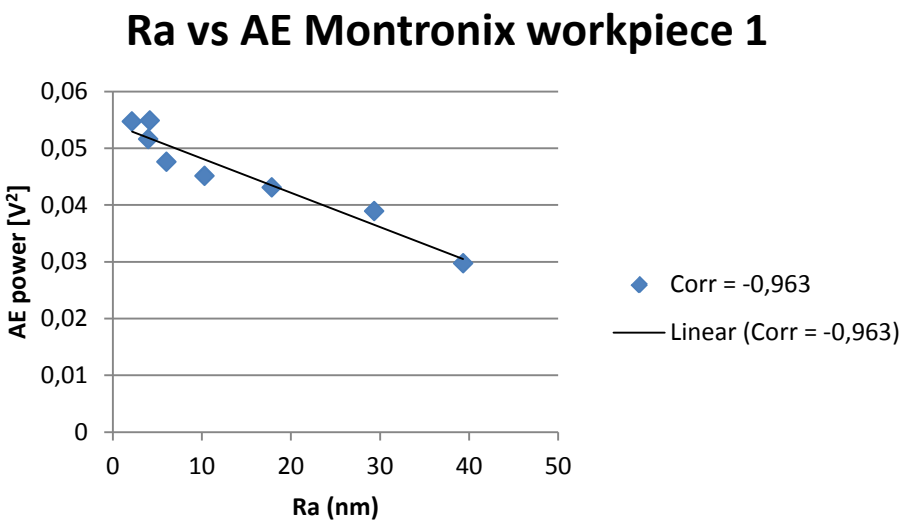

FIGURE 6.45 Correlation between Ra and AE for workpiece 1

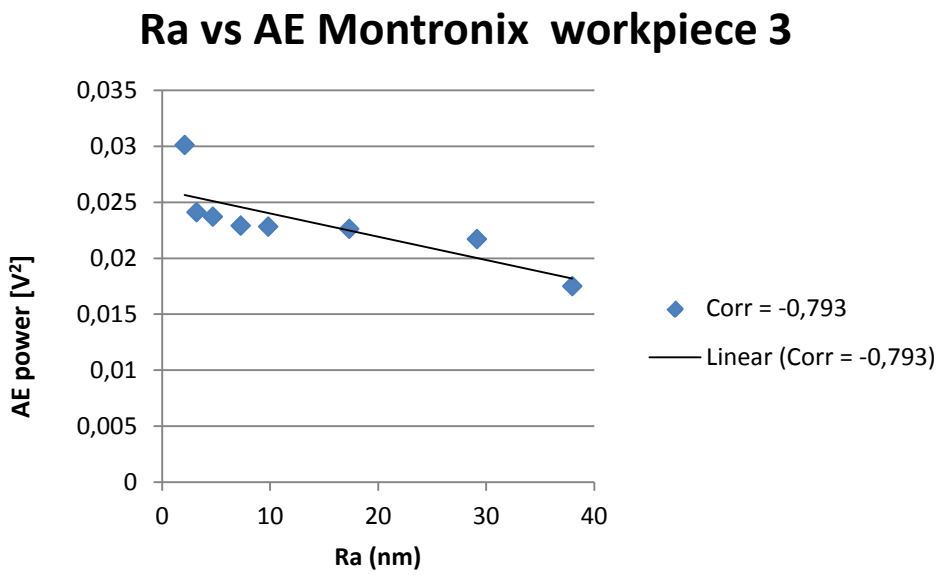

FIGURE 6.46 Correlation between Ra and AE for workpiece 3

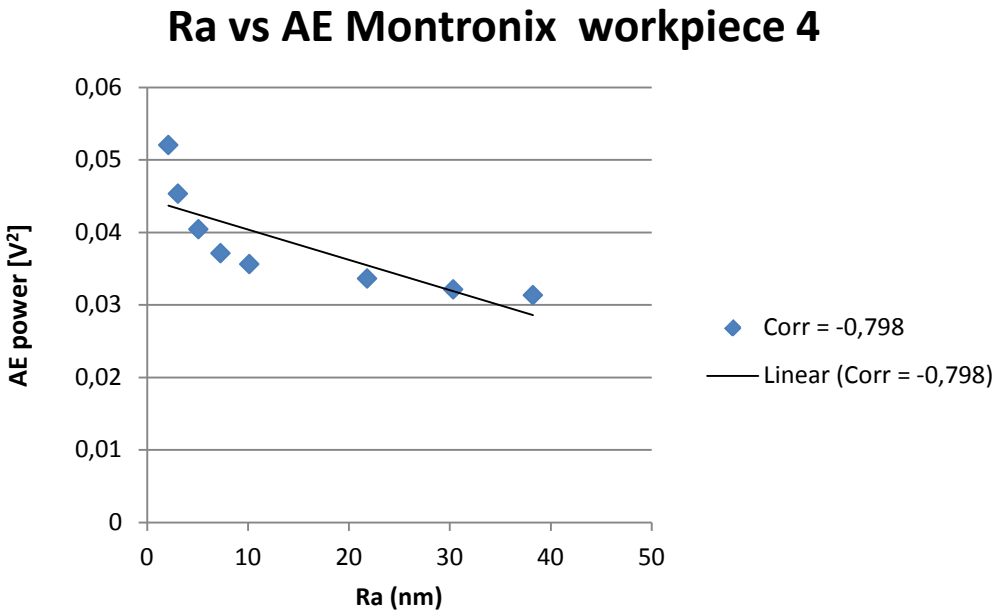

FIGURE 6.47 Correlation between Ra and AE for workpiece 4

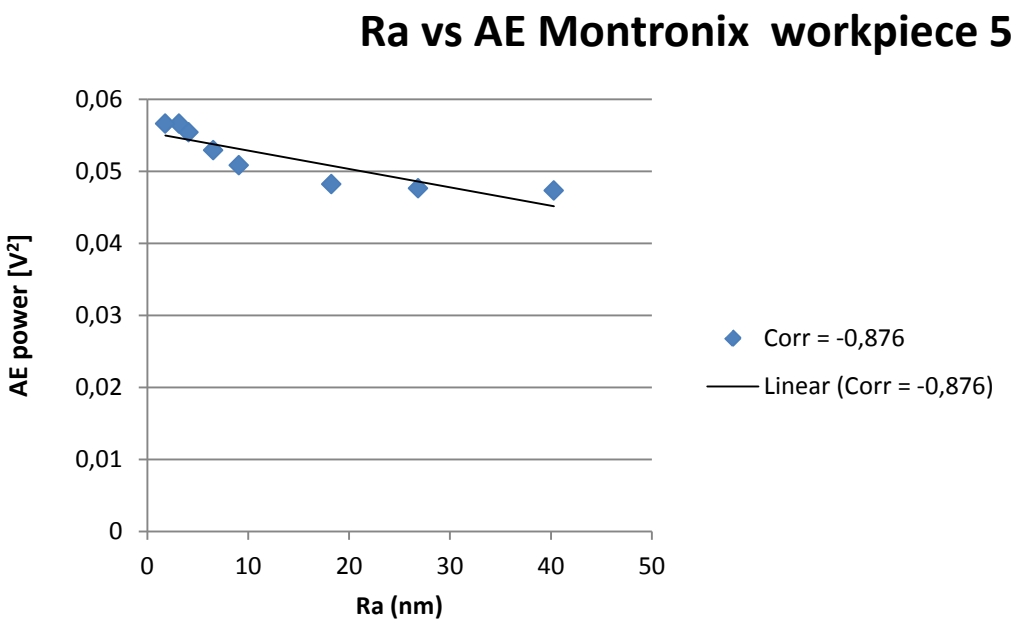

FIGURE 6.48 Correlation between Ra and AE for workpiece 5

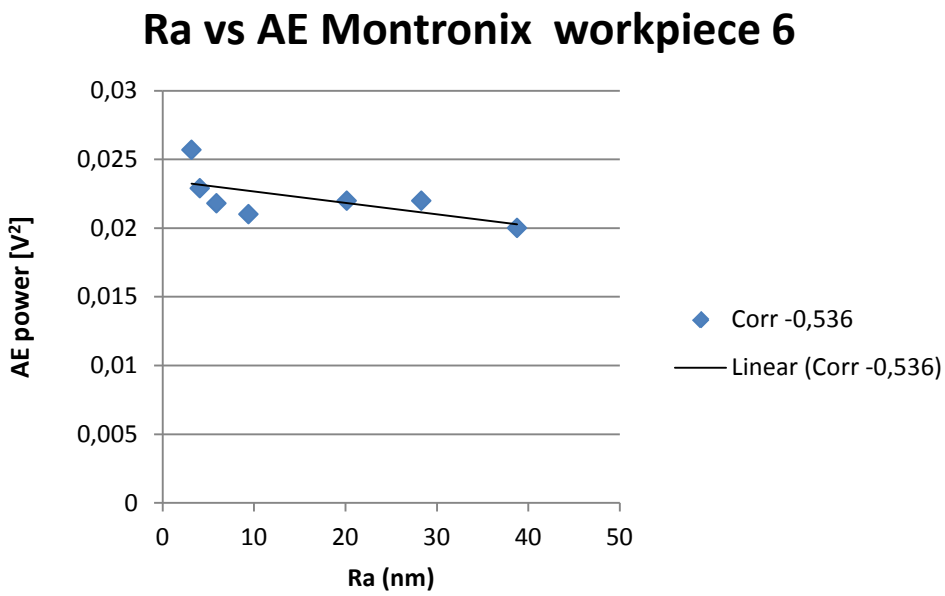

FIGURE 6.49 Correlation between Ra and AE for workpiece 6

The average correlation factor is -0,661.

6.3.3 Frequency analysis

On both signals a FFT (Fast Fourier Transform) was applied to detect which were the main frequencies acquired.

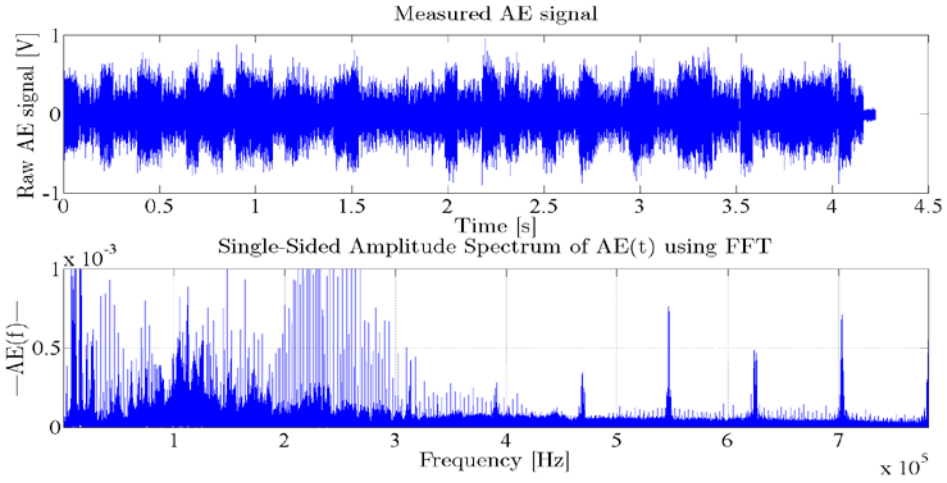

FIGURE 6.50 Signal, above, and FFT, below, from R15

For the R15 it is noticeable (fig. 6.52) that the main frequencies is around 120 kHz and 15 kHz, in accordance with the characteristics of the sensor that presents its peak sensitivity is 150 kHz (see Chapter 4).

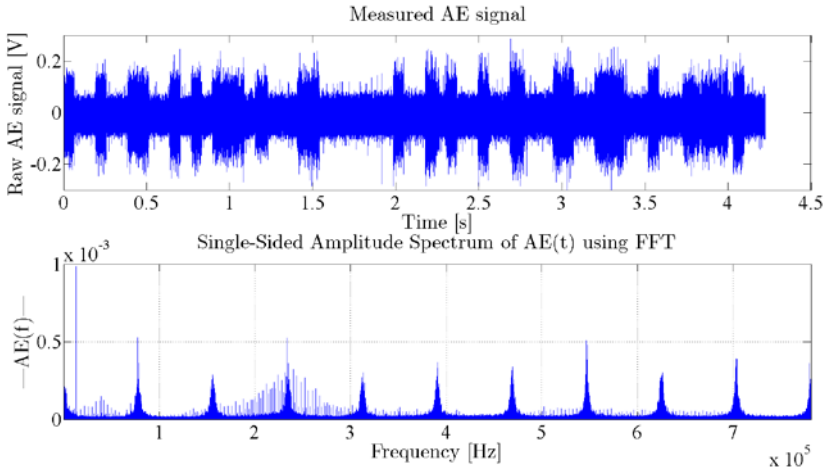

FIGURE 6.51 Signal, above, and FFT, below, from BV100

From the BV100 it is noticeable that there is not an evident main frequency, there is a big peak around 10 kHz.

Both sensors are characterized by several peaks equally spaced whose origin was studied analyzing the FFT of the back ground noise to evaluate if they are induced just by the noise.

From the FFT of the noise for both sensors, crosschecking it with the FFT of the whole signal, it was noticed that the R15 is detecting a lot under 200 kHz and the two big peaks underlined before are due definitely to the process.

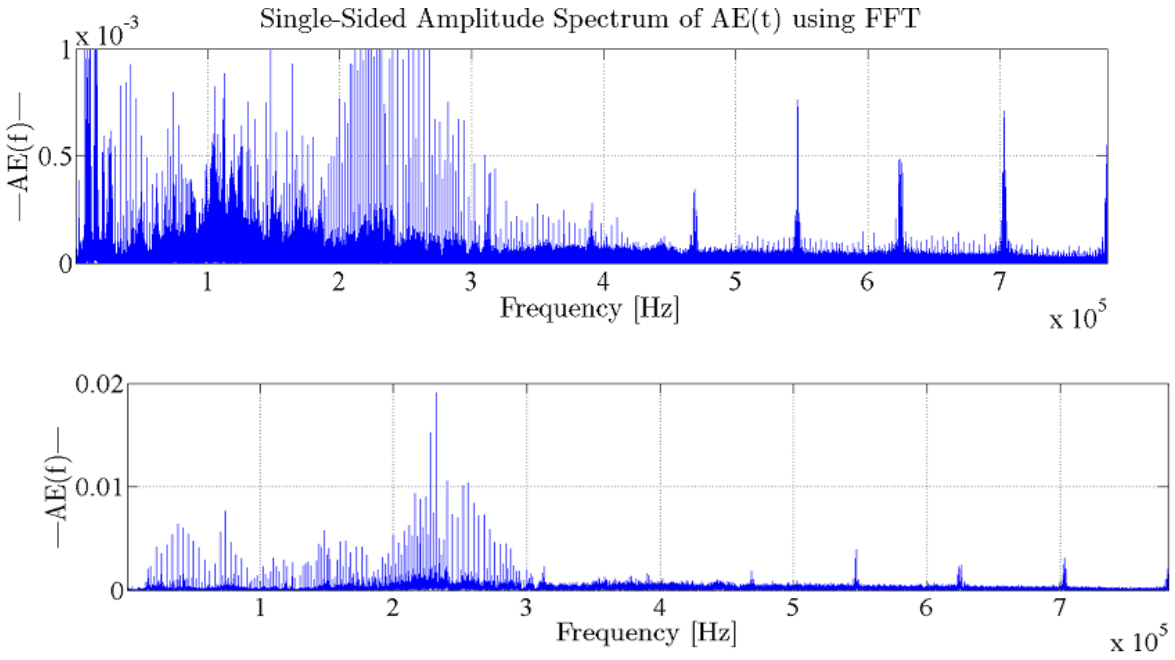

FIGURE 6.52 FFT of the background noise (below) and the signal from the process (above)for R15

On the other hand the comparison between the noise and the signal for the BV100 showed that the only difference is the amplitude of the peaks that reflect the presence of a main frequency characteristic of the process, most probably the one detected at 10 kHz that presents a different ratio with the other peaks if seen in the full signal FFT or only in the FFT of the noise.

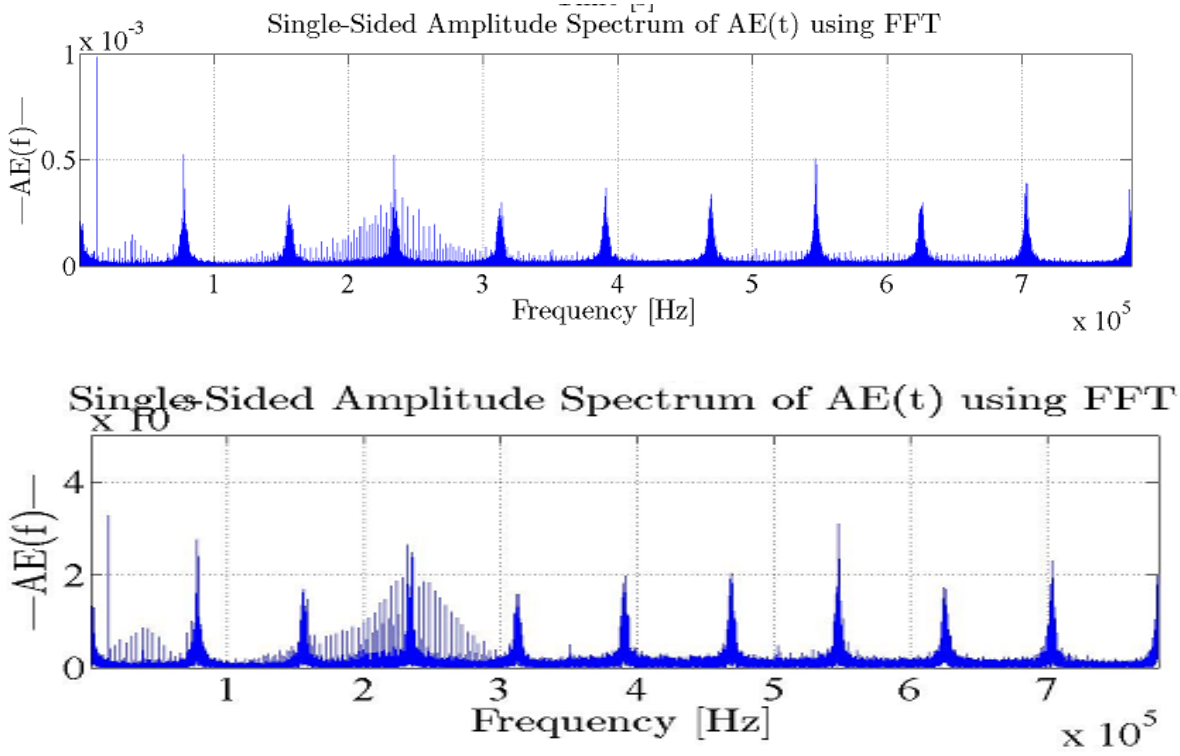

FIGURE 6.53 FFT of the background noise(below) and the signal from the process (above) for BV100

The presence of these well-spaced peaks in both sensor and also in the background noise led to state that they are probably induced by the CNC machine.

It is possible to say that the R15 “hears” definitely more than the BV100 that, from this analysis, cannot be used to monitor the polishing process failing to detect significant signal.

Graph with the correlation between AE and Ra for different amount of passes are shown in Appendix H.

6.4 Power consumption

The correlation between the power consumption signals and the roughness values measured with WLI are now presented for the total polishing work of 160 passes, corresponding to 2000 seconds.

The power we are interested in is the one consumed by the oscillation module during the polishing process. The power consumed should reflect the behavior of the friction forces that decrease with the progress of the process. Thus if the power consumed by bearing and the internal mechanisms is constant. It was acquired with a sample rate of 1 kHz manually started and stopped, leaving some time before and after the proper process acquisition to evaluate the possible errors due to the drift.

The values showed for the power are not the real power values but they are normalized to 100 which is the maximum value detectable by the setup.

At first glance the power does not follow any trend as it is possible to see in Figure 6.57.

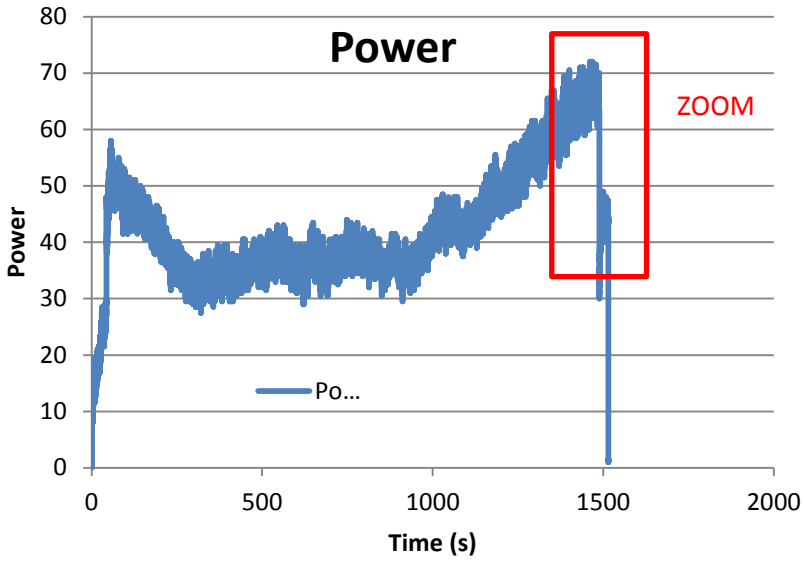

FIGURE 6.55 Rough power signal for workpiece 5

But with a more accurate vision one can see that there is a big drift error going to affect all of the data collected.

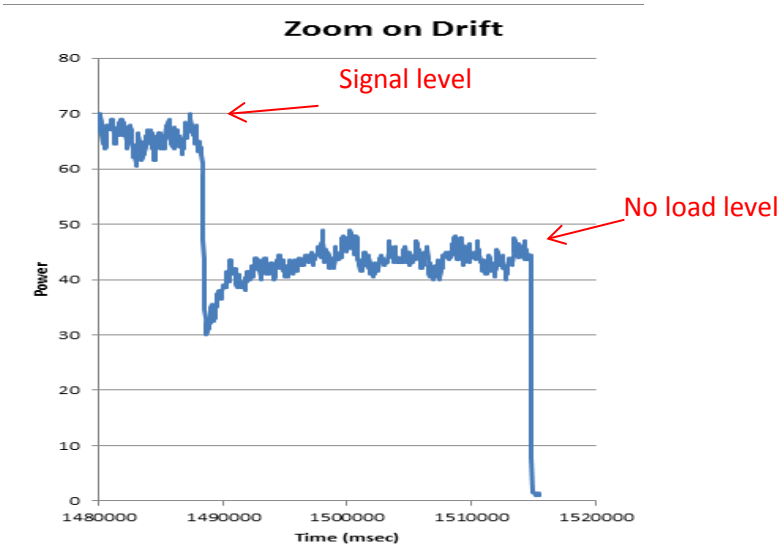

FIGURE 6.56 Zoom on drift error signal for workpiece 5

The no load is around 40 when the final signal is around 70, then the drift should be definitely corrected to properly evaluate the behavior of the power curve.

Assuming that the drift has a linear course, the data are easily correctable by subtracting the values subtended by a straight line to the values acquired.

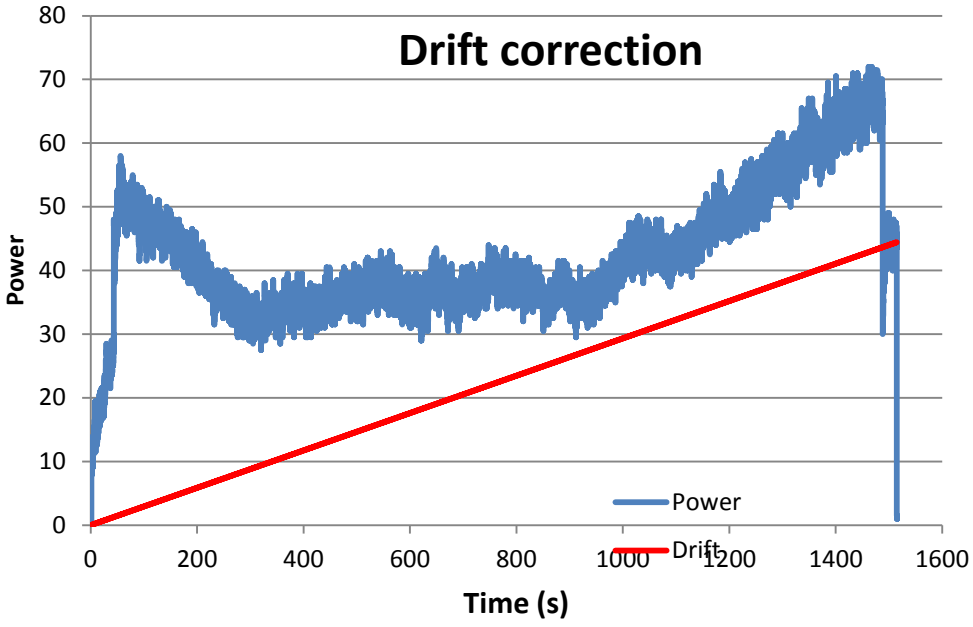

FIGURE 6.57 Drift correction for workpiece 5

After this a posteriori correction the curve can finally be compared with that of the surface roughness.

Below a comparison between the results obtained with WLI and Power consumption are presented showing on the same graph both the curves for the roughness behavior in Ra and the power.

On the X axis there is the time in seconds and on the Y axis there are the Ra value in nanometers and the power in arbitrary unit.

Graph with the correlation between Power and Ra for different amount of passes are in Appendix I.

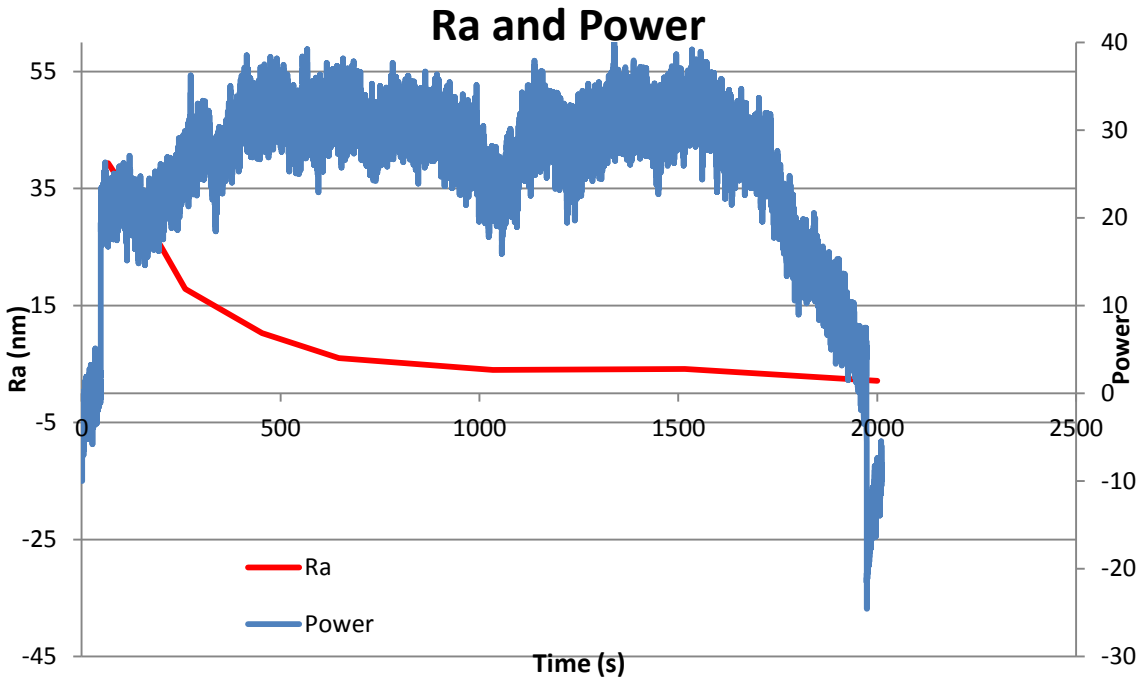

FIGURE 6.58 Correlation between power and Ra for 160 passes for workpiece 1

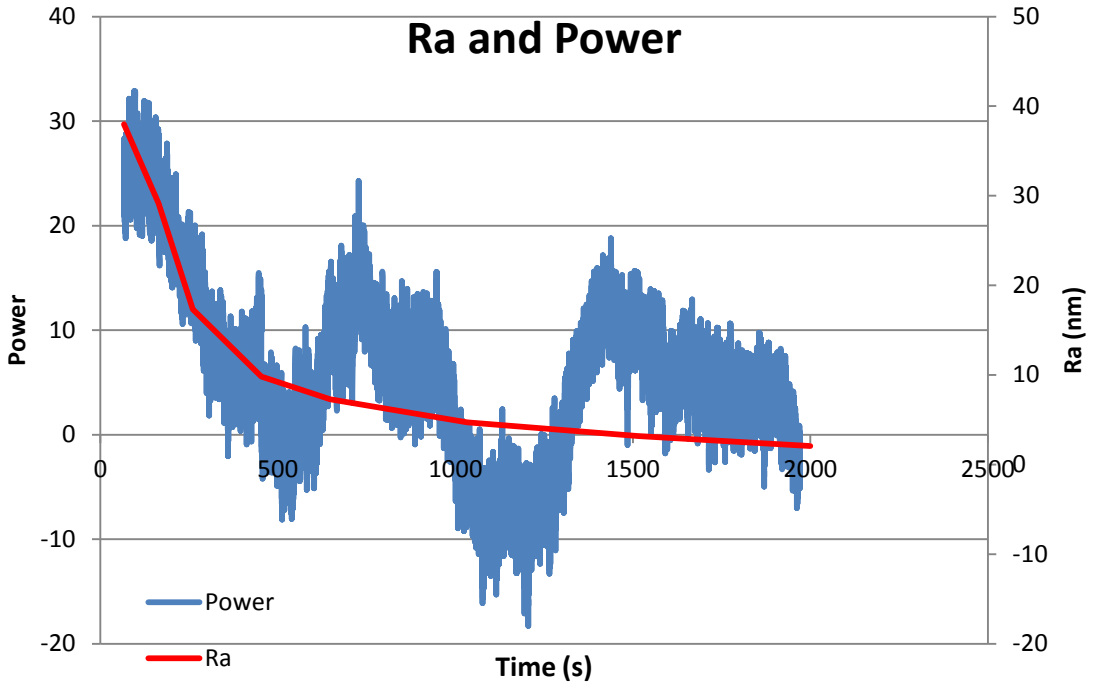

FIGURE 6.59 Correlation between power and Ra for 160 passes for workpiece 3

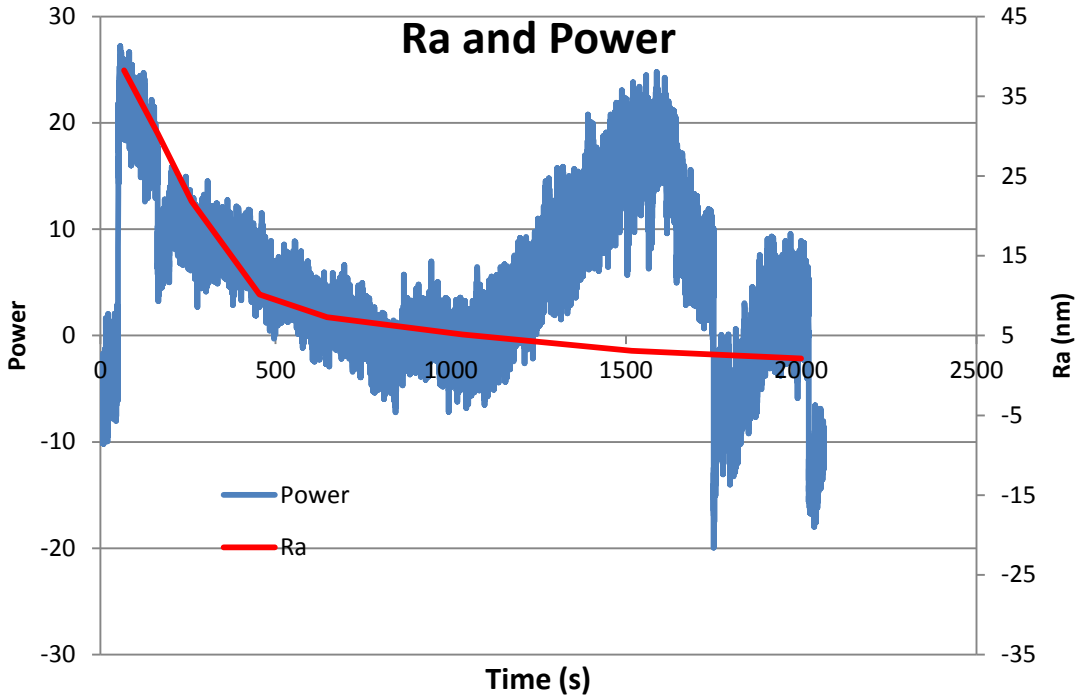

FIGURE 6.60 Correlation between power and Ra for 160 passes for workpiece 4

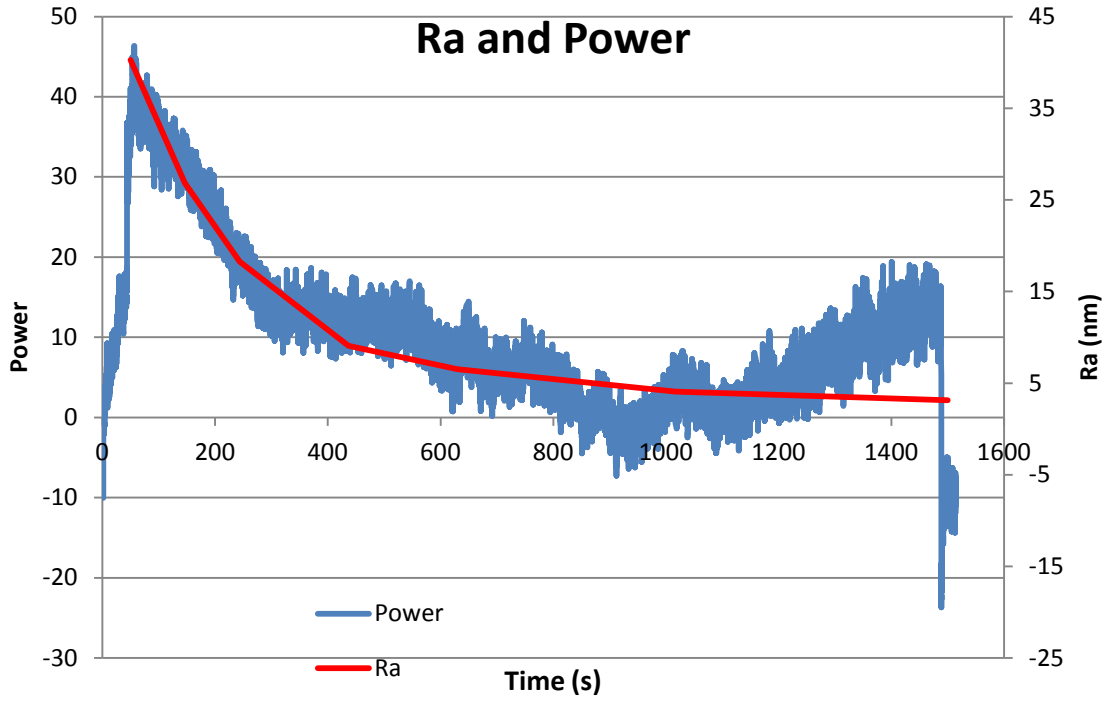

FIGURE 6.61 Correlation between power and Ra for 160 passes for workpiece 5

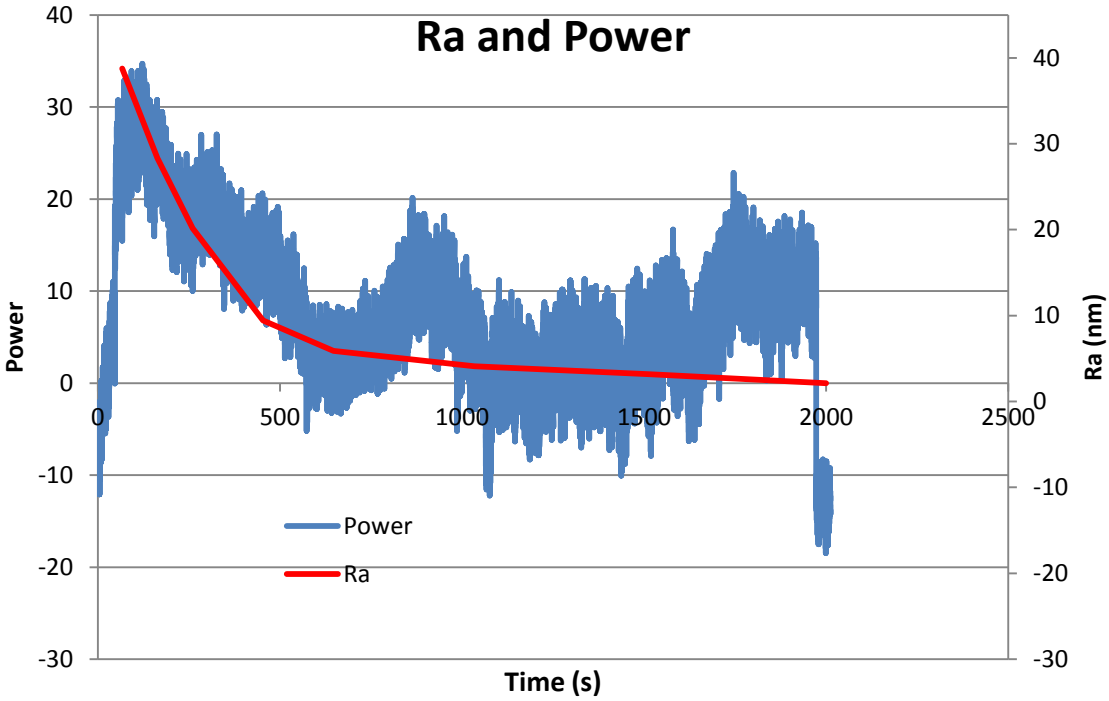

FIGURE 6.62 Correlation between power and Ra for 160 passes for workpiece 6

It is evident that the curve of the power and the curve of roughness are somehow correlated, except for the workpiece 1.

The behavior of power follows really well the roughness curve in the beginning of the process for all the workpieces, (neglecting always workpiece 1), up to more than a quarter of the process. Then in workpiece 3 there is a huge variation and then the curves are close again at the end of the process. In workpiece 4 a big deviation occurs after the middle of the process, but in the end the curves are close again also in this case. Workpiece 5 presents a very good correlation till the third quarter of the process than the signal increases strongly and does not return towards the Ra curve. In workpiece 6 the best correlation is noticeable; the curves are close during the whole process.

These distortions noticed in power consumption signal are not detectable in force or AE signals.

All these variation noticeable in the power curves could result from different factors that come into play. First of all the friction in the bearings.

It is known that Strecon is developing a new oscillation module, better designed with less mechanical joints and therefore less friction.

Below are showed the graphs that correlate directly the Ra values and the power consumption, with a trend line and the correlation factor value for each workpiece.

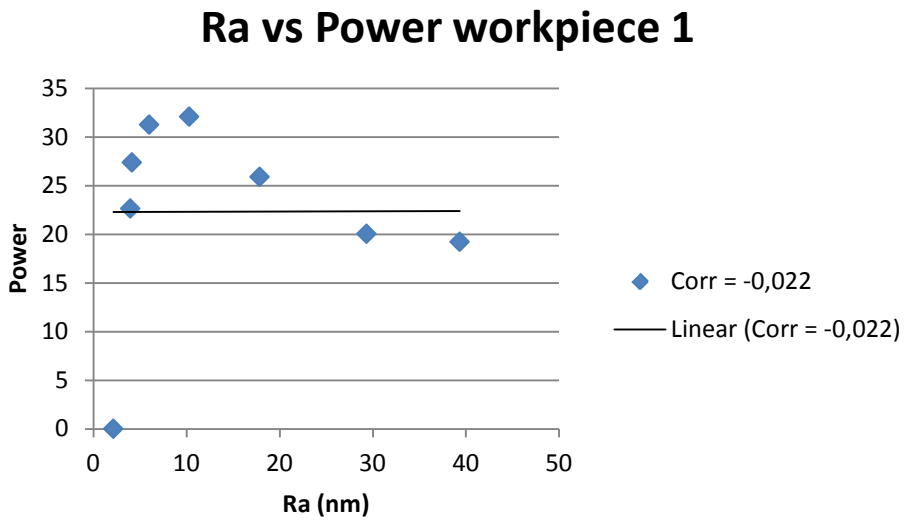

FIGURE 6.63 Correlation between Ra and power for workpiece 1

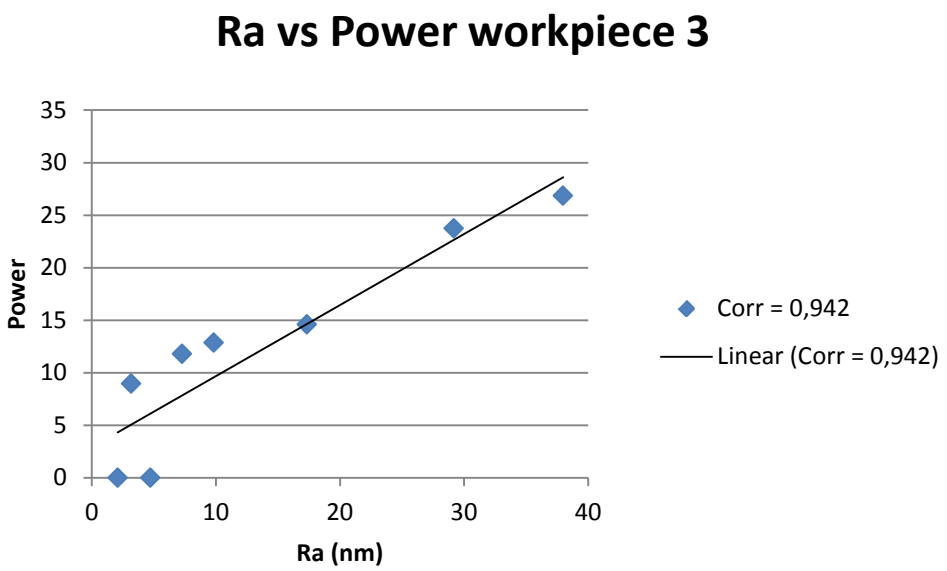

FIGURE 6.64 Correlation between Ra and power for workpiece 3

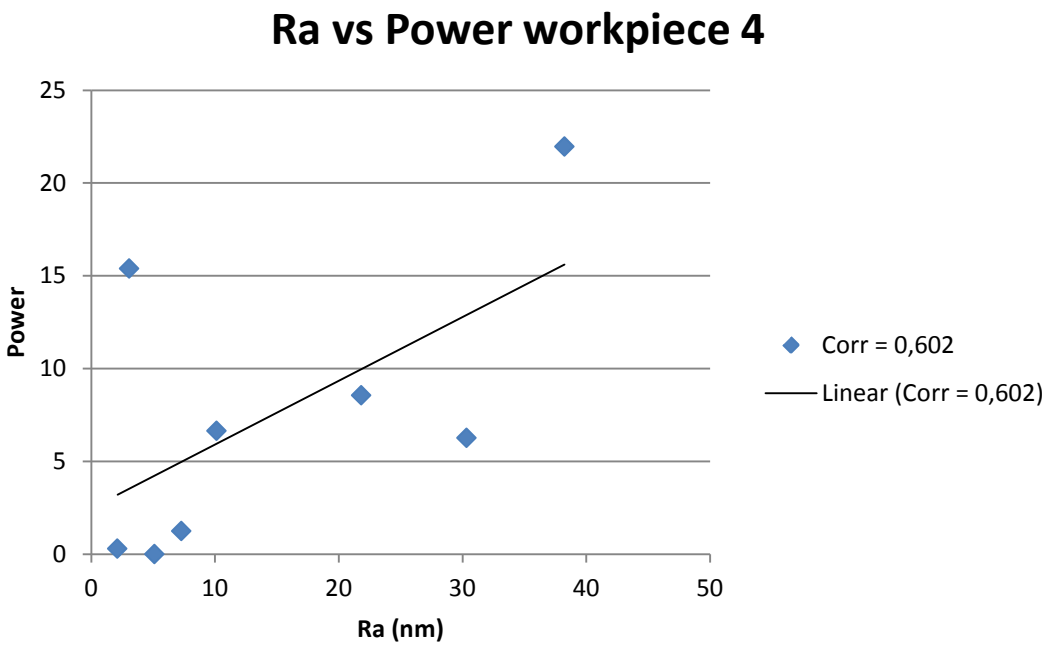

FIGURE 6.65 Correlation between Ra and power for workpiece 4

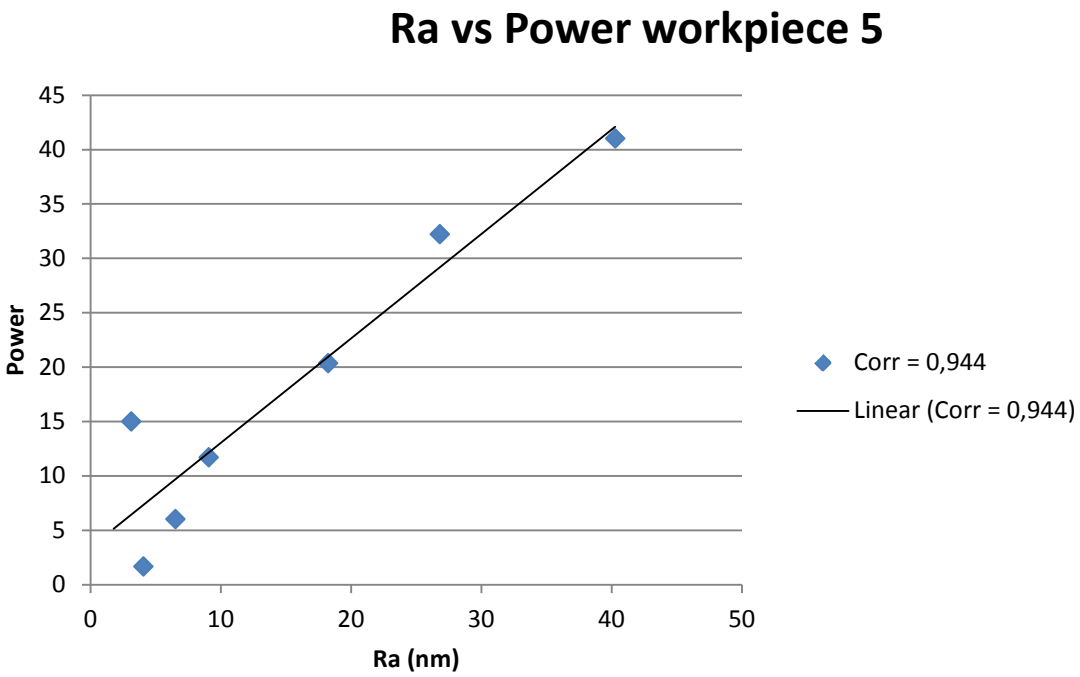

FIGURE 6.66 Correlation between Ra and AE for workpiece 5

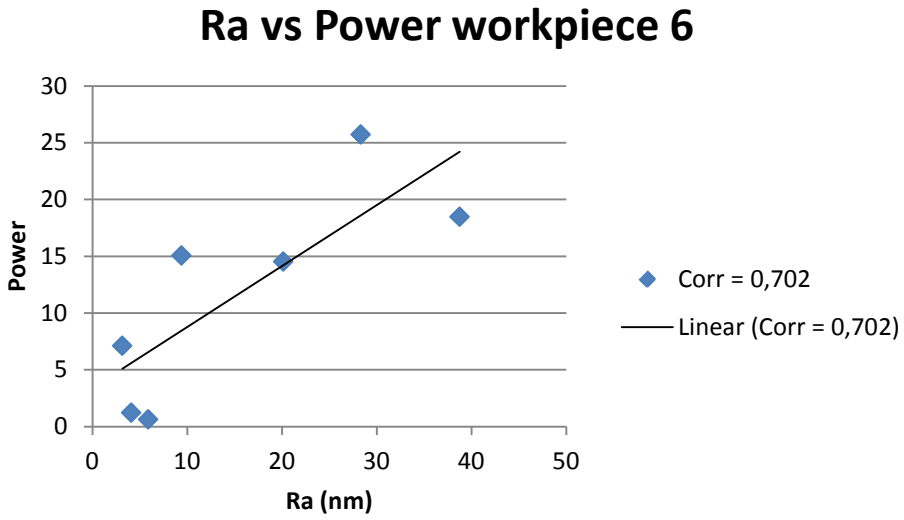

FIGURE 6.67 Correlation between Ra and power for workpiece 6

The average correlation factor is 0,529.

Another factor to take into account is the temperature of the oscillation module given by the software. During the final testing has been noticed that the temperature of the module increased with the progress of the process. Starting from the first surface when the

temperature was about 35 degrees and finishing with a temperature around 41 degrees. This increase of temperature due to Joule effect could influence the power consumption. It was also noticed that the temperature trend was almost the same for all the workpieces.

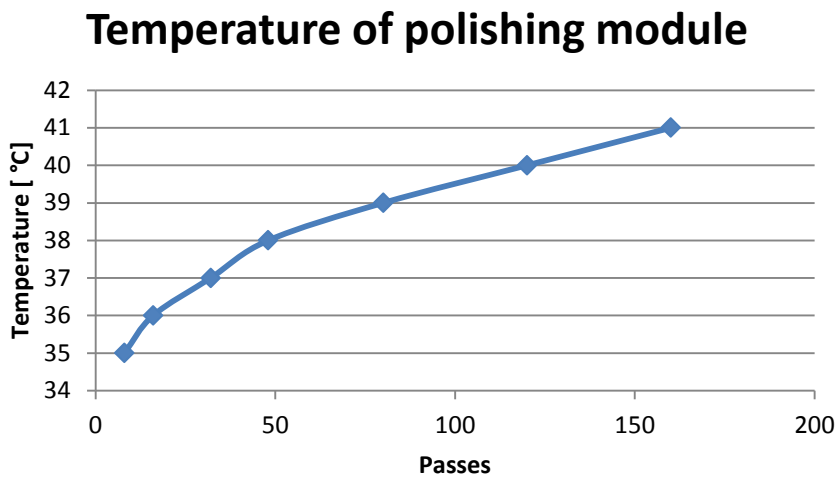

FIGURE 6.68 Temperature of the polishing module for workpiece 3

Summary and Conclusions

The objective was the validation of the correlation between process progress and sensors outputs.

The sensor system was composed by a three-component force transducer on which the workpiece was clamped, 2 AE sensors positioned on the workpiece and a Hall sensor for the measurement of the power consumed by oscillation module, applied in robot assisted flat diamond polishing and measurement of surface roughness by OptoSurf on machine. Evaluation of the correlation level between the surface roughness progress and the signals acquired with these sensors is the final result.

In order to evaluate the surface roughness the whole diamond polishing process was divided in intervals after which the roughness was measured both with a White light interferometer, used as reference instrument, and also with a Scattered light instrument (Optosurf) directly mounted on the CNC.

During the entire test campaign the polishing module that allows the oscillation of tool was mounted on CNC milling machine Cincinnati Milacron Sabre 750 with 3 CNC controlled axes.

Several preliminary tests were performed to achieve the maximum reliability level in the process and to understand properly how to plan the final test campaign.

The results from these preliminary tests brought to a final campaign in which a grounded workpiece with the starting surface roughness around Ra 200 nm were initially polished with stone for 10 passes back and forth perpendicular to the grinding marks up to reach a surface roughness around Ra 40 nm to prepare them for the final diamond polishing.

The test campaign was performed on a total diamond polishing process of 160 passes divided in 7 time intervals with a percentage of 5, 10, 20, 30, 50 and 75 % of the total polishing passes to characterize the surface roughness curve and finally compare it with the signals acquired with the different sensors. Every surface was 20 x 10 mm

The total number of passes was chosen in order to evaluate the stabilization of the process when the improvement of the surface is very low compared to the required time.

The polishing procedure was repeated 5 times on 5 different workpieces to have a quantity of reliable data to draw robust conclusion.

During the process the Acoustic emission signals and the forces from the workpiece and the power consumption data of the oscillation module are collected, in order to be afterward analyzed and correlate them with the surface roughness data.Each surface was measured both with a white light interferometer, as reference instrument, and with Optosurf before

and after the polishing process, to validate the applicability of this latter instrument mounted together with the polishing module on the CNC for machine measurement of the finished surfaces.

As shown by the analysis of the surface roughness measured with the white light interferometer showed that with the selected process settings and with the improvements described in Chapter 4 the process has proved to be highly repeatable. This was a prerequisite for the correlation alaysis. The starting Ra value was 40 nm down to 2 nm. The use of Optosurf for direct measurement on the machine tool has been validated; the curves produced by the analysis of the roughness measured with Optosurf and White light interferometer are really close and indicate a strong correlation (Correlation value between 0,87 and 0,99). Thus it has been proved that Optosurf could be used for inline roughness measurements.

The analysis of forces led to discover a correlation between them and the surface progress. Even though the behavior of the forces curve doesn't follow the Ra curve it is possible to define a correlation for all the workpiece demonstrating the reproducibility of the phenomenon, but it is not noticeable the stabilization in the end of the process.

The analysis of the acoustic emission, led for both sensors to bad results. The signal is not very repeatable and in some cases there is not a noticeable trend that could make sense to a possible correlation. The FFT analysis of the AE detected that between the two sensors, the R15 is more suitable for monitoring this process. It "heard" the signal from the process at frequency of 120 kHz and 15 KHz but it is also a lot influenced by the background noise. Filtering the frequency due to background noise didn't lead to different result from the non-filtered signal.

Finally the analysis of the power consumption led to unexpected results. What appeared to be a signal completely unrelated to the progress of the roughness proved, after careful post processing, looked to be quite reliable. For almost all the workpieces power consumption follows the roughness curve. Strong variations in the signal are still present, probably due to defects in the design of the module and the increase in temperature of the module itself due to Joule Effect. A deeper study of the module could bring to a possible implementation of the power consumption sensor on the machine.

Future developments could be made: fully integrating the Optosfurf with the CNC without relying on the little human precision in positioning, developing a correlation function between forces and surface roughness progress and evaluating its efficiency, improving the oscillation module in order to remove possible sources of interference in the power consumption acquisition and, dealing with acoustic emission, try to use sensors with higher sensitivity to tested ones to find a correlation with the roughness curve or to document definitively the impossibility of using the acoustic emission for this purpose.

References

[1] Toshio Kasai, *Lapping and Polishing Technology*, School of Engineering, Tokyo Denki University, Tokyo 101-8457, Japan

[2] J.H. Ahn, Y.F. Shen, H.Y. Kim, H.D. Jeong, K.K. Cho, *Development of a sensor information integrated expert system for optimizing die polishing,* Robotics and Computer Integrated Manufacturing 17 (2001) 269}276

[3] D. Dornfeld, *Application of acoustic emission techniques in manufacturing*, University of California, Berkeley, CA 94720, USA

[4] J. F. G. Oliveira, C. M. 0. Valente, *Fast Grinding Process Control with AE Modulated Power Signal*

[5] B. Karpuschewski, M. Wehmeier, I. lnasaki, *Grinding Monitoring System Based on Power and Acoustic Emission Sensors*

[6] C. J. Evans, E. Paul, D. Dornfeld, D.A. Lucca, G. Byrne, M. Tricard, F. Klocke, 0. Dambon and B. A. Mullany, *Material Removal Mechanisms in Lapping and Polishing*, CIRP Annals – Manufacturing Technology Volume 52, Issue 2, 2003, Pages 611–633

[7] D.E. Lee, I. Hwang, C.M.O. Valente, J.F.G. Oliveira, D.A. Dornfeld, *Precision manufacturing process monitoring with acoustic emission*, International Journal of Machine Tools & Manufacture 46 (2006) 176–188

[8] J. Webster, W. P. Dong, R. Lindsay, *Raw Acoustic Emission Signal Analysis of Grinding Process*, Center for Grinding Research and Development, University of Connecticut, USA

[9] Yongsong Xie, Bharat Bhushan, *Effects of particle size, polishing pad and contact pressure in free abrasive polishing*, Wear Volume 200, Issues 1–2, 1 December 1996, Pages 281–295

[10] Mark Irvin, *Diamond Lapping and Polishing*, Hyprez Product manager, Engis Corp.

[11] Shih-Chieh Lin *, Meng-Long Wu, *A study of the effects of polishing parameters on material removal rate and non-uniformity*, International Journal of Machine Tools & Manufacture 42 (2002) 99–103

[12] J. Webster, I. Marinescu, R. Bennett, *Acoustic Emission for Process Control and Monitoring of Surface Integrity during Grinding*

[13] S. H. Chang, S. Balasubramhanya, S. Chandrasekar, T. N. Farris, F. Hashimoto, *Forces and Specific Energy in Superfinishing of Hardened Steel*

[14] I. Inasaki, *Sensor Fusion for Monitoring and Controlling Grinding Processes*, Advanced Manufacturing Technology, 15:730–736

[15] Pete Theobald, Bajram Zeqiri and Janine Avison, *Couplants and their influence on ae sensor sensitivity*, National Physical Laboratory, Teddington, Middlesex, TW11 0LW, United Kingdom

[16] K. Saito, T. Miyoshi, T. Sasaki, *Automation of Polishing Process for a Cavity Surface on Dies and Molds by Using an Expert System*

[17] Stephenson, David. *Metal Cutting Theory and Practice*. 2nd. Boca Raton: CRC Press, 1997. 52-60.

[18] Salmon, Stuart, "What is Abrasive Machining?," *Manufacturing Engineering* Feb. 2010, Society of Manufacturing Engineers.

[19] Oberg, Erik; Jones, Franklin D.; Horton, Holbrook L.; Ryffel, Henry H. (2000), *Machinery's Handbook* (26 th. ed.), New York: Industrial Press Inc

[20] *Uddeholm Stavax® ESR*, Uddeholm

[21] *Polishing mould steel*, Uddeholm

[22] Rao V. Ddukkipati, *MATLAB for mechanical Engineers*, New Age Science

[23] S. Gasparin, *Verification of tolerance chains in micro manufacturing*, Ph.d Thesis, April 2012

[24] Rainer Brodmann, Jörg Seewig, *Non-Contact Surface Metrology by means of Light Scattering*

[25] *Surface Measurement System OS 500*, Optosurf operating manual

[26] Peter Norman, *Advanced Process Monitoring and Analysis of Machining*, Luleå University of Technology

[27] *Manuale generico serie Spectra*

[28] *Introduction to Piezoelectric Force Sensors*, Kistler

[29] Poulomi Ghosh, Abhisek Maiti*, Instantaneous Power Measurement using Hall Sensor*, International Journal of Scientific and Research Publications, Volume 2, Issue 8, August 2012

[30] Ron Pugh, *Current and Power Waveform Measurement Technique*

[31] C. Huynh, M. Rutten, R. Cheek, H. Linde, *A Study of Post-Chemical-Mechanical Polish Cleaning Strategies*, IBM Microelectronics Division, Essex Junction, Vermont

[32] F. Mazzucato, *Development of a suitable modeling approach for the robot assisted polishing process,* M. Sc. Thesis

[33] Susan Woods, *Understanding scanning white light interferometry,* MICROmanufacturing, Volume 2, Issue 4, December 2009

[34] L. Pilný, G. Bissacco, L. De Chiffre , *Monitoring of Robot Assisted Polishing through Acoustic Emission Measurement*

[35] http://www.accutransusa.com

[36] http://www.pacndt.com/

[37] http://www.mistrasgroup.com/products/technologies/acousticemission.aspx

[38] http://www.kistler.com

[39] http://www.piazzarosa.it/

[40] http://montronix.com/

[41] http://www.joke.de/

[42] http://www.struers.com

[43] http://www.allaboutcircuits.com

[44] http://www.ifacom.org/

[45] http://www.zygo.com/

[46] http://www.strecon.com/

Appendix A

Starting workpieces measurements with FTS

Numb	Ra	Rz	Rzmax	RSm
1	0,214	1,67	1,968	29,849
2	0,193	1,644	2,029	29,297
3	0,181	1,583	1,811	26,675
4	0,184	1,448	1,606	28,814
5	0,185	1,483	1,779	28,096
6	0,188	1,57	1,821	28,608
7	0,191	1,537	1,885	28,796
8	0,188	1,553	1,933	27,621
9	0,209	1,705	2,134	32,498
10	0,201	1,548	1,917	29,989
Avg	0,193	1,574	1,888	29,024
Std	0,011	0,08	0,146	1,576
Std%	5,7	5,1	7,7	5,4

Workpiece 1

Numb	Ra	Rz	Rzmax	RSm
1	0,179	1,559	2,432	34,169
2	0,196	1,633	1,965	34,035
3	0,188	1,512	1,827	31,313
4	0,187	1,398	1,616	29,527
5	0,187	1,317	1,574	29,82
6	0,187	1,388	1,699	30,45
7	0,165	1,235	1,344	27,901
8	0,185	1,504	1,907	30,547
9	0,192	1,536	1,738	29,187
10	0,208	1,625	1,866	30,734
Avg	0,188	1,471	1,797	30,768
Std	0,011	0,132	0,289	1,996
Std%	5,9	9	16,1	6,5

Workpiece 3

Numb	Ra	Rz	Rzmax	RSm
1	0,217	1,516	1,891	38,662
2	0,234	2,187	3,76	42,093
3	0,268	2,458	3,469	43,381
4	0,25	2,536	4,973	50,72
5	0,193	1,608	2,323	34,116
6	0,18	1,353	1,597	32,746
7	0,219	2,228	3,923	41,714
8	0,196	1,505	2,333	35,015
9	0,227	1,737	2,323	35,136
10	0,176	1,333	1,626	26,917
Avg	0,216	1,846	2,822	38,05
Std	0,03	0,461	1,139	6,703
Std%	13,9	25	40,4	17,6

Workpiece 4

Numb	Ra	Rz	Rzmax	RSm
1	0,204	1,927	2,851	33,772
2	0,186	1,572	1,709	34,217
3	0,188	1,595	1,779	29,839
4	0,203	1,61	1,818	30,69
5	0,191	1,452	2,086	31,874
6	0,203	1,654	2,115	32,452
7	0,223	1,686	2,154	32,339
8	0,186	1,426	1,619	29,708
9	0,225	1,754	2,378	40,19
10	0,216	1,581	1,706	32,244
Avg	0,203	1,626	2,021	32,733
Std	0,015	0,144	0,381	3,015
Std%	7,3	8,9	18,8	9,2

Workpiece 5

Numb	Ra	Rz	Rzmax	RSm
1	0,164	1,38	1,76	23,559
2	0,181	1,443	2,112	30,556
3	0,178	1,48	1,798	26,703
4	0,168	1,434	2,083	28,5
5	0,17	1,341	1,638	27,14
6	0,163	1,516	1,949	29,239
7	0,169	1,596	2,851	28,825
8	0,16	1,225	1,373	25,814
9	0,171	1,341	1,635	27,421
10	0,173	1,324	1,549	25,544
Avg	0,17	1,408	1,875	27,33
Std	0,007	0,108	0,415	2,05
Std%	3,9	7,6	22,1	7,5

Workpiece 6

Appendix B

3D starting workpieces measurements with Alicona

Workpiece 1	
Sa	184 nm
Sa	218 nm
Sa	220 nm
Avg	207 nm

Workpiece 1

Workpiece 3	
Sa	181 nm
Sa	198 nm
Sa	231 nm
Avg	203 nm

Workpiece 3

Workpiece 4	
Sa	185 nm
Sa	226 nm
Sa	259 nm
Avg	213 nm

Workpiece 4

Workpiece 5	
Sa	256 nm
Sa	209 nm
Sa	200 nm
Avg	211 nm

Workpiece 5

Workpiece 6	
Sa	176 nm
Sa	173 nm
Sa	166 nm
Avg	172 nm

Workpiece 6

Appendix C

3D starting workpieces measurements with FTS

Workpiece 1	
Sa	199 nm
Sa	162 nm
Sa	211 nm
Avg	190 nm

Workpiece 1

Workpiece 3	
Sa	210 nm
Sa	173 nm
Sa	191 nm
Avg	191 nm

Workpiece 3

Workpiece 4	
Sa	231 nm
Sa	225 nm
Sa	174 nm
Avg	199 nm

Workpiece 4

Workpiece 5	
Sa	201 nm
Sa	192 nm
Sa	194 nm
Avg	193 nm

Workpiece 5

Workpiece 6	
Sa	163 nm
Sa	161 nm
Sa	170 nm
Avg	165 nm

Workpiece 6

Appendix D

Starting surface measurements with WLI

workpiece 1 (Ra [nm])						
surface	m1	m2	m3	m4	m5	Avg
1	41	31	36	37	42	37,4
2	35	33	33	38	48	37,4
3	34	32	39	46	41	38,4
4	37	45	34	36	38	38
5	39	36	35	34	38	36,4
6	56	54	52	56	57	55
7	35	36	39	40	39	37,8
8	34	40	39	33	37	36,6
9	35	40	34	37	39	37

Workpiece 1

workpiece 3 (Ra [nm])						
surface	m1	m2	m3	m4	m5	Avg
1	35	36	34	39	37	36,2
2	30	36	40	39	41	37,2
3	45	40	39	39	37	40
4	36	39	35	40	42	38,4
5	46	32	35	43	41	39,4
6	44	35	36	37	40	38,4
7	35	40	30	37	39	36,2
8	40	47	36	37	42	40,4
9	35	34	34	36	39	35,6

Workpiece 3

workpiece 4 (Ra [nm])						
surface	m1	m2	m3	m4	m5	Avg
1	40	36	42	35	44	39,4
2	43	47	45	30	40	41
3	39	33	34	37	39	36,4
4	49	32	43	45	39	41,6
5	35	49	33	35	40	38,4
6	33	34	38	35	35	35
7	38	36	37	40	42	38,6
8	35	35	38	41	39	37,6
9	37	32	36	38	38	36,2

Workpiece 4

workpiece 5 (Ra [nm])						
surface	m1	m2	m3	m4	m5	Avg
1	36	38	34	38	39	37
2	40	45	43	41	37	41,2
3	43	46	39	42	35	41
4	49	37	47	45	41	43,8
5	48	44	36	40	43	42,2
6	47	41	39	49	42	43,6
7	35	40	30	37	39	36,2
8	47	36	36	38	41	39,6
9	46	42	31	34	37	38

Workpiece 5

workpiece 6 (Ra [nm])						
surface	m1	m2	m3	m4	m5	Avg
1	40	46	33	34	38	38,2
2	49	48	33	36	37	40,6
3	41	37	33	30	35	35,2
4	48	41	36	39	42	41,2
5	36	47	40	40	43	41,2
6	46	40	35	35	36	38,4
7	36	37	40	38	41	38,4
8	34	45	47	36	39	40,2
9	32	38	33	39	36	35,6

Workpiece 6

Appendix E

Starting surface measurements with Optosurf

workpiece 1 (Aq [non-dimensional])							
surface	m1	m2	m3	m4	m5	m6	Avg
1	45,28	42,55	56,09	59,45	47,75	42,13	48,88
2	43,01	40,83	39,26	39,39	38,24	43,3	40,67
3	43,54	42,76	45,93	40,29	41,3	40,01	42,31
4	38,87	54,19	34,69	39,5	52,38	32,87	42,08
5	41,77	54,98	34,686	30,28	53,41	44,38	43,25
6	63,89	71,5	60,38	60,5	67,79	60,1	64,03
7	37,12	36,2	56,23	56,67	48,26	39,5	45,66

Workpiece 1

workpiece 3 (Aq [non-dimensional])							
surface	m1	m2	m3	m4	m5	m6	Avg
1	55,24	34,69	48,92	9,88	37,31	49,68	39,29
2	34,78	38,04	38,77	40,06	35,33	38,73	37,62
3	36,19	33,64	37,57	31,93	29,46	35,46	34,04
4	37,14	41,47	40,78	44,75	36,61	36,84	39,60
5	47,38	28,72	47,32	33,76	33,74	47,42	39,72
6	36,92	37,06	42,82	38,21	36,17	32,46	37,27
7	34,68	41,39	42,71	41,19	42,14	32,23	39,06

Workpiece 3

workpiece 4 (Aq [non-dimensional])							
surface	m1	m2	m3	m4	m5	m6	Avg
1	43,23	31,93	55,48	55,23	28,74	45,65	43,38
2	55,86	59,86	61,54	60,74	53,26	58,84	58,35
3	40,91	67,04	50,62	53,07	64,09	41,25	52,83
4	43,68	39,43	52,83	52,43	32,27	41	43,61
5	35,71	36,48	59,6	55,55	36,53	37,25	43,52
6	46,89	58,2	27,69	27,38	48,58	43,39	42,02
7	45,33	31,04	49,53	44,71	33,61	36,1	40,05

Workpiece 4

workpiece 5 (Aq [non-dimensional])							
surface	m1	m2	m3	m4	m5	m6	Avg
1	57,04	62,61	52,1	48,12	59,08	52,76	55,29
2	47,08	51,67	63,88	58,78	50,92	47,83	53,36
3	60,59	44,15	48,98	51,56	45,49	63,26	52,34
4	52,06	45,02	54,48	50,06	47,35	53,48	50,41
5	47,6	39,48	56,8	58,37	37,23	47,31	47,80
6	41,4	62,95	50,34	50,07	62,45	43,87	51,85
7	59,12	31,36	60,21	54,26	31,74	63,09	49,96

Workpiece 5

workpiece 6 (Aq [non-dimensional])							
surface	m1	m2	m3	m4	m5	m6	Avg
1	46,83	49,18	67,95	65,73	49,08	49,81	54,76
2	43,18	50,65	51,31	48,98	48,55	48,32	48,50
3	61,65	39,89	33,76	32,39	41,47	56,77	44,32
4	34,71	46,82	41,59	43,44	43	43,1	42,11
5	41,88	48,47	41,15	37,91	46,4	44,32	43,36
6	41,9	45,61	39,07	35,47	40,68	42,5	40,87
7	40,98	49,17	41,93	38,78	45,86	43,74	43,41

Workpiece 6

Appendix F

Sa measurements on final surfaces

workpiece1 Sa (nm)								
surface	m1	m2	m3	m4	m5	m6	AVG	St.Dev
1		26,5	29	28	27	28	33	28,6	2,12
2		21	19	18,5	21	18	19	19,4	1,16
3		11	8,5	8,7	10,5	9	9,8	9,6	0,92
4		5,5	8,2	7,4	7,6	6,5	5,9	6,9	0,96
5		4,5	4,6	4,2	4,7	4,1	3,5	4,3	0,40
6		3,4	3,6	3,2	3	3,2	2,8	3,2	0,25
7		2,3	2,2	2,4	1,9	2,3	2,4	2,3	0,17

Sa value for workpiece 1

workpiece 3 Sa (nm)								
surface	m1	m2	m3	m4	m5	m6	Avg	St.Dev
1	25	31	27	25	28	28	27,3	2,05
2	19	19	17,5	21	17	16	18,3	1,63
3	9,8	9	11	9,1	10,5	10,2	9,9	0,72
4	7,4	7,6	5,1	5,9	6	5,5	6,3	0,93
5	4,7	4,1	4,4	4,6	4,4	3,5	4,3	0,40
6	3,2	3,8	2,7	2,7	2,8	2,6	3,0	0,42
7	2,2	2,4	1,6	2,4	1,8	2,1	2,1	0,30

Sa value for workpiece 3

Workpiece 4 Sa (nm)								
surface	m1	m2	m3	m4	m5	m6	Avg	St.Dev
1	27,5	34	29	31	26	33	30,1	2,86
2	22	22	20	21,8	16	19	20,1	2,17
3	8,5	11,2	9	10,5	9,7	9,8	9,8	0,89
4	6,8	8,2	5,5	6,4	6,5	6,8	6,7	0,80
5	4,7	3,8	4,6	4,1	3,5	4,6	4,2	0,45
6	3	3,2	2,9	3,5	2,8	3,4	3,1	0,26
7	2,4	1,5	2,6	1,8	1,9	1,6	2,0	0,40

Sa value for workpiece 4

Workpiece 5 Sa (nm)								
surface	m1	m2	m3	m4	m5	m6	Avg	St.Dev
1	31	28	29	27	33	31	29,8	2,03
2	19	19	20	18	21	18,5	19,3	0,99
3	9	9	10	10,5	9	11	9,8	0,80
4	7,6	7,8	6,4	5,9	6	6,8	6,8	0,73
5	4,2	4,5	4,2	3,6	4,7	4	4,2	0,35
6	3,6	3	3,3	3	3,8	3,4	3,4	0,29
7	2	1,9	1,9	2,2	2,1	2	2,0	0,11

Sa value for workpiece 5

Workpiece 6 Sa (nm)								
surface	m1	m2	m3	m4	m5	m6	Avg	St.Dev
1	28	27	33	26,5	25	33	28,8	3,13
2	21	19	18,5	22	18	19	19,6	1,43
3	9,8	9	8,7	10,5	9	9,7	9,5	0,61
4	6,8	5,1	6,8	7,6	7,8	5,6	6,6	0,98
5	4	3,8	4,6	4,2	4,2	4,6	4,2	0,29
6	2,8	2,8	3,4	3,2	3,2	3,3	3,1	0,23
7	2,3	1,5	1,9	2,5	1,3	1,4	1,8	0,46

Sa value for workpiece 6

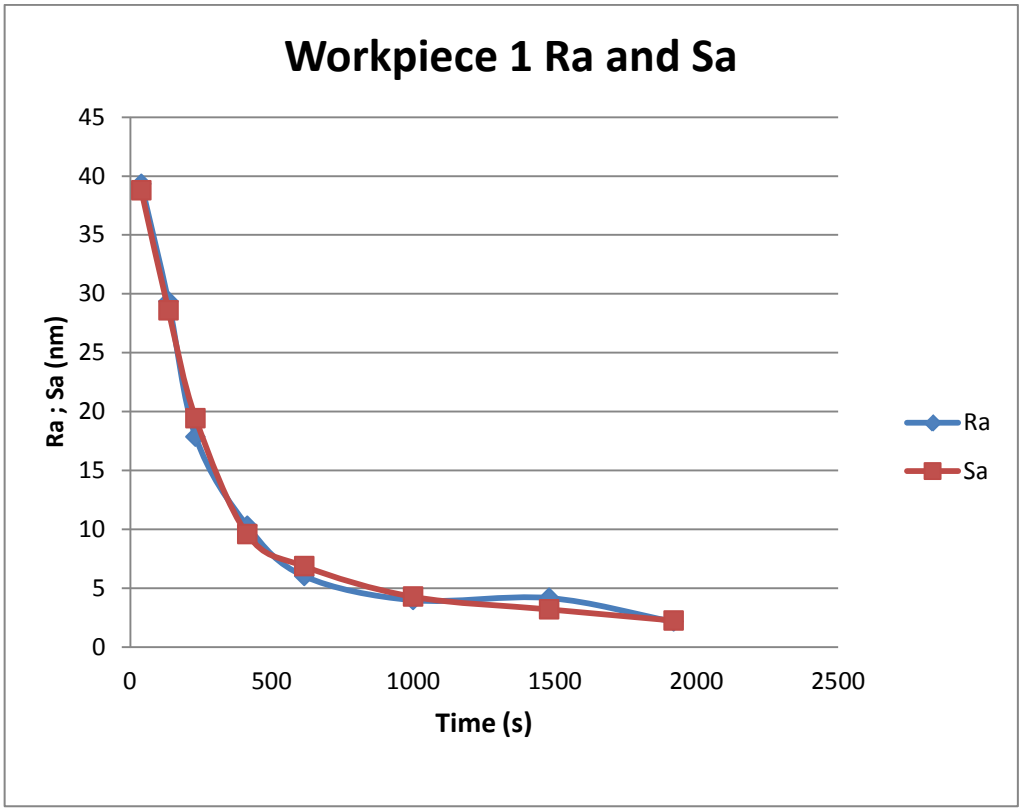

Comparaison betweene Ra and Sa for workpiece 1

Comparaison betweene Ra and Sa for workpiece 3

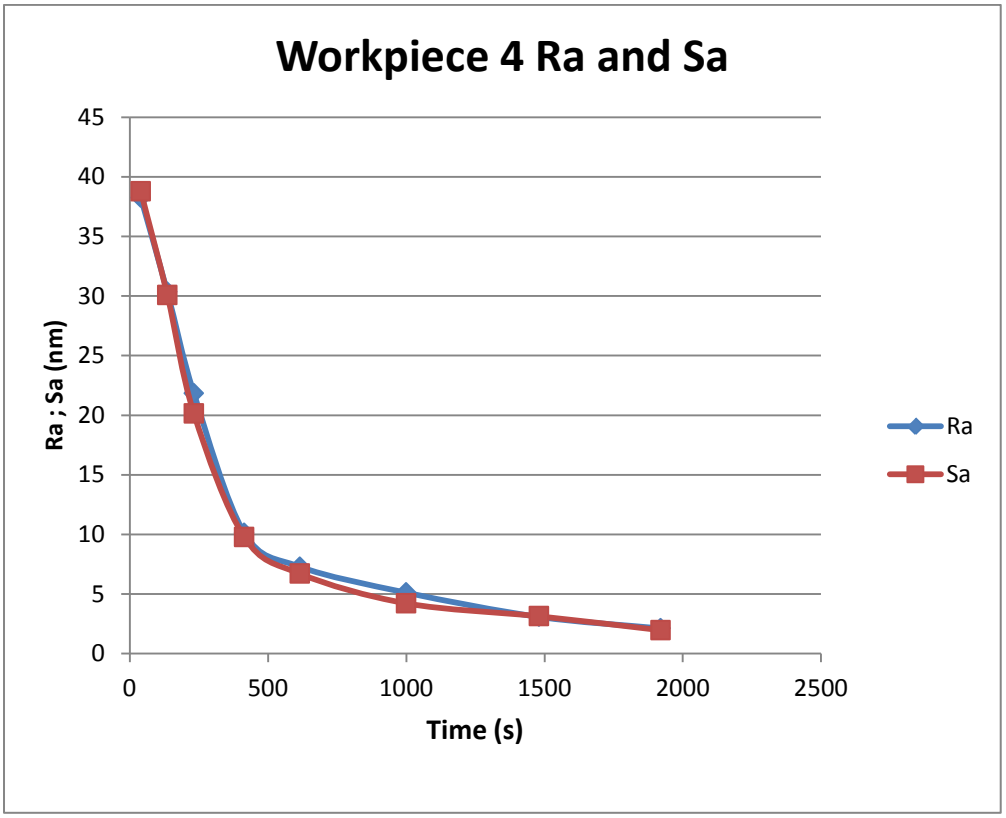

Comparaison betweene Ra and Sa for workpiece 4

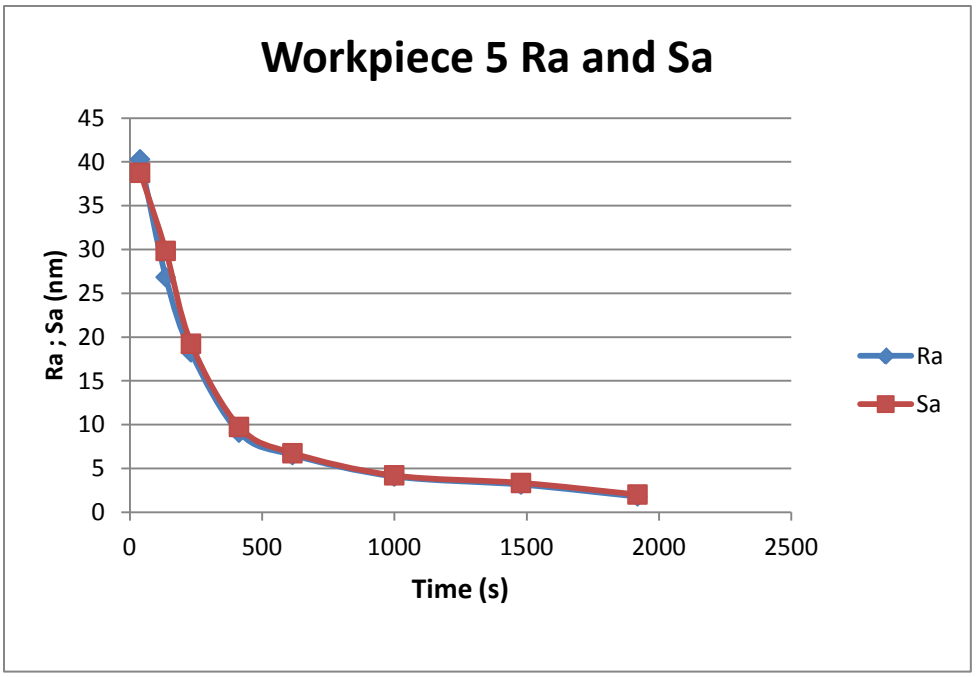

Comparaison betweene Ra and Sa for workpiece 5

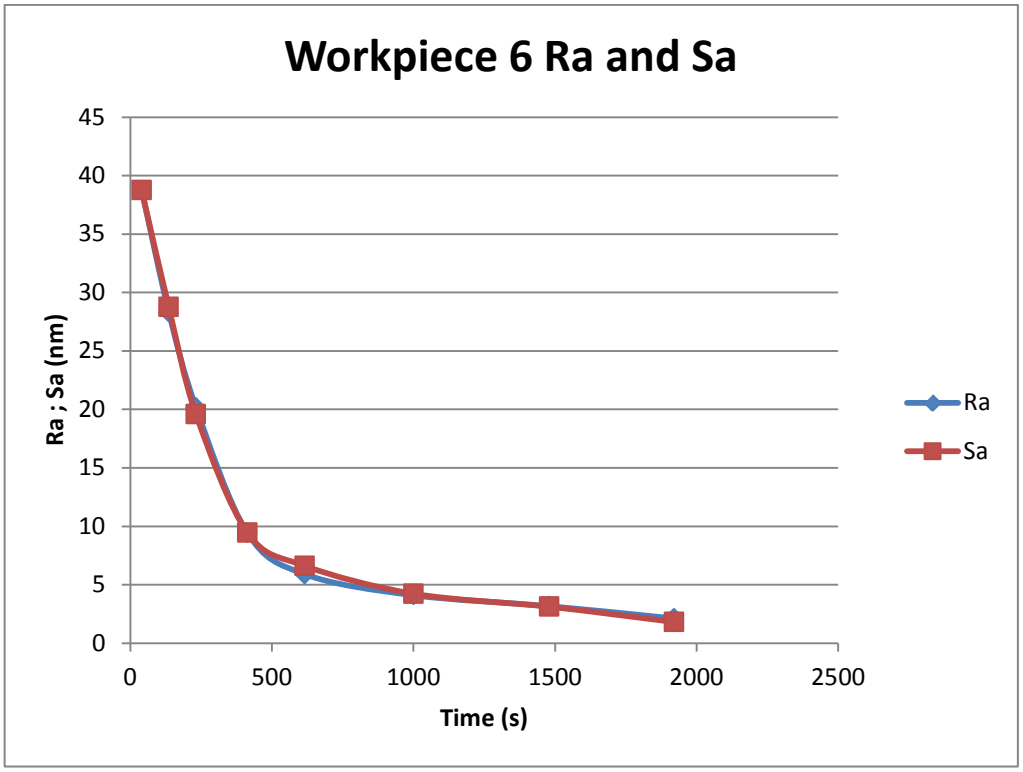

Comparaison betweene Ra and Sa for workpiece 6

Appendix G

Correlation graphs between forces and Ra for different time intervals

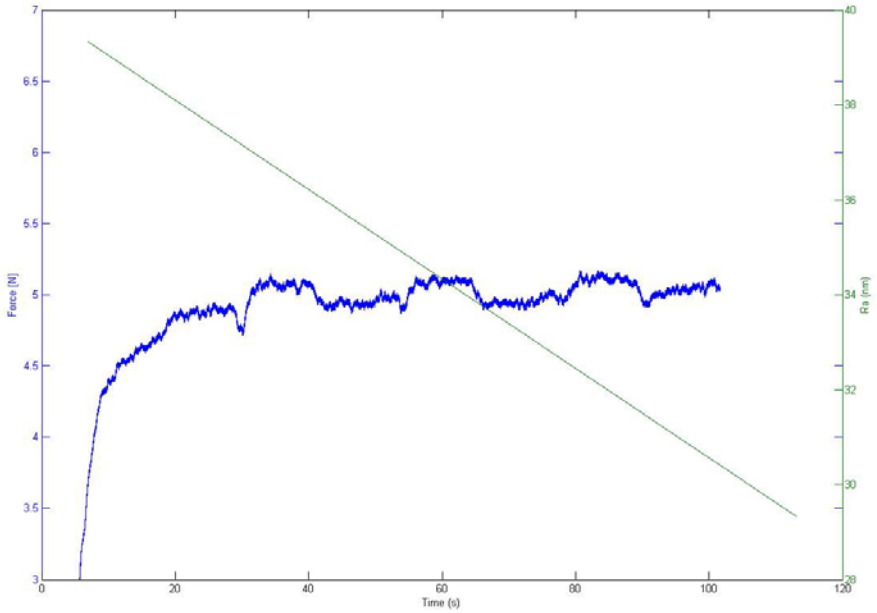

Correlation between force and Ra for 8 passes

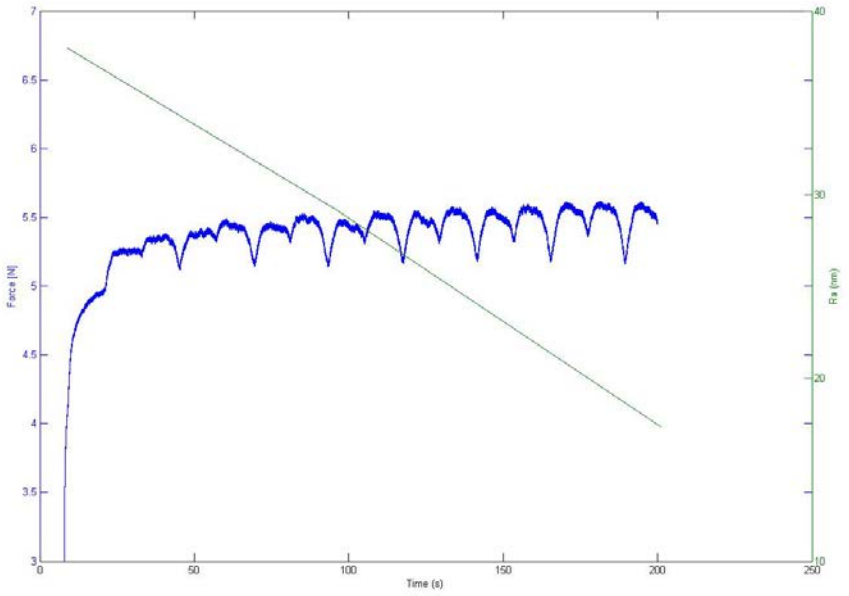

Correlation between force and Ra for 16 passes

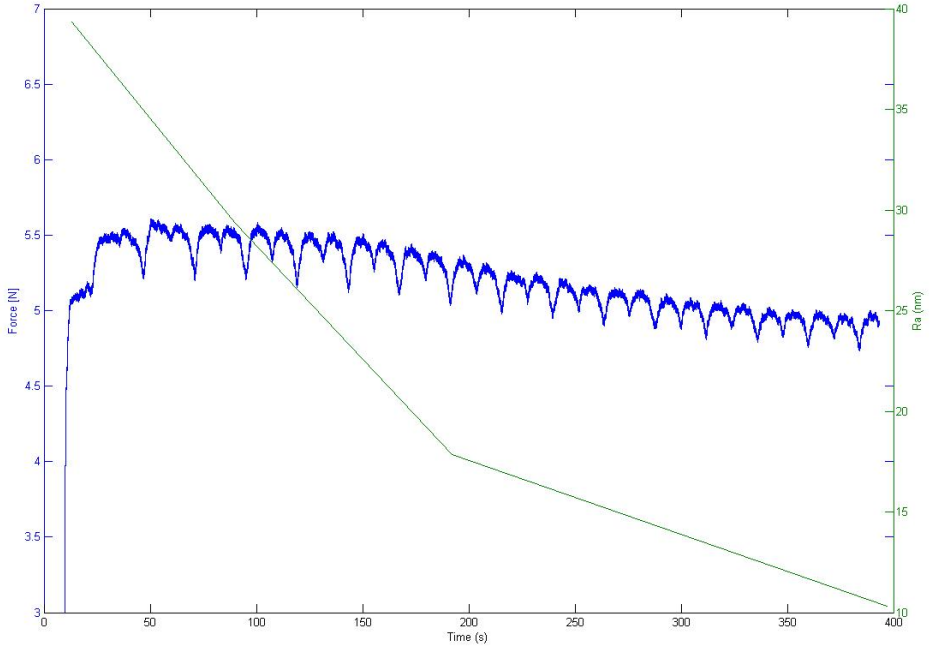

Correlation between force and Ra for 32 passes

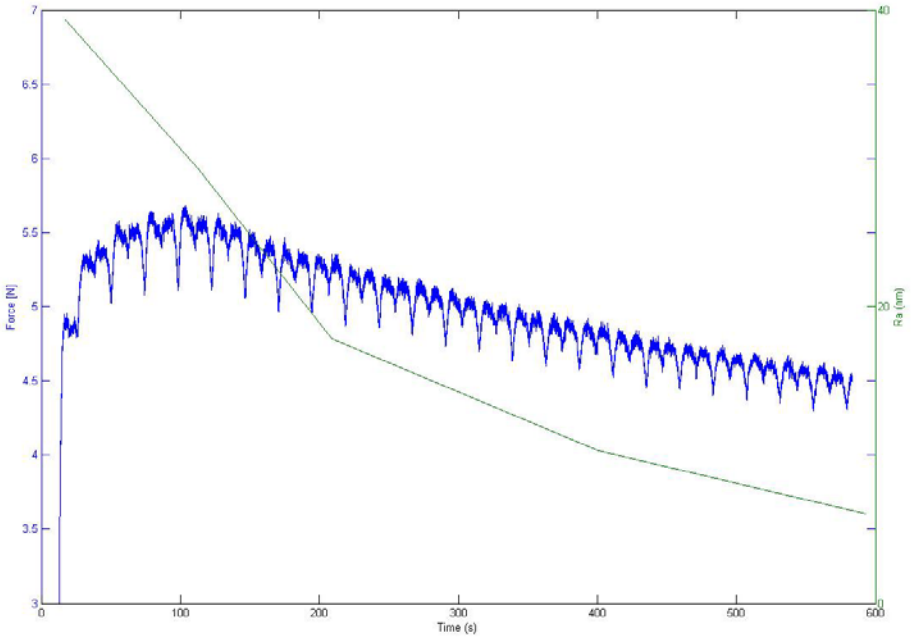

Correlation between force and Ra for 48 passes

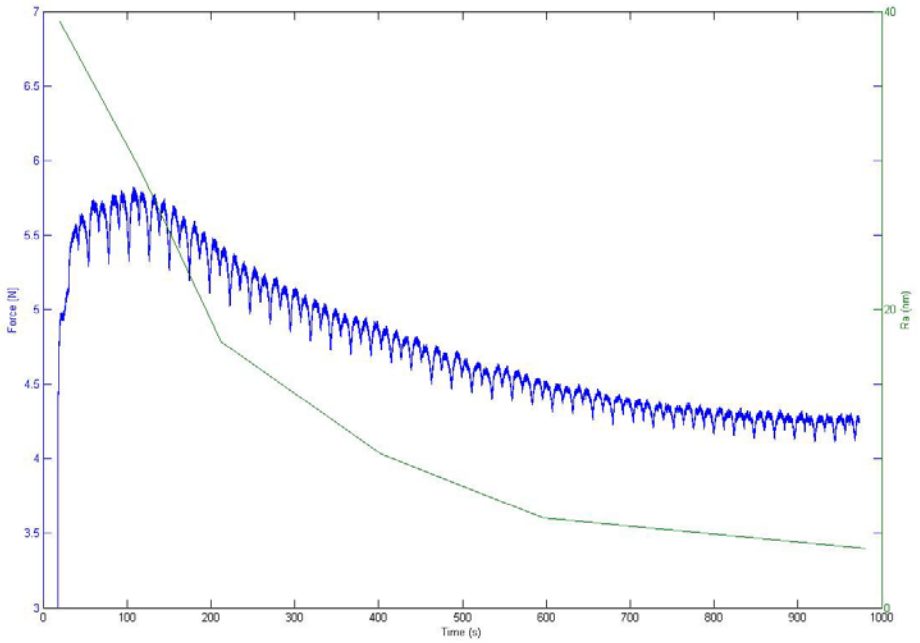

Correlation between force and Ra for 80 passes

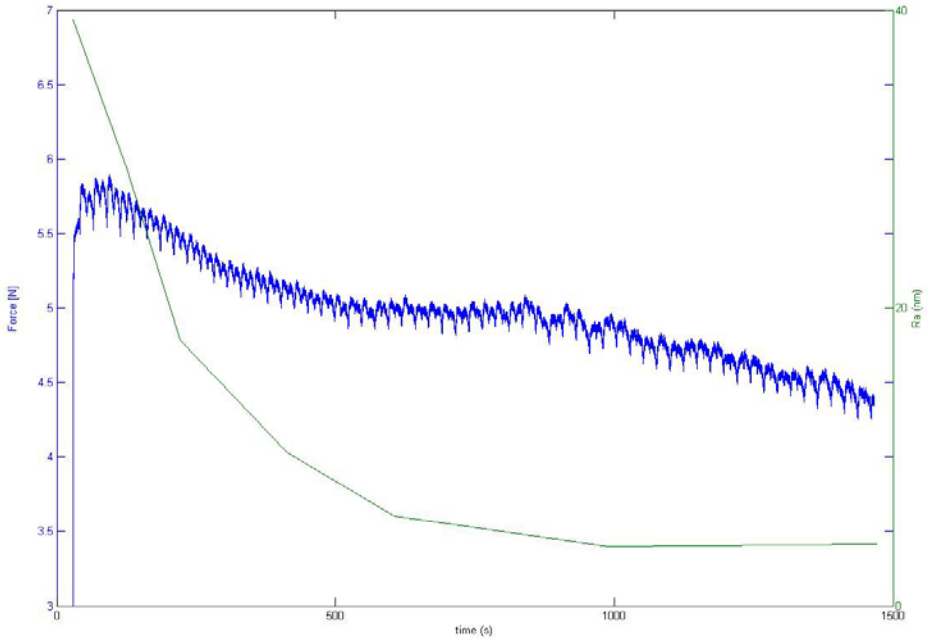

Correlation between force and Ra for 120 passes

Appendix H

Correlation graphs between AE power and Ra for different time intervals

- **Mistras R15**

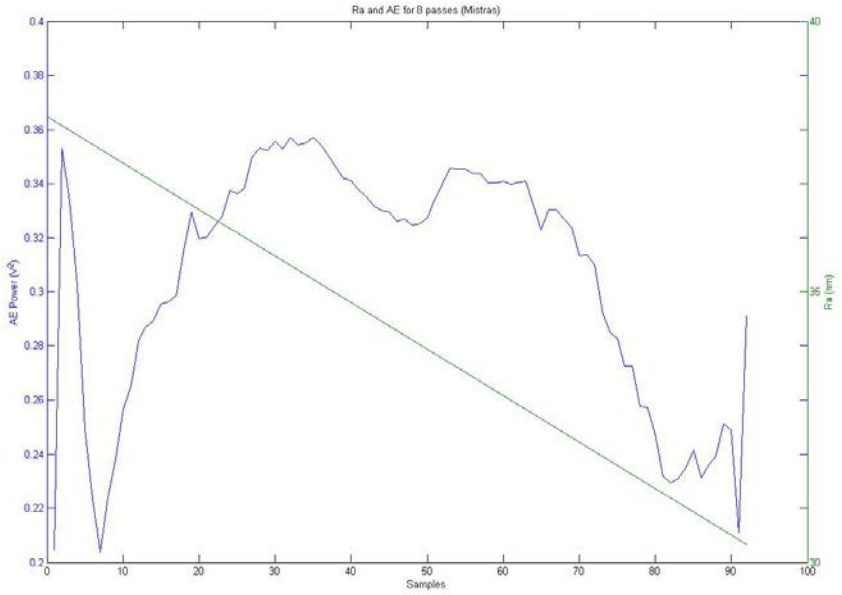

Correlation between AE and Ra for 8 passes (Mistras R15)

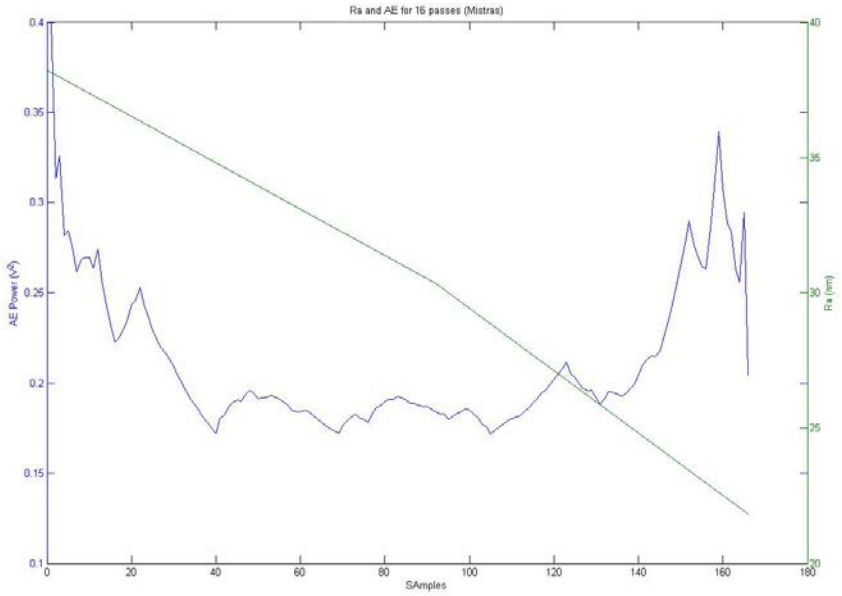

Correlation between AE and Ra for 16 passes (Mistras R15)

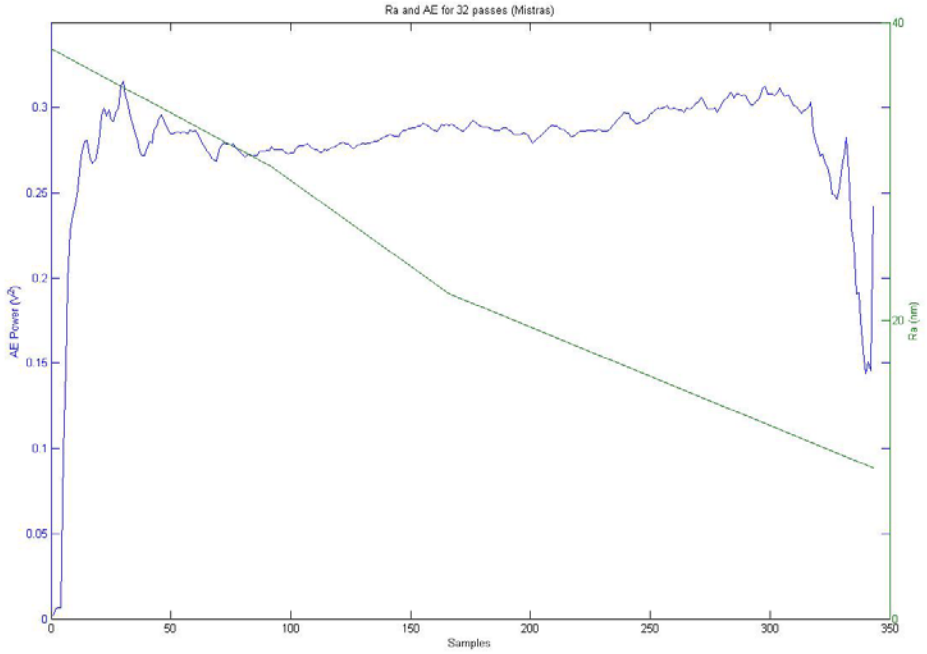

Correlation between AE and Ra for 32 passes (Mistras R15)

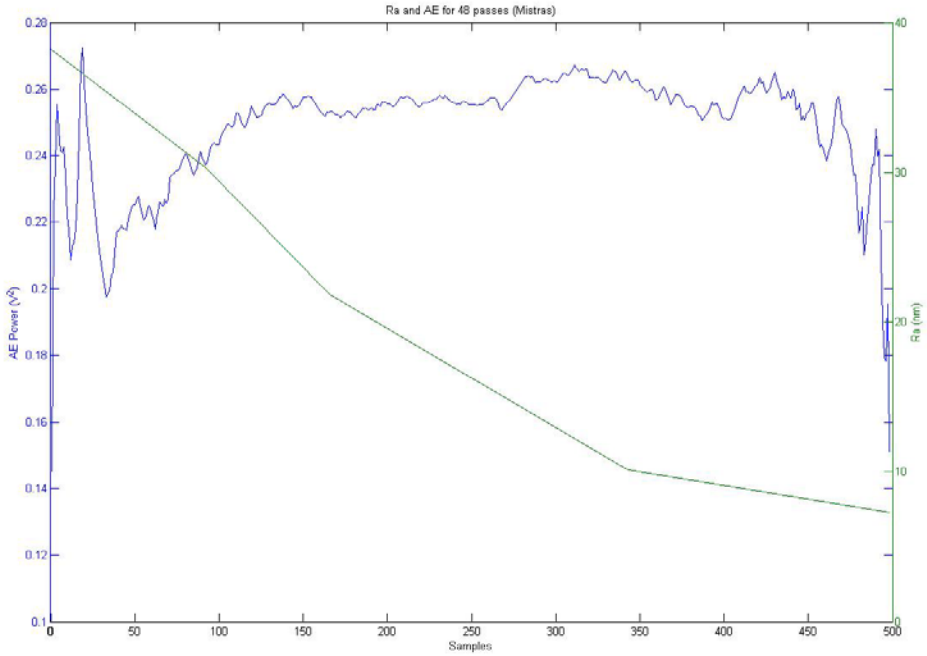

Correlation between AE and Ra for 48 passes (Mistras R15)

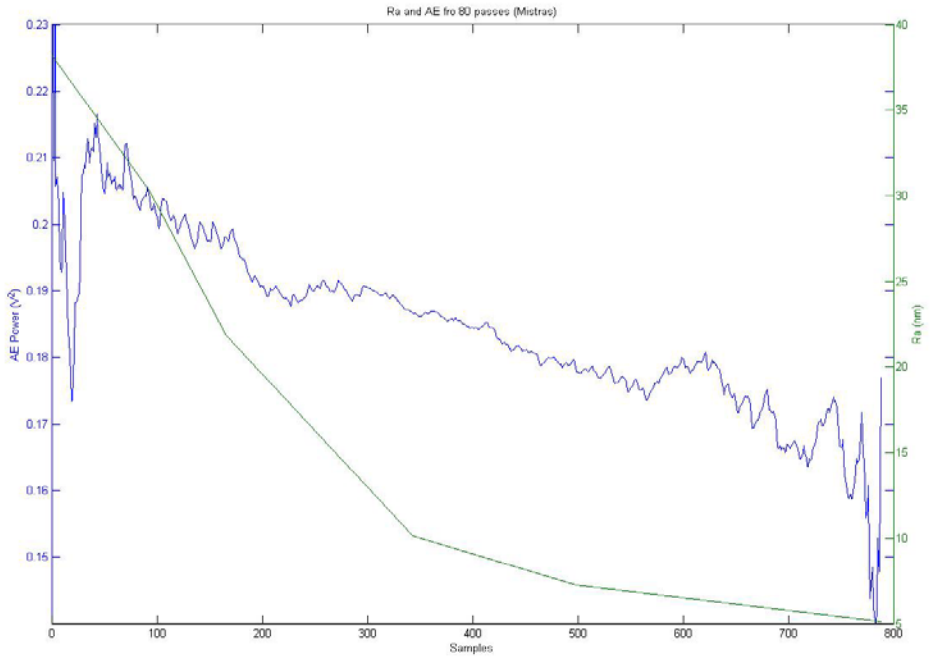

Correlation between AE and Ra for 80 passes (Mistras R15)

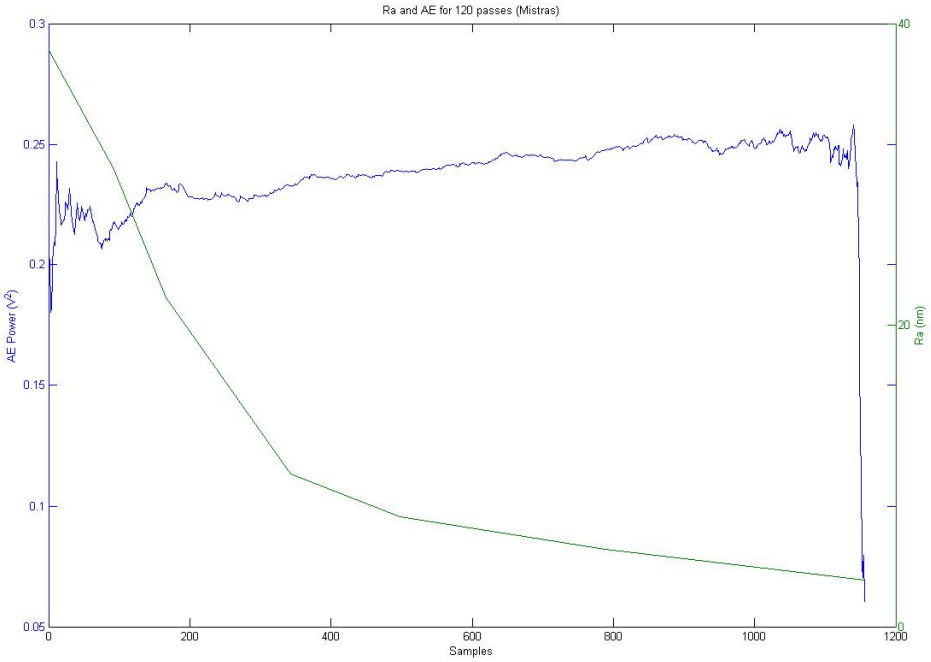

Correlation between AE and Ra for 120 passes (Mistras R15)

- **Montronix BV100**

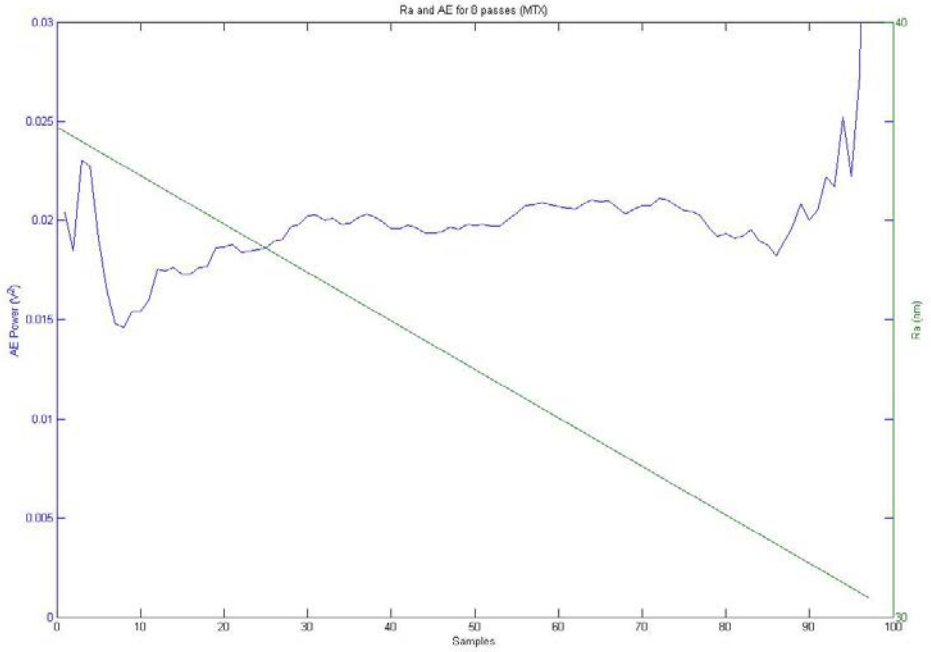

Correlation between AE and Ra for 8 passes (Montronix BV100)

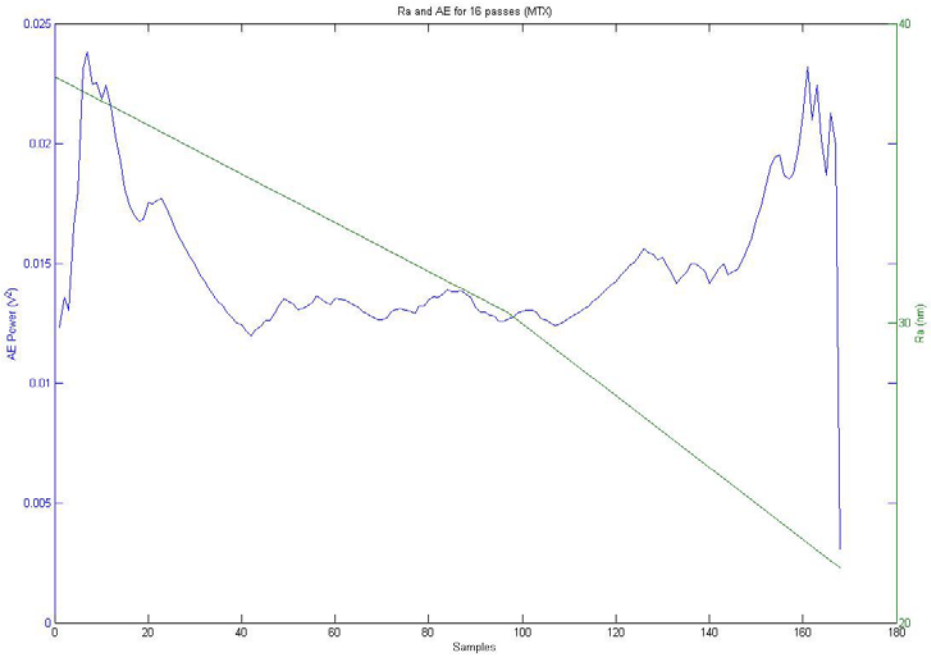

Correlation between AE and Ra for 16 passes (Montronix BV100)

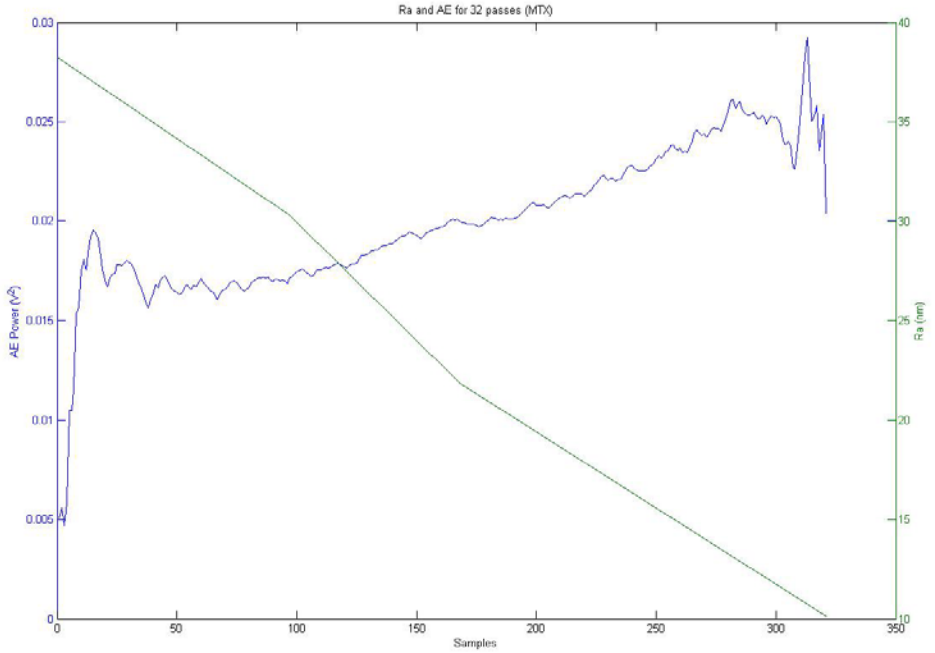

Correlation between AE and Ra for 32 passes (Montronix BV100)

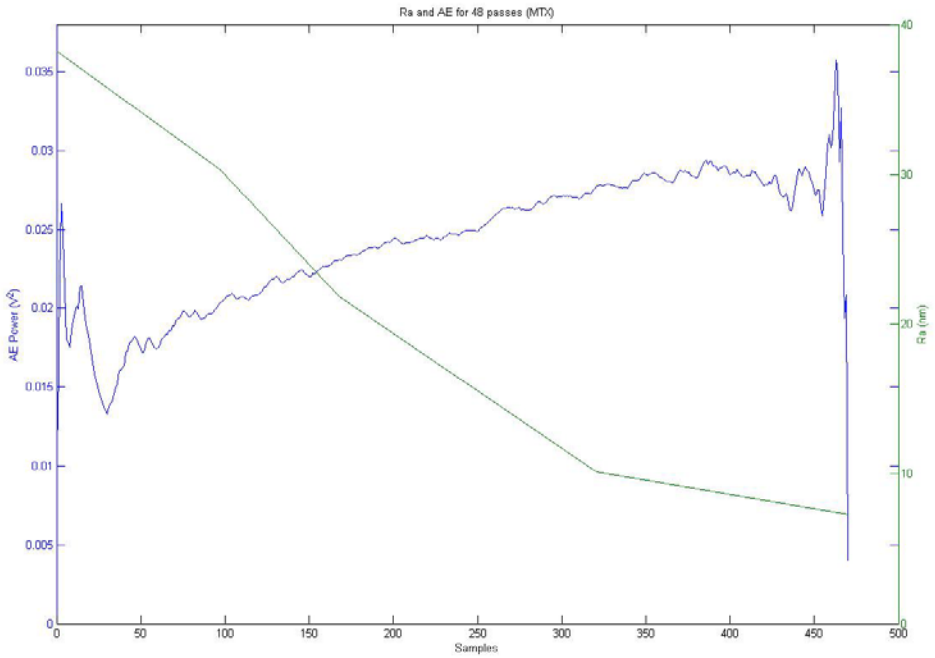

Correlation between AE and Ra for 48 passes (Montronix BV100)

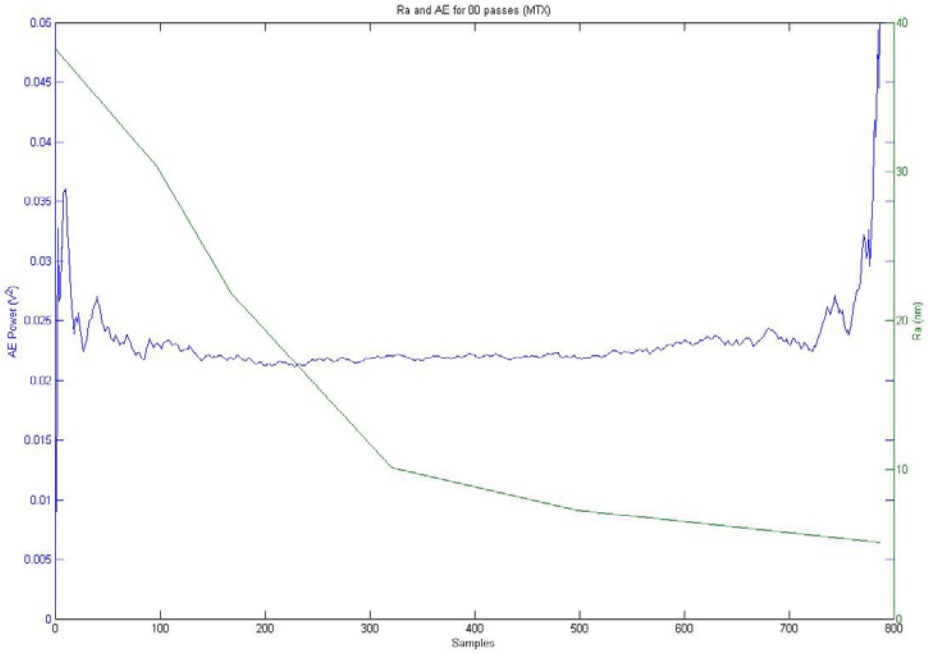

Correlation between AE and Ra for 80 passes (Montronix BV100)

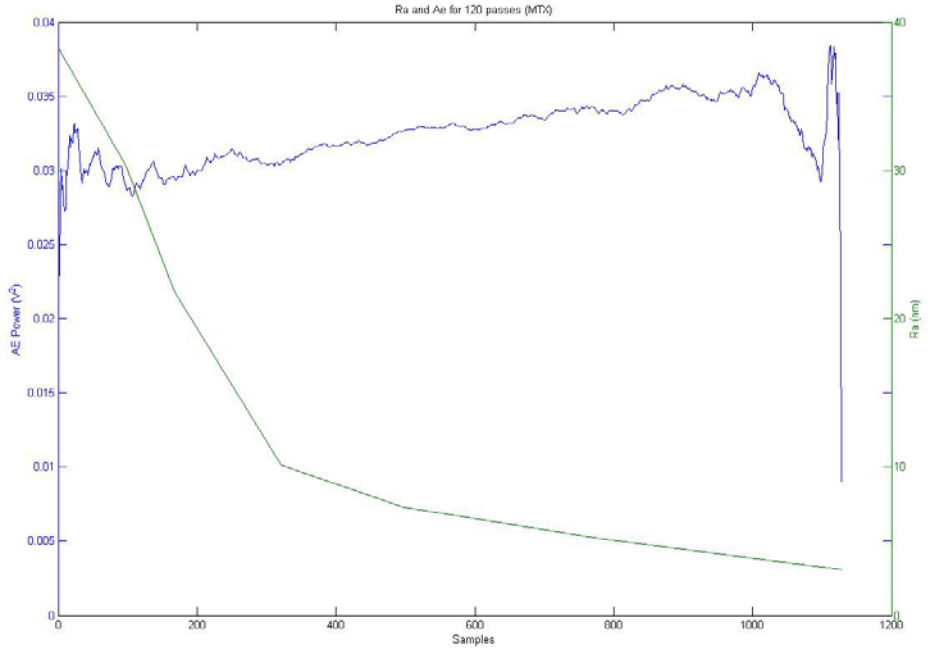

Correlation between AE and Ra for 120 passes (Montronix BV100)

Appendix I

Correlation graphs between power and Ra for different time intervals

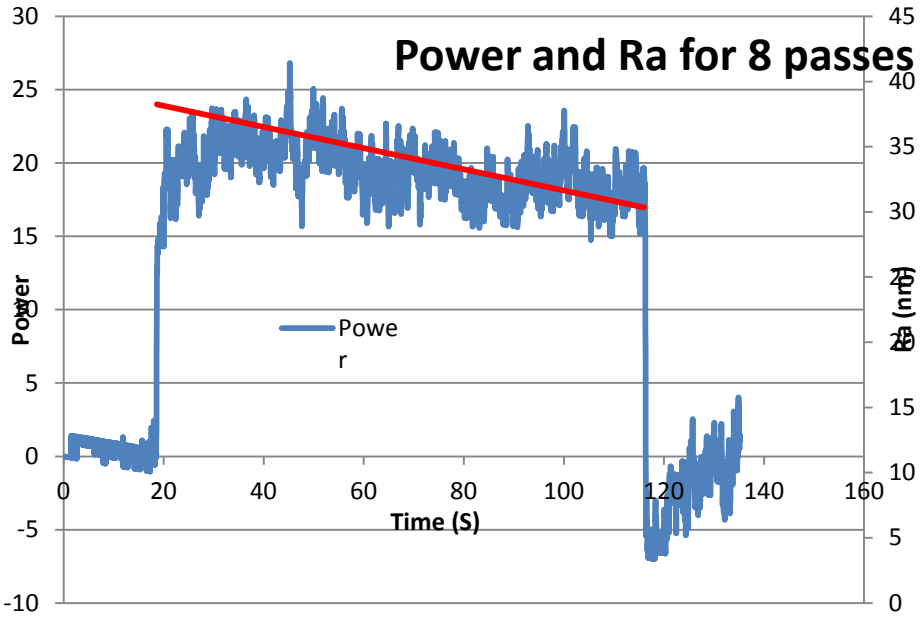

Correlation between force and Ra for 8 passes

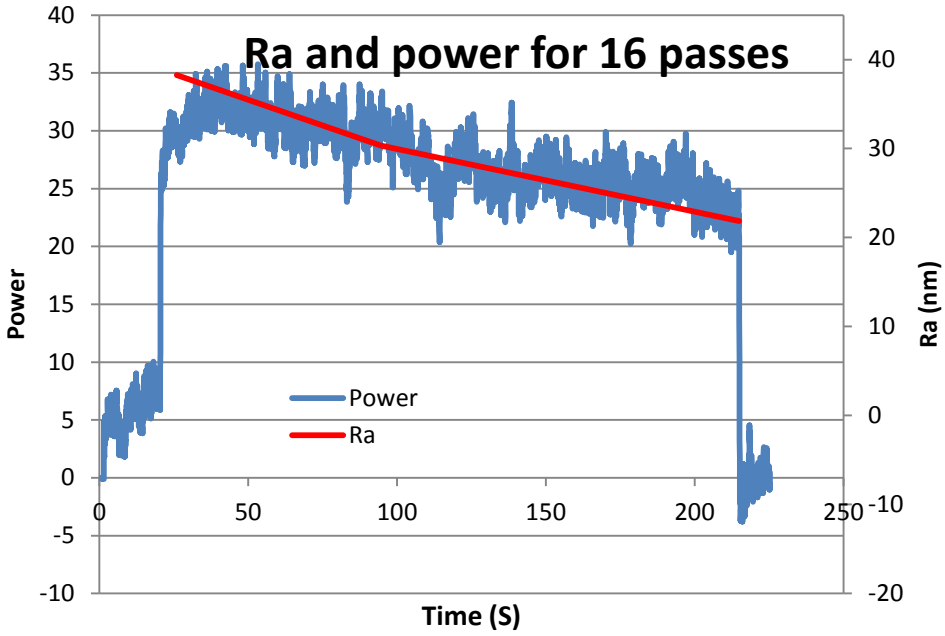

Correlation between force and Ra for 16 passes

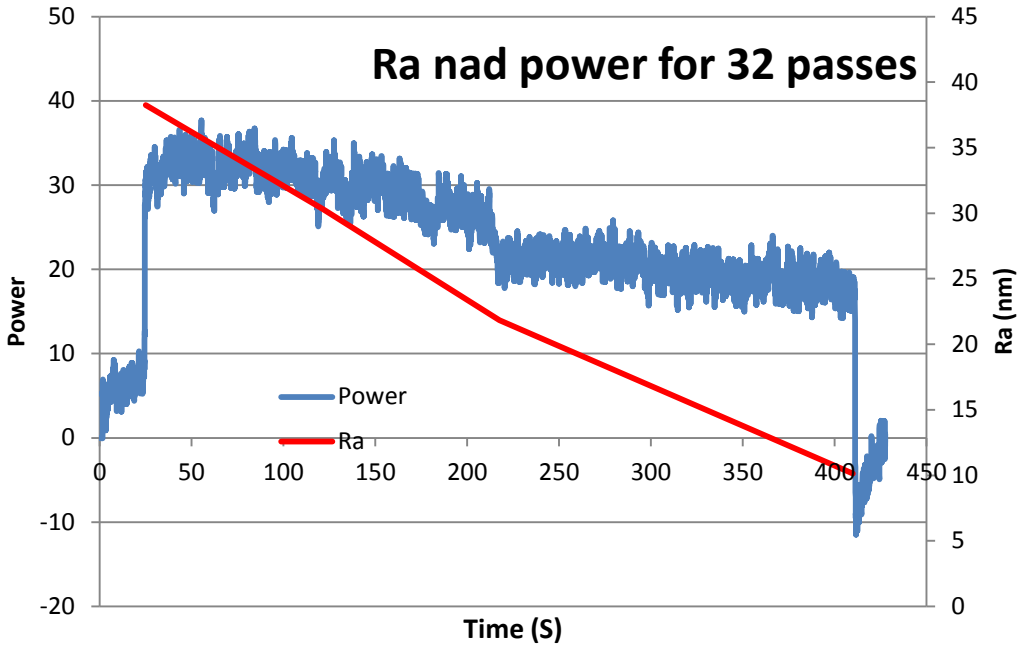

Correlation between force and Ra for 32 passes

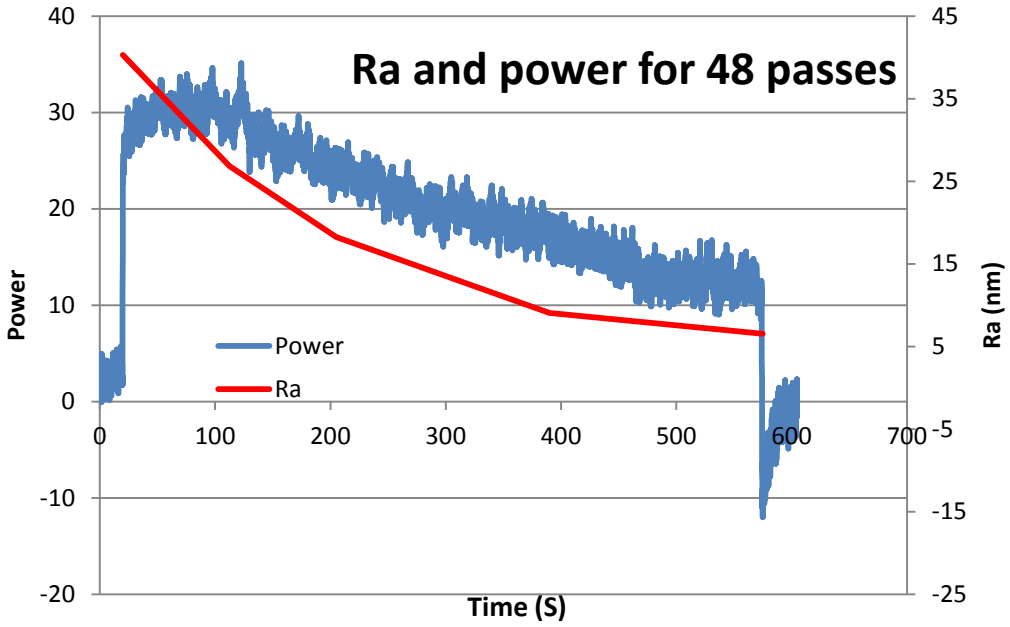

Correlation between force and Ra for 48 passes

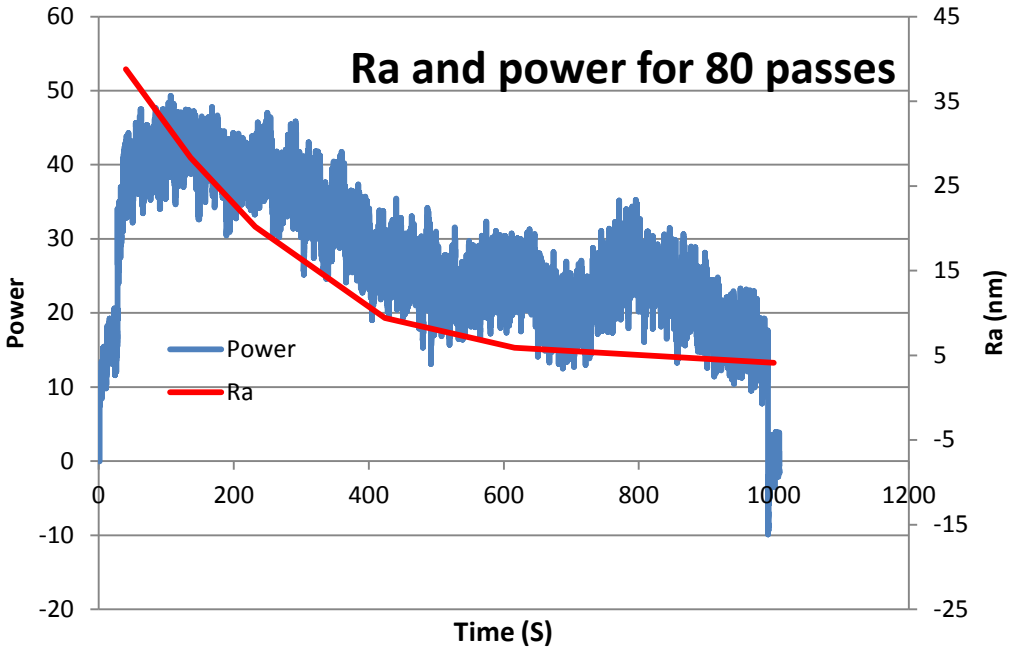

Correlation between force and Ra for 80 passes

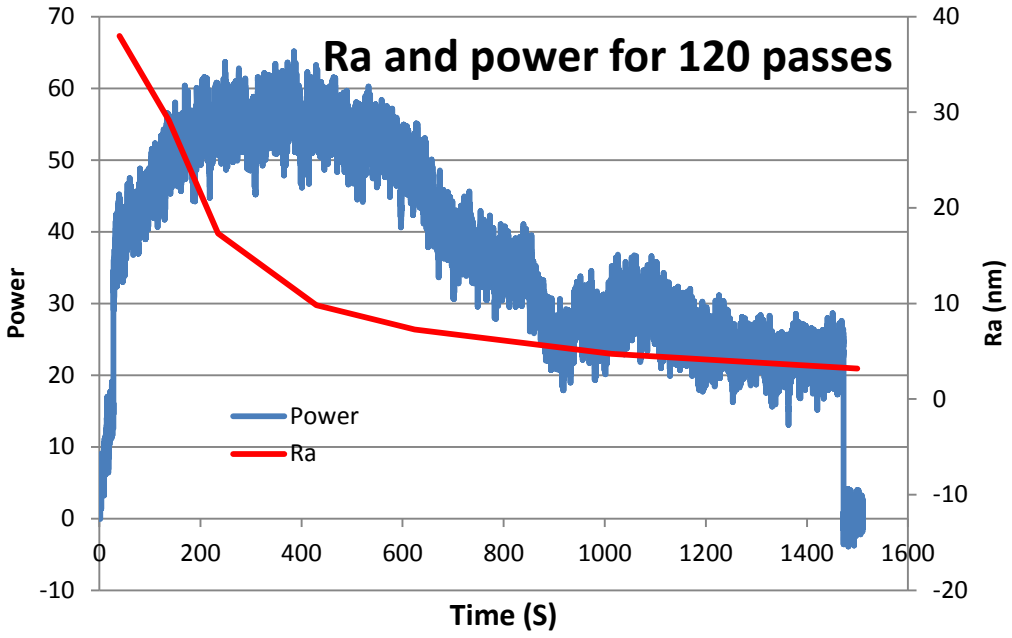

Correlation between force and Ra for 120 passes

Acknowledgements

I would like to express my gratitude to everyone who has helped and guided me during my exchange period and through this project.

First of all, I would like to thanks my family for always encouraging, supporting and assisting me.

Thanks to Professor Giuliano Bissacco for being my supervisor.

Special thanks to Lukas Pilny that followed me during the whole project, helped me every time I need, stood me and my infinite questions like a “guardian angel”.

Great thanks are due to the staff of DTU: Peter Sanderhoff, Lars Peter Holmbæk, Jakob Rasmussen and Rene Sobiecki

Then I want to thank to all my colleagues and friends I have met during my satying in Denmark for enjoyable time together.